



Western Michigan University  
ScholarWorks at WMU

---

Masters Theses

Graduate College

---

4-2012

## Design of a Catenoidal Shaped Anechoic Termination

Kyle Myers  
*Western Michigan University*

Follow this and additional works at: [https://scholarworks.wmich.edu/masters\\_theses](https://scholarworks.wmich.edu/masters_theses)



Part of the Mechanical Engineering Commons

---

### Recommended Citation

Myers, Kyle, "Design of a Catenoidal Shaped Anechoic Termination" (2012). *Masters Theses*. 41.  
[https://scholarworks.wmich.edu/masters\\_theses/41](https://scholarworks.wmich.edu/masters_theses/41)

This Masters Thesis-Open Access is brought to you for free and open access by the Graduate College at ScholarWorks at WMU. It has been accepted for inclusion in Masters Theses by an authorized administrator of ScholarWorks at WMU. For more information, please contact [wmu-scholarworks@wmich.edu](mailto:wmu-scholarworks@wmich.edu).



DESIGN OF A CATENOIDAL SHAPED  
ANECHOIC TERMINATION

by

Kyle Myers

A Thesis  
Submitted to the  
Faculty of The Graduate College  
in partial fulfillment of the  
requirements for the  
Degree of Master of Science in Engineering (Mechanical)  
Department of Mechanical and Aeronautical Engineering  
Advisor: Koorosh Naghshineh, Ph.D.

Western Michigan University  
Kalamazoo, Michigan  
April 2012

THE GRADUATE COLLEGE  
WESTERN MICHIGAN UNIVERSITY  
KALAMAZOO, MICHIGAN

Date February 17, 2012

WE HEREBY APPROVE THE THESIS SUBMITTED BY

Kyle Myers

ENTITLED Design of a Catenoidal Shaped Anechoic Termination

AS PARTIAL FULFILLMENT OF THE REQUIREMENTS FOR THE

DEGREE OF Master of Science in Engineering (Mechanical)

Mechanical and Aeronautical Engineering

(Department)



Koorosh Naghshineh, Ph.D.  
Thesis Committee Chair

Mechanical Engineering

(Program)



Kapseong Ro, Ph.D.  
Thesis Committee Member



Richard Hathaway, Ph.D.  
Thesis Committee Member

APPROVED



Dean of The Graduate College

Date April 2012

# DESIGN OF A CATENOIDAL SHAPED ANECHOIC TERMINATION

Kyle Myers, M.S.E.

Western Michigan University, 2012

An analytical model is developed in this thesis to predict the reflection coefficient of an anechoic termination consisting of a catenoidal horn connected to a tube lined with absorbing material. The theoretical predictions are compared to experimental measurements on a prototype. Comparisons are made for a variety of arrangements, including, an open horn, and a horn connected to absorbing terminations of two different lengths. The absorbing terminations are either open or closed to the environment and the analytical model can account for both these scenarios. The results indicate that the new model can accurately predict the reflection coefficient for each case presented, especially at low frequencies and for long absorbing terminations. A comparison with experimentally measured reflection coefficient is made between the analytical model presented in this thesis and the model of Bolton [1] in order to highlight the improvement over existing models.

© 2012 Kyle Myers

## ACKNOWLEDGEMENTS

I would like to express how thankful I am to my advisor, Dr. Koorosh Naghshineh, for his care and attention throughout this project. He has provided countless helpful suggestions and resources to enable me to complete this work and has pushed me to be my best. I would also like to thank committee members Dr. Kapseong Ro and Dr. Richard Hathaway for their suggestions and support while writing this thesis.

A special thanks to the people who have helped me with the experimental setup, including Dan Selvidge and Mitch Button for their handy work in the construction process, and Eric Gassman, who drew the horn model in AutoCAD. Also thanks to Phil Eppard at Johnson Controls, Inc. for taking the time out of a busy schedule to make measurements on polyester fiber samples for me.

Finally, I thank my parents, Mark and Bonnie, and all of my family for supporting me all throughout my academic life. They have instilled in me the importance of education and it has made me who I am today.

Kyle Myers

## TABLE OF CONTENTS

ACKNOWLEDGEMENTS .....	ii
LIST OF TABLES .....	vii
LIST OF FIGURES .....	viii
CHAPTER	
1. INTRODUCTION .....	1
1.1 Project Overview .....	1
1.2 Pressure Reflection Coefficient .....	2
1.3 Anechoic Termination Model Description .....	3
1.4 Thesis Organization .....	5
2. LITERATURE REVIEW AND RESEARCH MOTIVATION .....	6
2.1 ISO 5136 Standard .....	6
2.2 Need for an Anechoic Termination .....	7
2.2.1 Sound Power Measurement .....	8
2.2.2 Transmission Loss Measurement .....	10
2.3 Anechoic Terminations using Wedges .....	12
2.4 Anechoic Terminations using Absorbing Layers .....	14
2.5 Anechoic Terminations using Stepped Cross-Sections .....	20
2.6 Anechoic Terminations using Horns and Cones .....	22
2.7 Anechoic Terminations using Active Cancellation .....	25

## Table of Contents—Continued

### CHAPTER

2.8 Research Motivation .....	26
3. ANALYTICAL MODEL DEVELOPMENT .....	28
3.1 Acoustic Impedance .....	29
3.2 The Catenoidal Horn .....	33
3.2.1 Webster's Horn Equation .....	34
3.2.2 Impedance at the Horn Mouth .....	36
3.2.3 Motivation for Using a Catenoid .....	40
3.3 The Absorbing Termination .....	44
3.3.1 Acoustic Pressure Field in a Cylinder .....	45
3.3.2 Rigid Wall Boundary Condition .....	46
3.3.3 Absorbing Wall Boundary Condition .....	49
3.3.4 Normal Specific Acoustic Impedance, $z_w$ .....	52
3.3.5 Complex Axial Wavenumber, $k_x$ .....	57
3.3.6 Impedance at Termination Inlet .....	59
3.4 Summary of Analytical Model .....	61
4. EXPERIMENTAL VALIDATION .....	65
4.1 Description of the Prototype .....	65
4.2 Experimental Setup .....	70



## Table of Contents—Continued

### CHAPTER

4.2.1 Sound Source and Impedance Tube.....	71
4.2.2 Data Acquisition System.....	73
4.3 Experimental Measurement Procedure .....	75
4.3.1 Complex Reflection Coefficient .....	75
4.3.2 Benchmark for Experimental Measurements.....	77
4.4 Experimental Results vs. Analytical Predictions .....	79
4.4.1 Open Horn, No Termination .....	80
4.4.2 Horn with Open Termination.....	82
4.4.3 Horn with Closed Termination (Rigid Cap) .....	87
4.4.4 Horn with Closed Termination (Layered Rigid Cap) .....	90
4.4.5 Comparison between Experimental Arrangements .....	91
4.4.6 Analytical Model Compared to Bolton's Model .....	96
5. OPTIMUM DESIGN OF A TERMINATION .....	100
5.1 Parametric Study of Horn Geometry .....	100
5.1.1 An Infinitely Long Absorbing Termination.....	100
5.1.2 An Open Catenoid.....	102
5.2 Optimization Cost Function .....	104
5.3 Example of an Optimum Anechoic Termination.....	106

## Table of Contents—Continued

### CHAPTER

6. CONCLUSIONS AND RECOMMENDATIONS .....	109
REFERENCES .....	113
APPENDICES .....	117
A. MATLAB® Files .....	117
B. Derivation of Acoustic Pressure in Cylindrical Coordinates .....	125
C. Polyester Fiber Specifications .....	129
D. Figure Copyright Documentation.....	132
E. Impedance Data for Polyester Fiber .....	137

## LIST OF TABLES

1. Maximum reflection coefficient as a function of frequency for measuring fan sound power in-duct [2] .....	7
2. Maximum error in sound power level as a function of reflection coefficient from Eq. (2.2.2).....	10
3. Dimensions of each component of the anechoic termination prototype.....	67
4. Impedance tube specifications .....	73
5. Optimized anechoic termination dimensions.....	107

## LIST OF FIGURES

1. Schematic of the modeled anechoic termination. Horn throat and mouth are shown. The horn shape approximates a catenoid .....	4
2. A schematic of measuring muffler transmission loss using three microphones [5]. Microphones 1 and 2 are located upstream of the muffler and microphone 3 is downstream. ....	11
3. A pipe anechoic termination stuffed with absorbing material. Sound traveling to the right in air meets the absorbing material at the boundary shown and partially reflects due to the change in impedance.....	16
4. Three material layers lining a flat wall in an impedance tube. Shown are incident and reflected components at each boundary with impedance $Z_i$ . The three layers have different material characteristics.....	19
5. An acoustic wave incident on the boundary between the two pipes will have reflected and transmitted pressure components.....	21
6. A six stepped anechoic termination [1]. The incident wave travels to the right towards the terminator body at the far right .....	22
7. Horn shaped anechoic termination developed by Wollherr and modified to its present form by Neise [22] .....	24
8. Incident, reflected, and transmitted acoustic pressures at a boundary .....	31
9. A schematic of an anechoic termination with specific acoustic impedances shown at each boundary. A plane wave travels to the right in the test tube .....	33
10. Specific acoustic impedance ratio for a catenoidal horn of length 64 in. with throat and mouth diameters of 1 in. and 20 in. The horn terminates into an infinite tube .....	39
11. Magnitude of the specific acoustic impedance ratio for the example horn .....	40

12. On the left, two pipes of different area are connected to each other. On the right, a horn is used to transition the same two pipes. The wave travels from left to right .....	42
13. Comparison of reflection coefficient between two pipes of different diameters with a horn transition and without.....	42
14. Normal mode shapes at a cross section of the cylindrical cavity .....	47
15. Cross-section of the absorbing termination with absorbing material of thickness $a - r_0$ around the wall.....	49
16. Characteristic impedance ratio of the polyester fiber .....	55
17. Propagation constant of the polyester fiber (absolute value of imaginary part) plotted with the wavenumber in air.....	56
18. Specific acoustic impedance normal to the polyester fiber surface (normalized with the characteristic impedance of air).....	56
19. Real and imaginary components of the axial wavenumber. Also shown is the wavenumber in air.....	59
20. Anechoic termination prototype with catenoidal horn (white) and absorbing termination (black) of length 0.91 m (36 in.) and diameter 0.305 m (12 in.).....	66
21. An absorbing termination 3.28 m (129 in.) in length and diameter 0.305 m (12 in.). The mouth of the horn connects to the end shown on the left .....	66
22. Inlet of the absorbing termination with the horn unattached to the medium density fiberboard. A layer of polyester fiber lines the circumference throughout the termination.....	68
23. Connection of the horn mouth to the absorbing termination inlet .....	68
24. Absorbing termination with open end. Horn is partially visible on the far left.....	69
25. A bare cap (a) and the same cap with a layer of polyester fiber (b) is used to close the termination end shown in Figure 24.....	69

26. Experimental arrangement with sound source, impedance tube, catenoid, absorbing termination, and data acquisition system.....	70
27. Enclosure for sound source (a) and front wall open (b) with speaker mounted.....	71
28. Impedance tube (left) and close-up of microphone mounts (right) .....	72
29. Schematic of the signal flow for data collection.....	74
30. Open impedance tube used as a benchmark arrangement to validate experimental procedure.....	77
31. Side and front view of a baffled piston representing the open end of a tube.....	78
32. Experimental measurement of reflection coefficient for an open tube compared to theoretical predictions made using Eq. (4.3.7).....	79
33. Horn prototype open to the air .....	80
34. Measured and predicted reflection coefficient for open catenoid.....	81
35. Plot of power absorption coefficient for the open catenoid.....	82
36. Horn (partially shown) and absorbing termination open to the air (picture, far left) .....	83
37. Reflection coefficient magnitude for the horn and absorbing termination (length = 36 in.) open to the air .....	84
38. Power absorption coefficient for horn and absorbing termination (length = 36 in.) open to the air .....	85
39. Reflection coefficient magnitude for the horn and absorbing termination (length = 129 in.) open to the air .....	86
40. Absorption coefficient for horn and absorbing termination (length = 129 in.) open to the air .....	86
41. Horn (partially shown) and absorbing termination with rigid cap attached (picture, far left).....	87

42. Reflection coefficient magnitude for the horn and absorbing termination (length = 36 in.) closed with a rigid cap.....	88
43. Absorption coefficient for horn and absorbing termination (length = 36 in.) closed with a rigid cap.....	88
44. Reflection coefficient magnitude for the horn and absorbing termination (length = 129 in.) closed with a rigid cap.....	89
45. Absorption coefficient for horn and absorbing termination (length = 129 in.) closed with a rigid cap.....	90
46. Experimentally measured reflection coefficient for each boundary condition (36 in. absorbing termination) .....	91
47. Experimentally measured power absorption coefficient for each boundary condition (36 in. absorbing termination) .....	92
48. Experimentally measured reflection coefficient for each boundary condition (129 in. absorbing termination) .....	93
49. Experimentally measured power absorption coefficient for each boundary condition (129 in. absorbing termination) .....	94
50. A relative comparison of experimentally measured reflection coefficient between two different length absorbing terminations (when both are open) .....	95
51. A relative comparison of experimentally measured absorption coefficient between two different length absorbing terminations (when both are open) .....	95
52. Bolton's model vs. the present analytical model (catenoid and 129" open absorbing termination) compared to experimentally measured reflection coefficient .....	98
53. Bolton's model vs. the present analytical model (catenoid and 129" open absorbing termination) compared to experimentally measured absorption coefficient.....	99
54. Reflection coefficient of a catenoid 1 meter in length connected to an infinitely long tube for several flare values .....	102

55. Comparison of reflection coefficient for an open catenoid (6 in. throat diameter, 36 in. length) of various mouth diameters .....	104
56. The cost function is the normalized area under the reflection coefficient magnitude bounded between lower and upper frequencies .....	105
57. Reflection coefficient magnitude of optimized anechoic termination .....	107



## CHAPTER 1

### INTRODUCTION

#### 1.1. Project Overview

Anechoic terminations are assemblies that function to absorb all sound energy incident on the end of a duct opposite to a sound source. Acoustic quantities such as sound power and transmission loss are commonly measured in an in-duct arrangement, which requires the use of an anechoic termination. For example, the heating, ventilation and air conditioning (HVAC) industry uses an anechoic termination as part of their experimental setup to measure sound power emitted into a duct from fans or other air-moving devices. The automotive industry implements an anechoic termination on test bench arrangements as part of a technique to measure the transmission loss of mufflers or other intake manifolds. However, the acoustical measurements are subject to errors and other experimental difficulties when the duct end is too reflective. To create a non-reflective boundary condition, an anechoic termination is connected to the duct end opposite the sound source.

The non-reflective condition is typically achieved with the use of long pipes lined with absorbing material, horns, or other expanding cross-sections terminating into absorbing tubes. In practice, it is difficult to design a completely non-reflective termination, as some reflection will always exist over a broad

spectrum. Redesigning the horn geometry, changing the length of the absorbing tube, or changing the type of absorbing material all affect the reflection characteristics of the anechoic termination. It will then be of interest to the engineer to predict the effect these design changes will have on the reflection characteristics over a certain frequency range. The goal of this thesis is to help develop a new analytical model to be used in order to predict the effect that changes in horn geometry, absorbing tube length, and absorbing material have on the reflection characteristics of anechoic terminations. The validity of this analytical model is then proven through experimental measurements.

## 1.2. Pressure Reflection Coefficient

An anechoic termination describes a non-reflective boundary condition (e.g., at a duct end located opposite to the sound source). The termination reflects no sound in principle, although this is very difficult to achieve in practice. In Chapter 3, it will be shown that this is especially true for low frequencies. The amount of reflection created by the anechoic termination can be quantified and is frequency dependent. If the complex amplitude of the reflected and incident acoustic pressure <sup>1</sup> is  $p_r$  and  $p_i$  respectively, then the *pressure reflection coefficient*  $\eta$  is defined as

$$\eta = \frac{p_r}{p_i} \tag{1.2.1}$$

---

<sup>1</sup> Acoustic pressure, being a function of space and time, has both magnitude and phase. It is commonly expressed as a complex quantity purely for mathematical convenience.

The magnitude of Eq. (1.2.1) quantifies the amount of reflection at a particular plane. The magnitude of this quantity, which varies from zero to one, is of primary interest in this thesis. A reflection coefficient equal to zero indicates the incident wave is completely transmitted (i.e. everything is absorbed); a reflection coefficient equal to one indicates the incident wave is completely reflected (i.e. nothing is absorbed). Throughout the remainder of this text, the pressure reflection coefficient will be simply stated as *reflection coefficient*.<sup>2</sup> The reflection coefficient of a particular termination is an important quantity that determines the effectiveness of the design.

### 1.3. Anechoic Termination Model Description

An anechoic termination could be constructed from a long tube filled with one or more different absorptive layers, a horn shaped pipe coupled with an absorptive tube, a wedge or panel of wedges, or multiple stepped circular cross sections lined with absorptive material. The models treated in this thesis will consist of two parts: the first is a gradually expanding cross sectional area taking the shape of a catenoidal horn, and the second is a cylindrical tube lined with absorbing material around its inner circumference. This tube connects to the end of the horn section. Figure 1 shows a schematic of this concept, where the horn shape approximates a catenoid (Chapter 3 will define the catenoidal profile).

---

<sup>2</sup> In general, it is important to distinguish between types of reflection coefficient (e.g., pressure, power, intensity). However, since the latter two are not used in this thesis, reflection coefficient is understood to mean pressure reflection coefficient.

A sound source generates sound that travels through the test tube towards the anechoic termination. The test tube is the location where the incident and reflected components of sound are separated (decomposed) in order to measure the reflection coefficient of the anechoic termination. The end of the test tube opposite the sound source connects to the horn throat. The horn mouth connects to the terminator body, shown in the figure with both its circumference and end cap lined with absorbing materials. The end cap is removable so that the terminator body can open to the air (not shown). The gradual flare of the horn diminishes reflected waves created by propagation through sections of different diameter. The absorbing tube attenuates the sound waves coming from the horn by means of an absorptive material lining such as polyester fiber. These concepts will be explained in detail in Chapter 3.

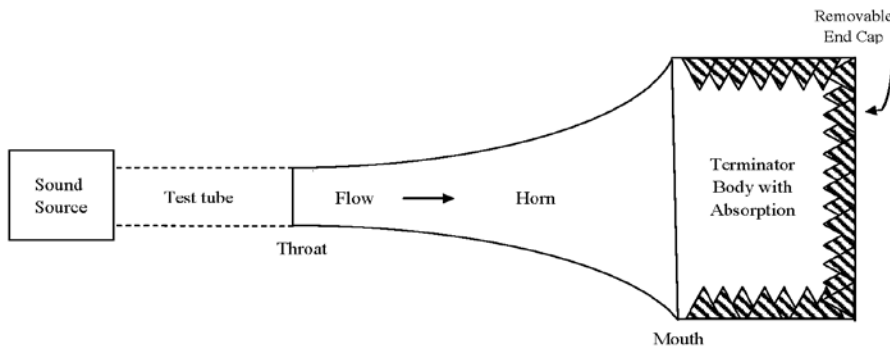


**Figure 1** Schematic of the modeled anechoic termination. Horn throat and mouth are shown. The horn shape approximates a catenoid

#### 1.4. Thesis Organization

Anechoic terminations are an important requirement to obtain accurate experimental measurements of fan noise or automotive intake/exhaust component transmission loss. This will be shown in Section 2.2 of the pertinent literature review. Sections 2.3-2.7 will demonstrate that the justification for particular anechoic termination designs have relied on extensive experimentation, numerical optimization, or simplified analytical models. The remainder of Chapter 2 will discuss the motivation for this research. Chapter 3 will show the steps taken to construct a new analytical model to predict the reflection coefficient of a catenoidal horn terminating into an absorbing pipe. A variety of boundary conditions for the pipe end will be considered. Chapter 3 will conclude with a procedural summary showing how to use the analytical model to calculate the reflection coefficient of the anechoic termination. Chapter 4 will compare the predictions from the analytical model against experimental measurements conducted at Western Michigan University's Noise and Vibration Laboratory. Predictions of the reflection coefficient using the analytical model presented in this thesis are compared to an existing simplified model at the chapter end. A study of various horn geometries will be carried out in Chapter 5 along with an example of an anechoic termination optimized for minimum reflection coefficient across a particular frequency range. Finally, Chapter 6 will provide a summary of this thesis and recommendations for future work.

## CHAPTER 2

### LITERATURE REVIEW AND RESEARCH MOTIVATION

This chapter contains a literature survey of the different kinds of anechoic terminations that have been constructed and the theoretical motivation for these designs. First, the need for anechoic terminations as part of an in-duct arrangement to measure acoustical quantities will be discussed. Then, different ways of designing anechoic terminations are summarized in the latter sections. These will include anechoic terminations that use wedges, absorbing layers, stepped sections, horns, and active cancellation. The chapter will conclude with a discussion of the motivation for the current research.

#### 2.1. ISO 5136 Standard

Of particular importance in the documentation relevant to anechoic terminations is the ISO 5136 standard [2]. This standard describes a technique to measure the sound power of fans and other air moving devices using an in-duct method. It gives recommendations for anechoic termination design and provides many examples of anechoic terminations that have been successfully implemented in the field. Many of the designs present in the standard come from papers discussed in this chapter. These designs can be useful if the dimensions suit the needs of the particular project, but significant scaling is discouraged to

obtain different size anechoic terminations. An analytical model that would allow the designer to quantify changes in the geometry is not available.

The standard also gives experimental techniques to measure reflection coefficient, and sets guidelines for the maximum reflection coefficient tolerated in an experimental arrangement. Table 1 shows the maximum reflection coefficient permitted by the standard. More reflection is tolerated at low frequencies since those frequencies are most difficult to absorb. The motivation behind setting maximum reflection is to limit measurement error in sound power, as will be shown in the next section.

**Table 1** Maximum reflection coefficient as a function of frequency for measuring fan sound power in-duct [2]

<b>½ Octave Band Center Frequency (Hz)</b>	<b>Maximum Pressure Reflection Coefficient</b>
50	0.40
63	0.35
80	0.30
100	0.25
125	0.15
≥160	0.15

## 2.2. Need for an Anechoic Termination

The need for anechoic terminations arises from the measurement techniques used to quantify sound power level and transmission loss inside a duct. The following two sections will describe the reasons for implementing an

anechoic termination in an experimental setup that measures these acoustic quantities.

### 2.2.1. Sound Power Measurement

First, consider the heating, ventilation and air-conditioning (HVAC) example of calculating sound power radiated into a duct from a fan. The sound power is the amount of energy the fan emits inside the duct per second. In the absence of reflections inside the duct, the sound power  $P_W$  for plane waves<sup>3</sup> is [3]

$$P_W = \frac{p^2}{\rho c} S, \quad (2.2.1)$$

where  $p$  is the root-mean-square (rms) amplitude of the acoustic pressure,  $\rho$  and  $c$  are the density and speed of sound of the acoustic medium (air in this case), and  $S$  is the duct cross-sectional area. Based on Eq. (2.2.1), sound power is independent of microphone measurement location since the root-mean-square of the acoustic pressure throughout the duct is constant. In practice where reflections create standing waves within the duct, sound power becomes a function of the duct reflection coefficient and source location within the duct [4]. Through use of an anechoic termination, these reflections can be eliminated, and the sound power is calculated using Eq. (2.2.1) (see Ref. [2] for corrections involving microphone response, microphone shields, and airflow). Therefore, the use of an anechoic termination as a boundary condition is preferred because it standardizes in-duct

---

<sup>3</sup> Waves for which pressure and velocity have constant magnitude and phase on any plane perpendicular to the direction of wave propagation



measurements of sound power between different laboratories. The ISO 5136 [2] adopts the non-reflective boundary condition for this reason as a standard for measuring fan sound power in ducts.

Expanding on this idea, consider an in-duct arrangement in the absence of an anechoic termination. Reflections at the end of the duct will interfere with incoming sound waves, creating a standing wave. This makes the acoustic pressure vary with location along the length of test section, implying that the sound power calculated using Eq. (2.2.1) would also vary depending on the axial location of the microphone. Therefore, the pressure measured in the actual non-anechoic duct is different from the desired pressure in an anechoic duct, leading to systematic errors in measurement of sound power level. Differences in acoustic pressure between the two cases depend on the particular frequency and the particular measurement location of the microphone. For a given frequency, the acoustic pressure measured at a specific location in the non-anechoic duct may equal the pressure in a duct with an anechoic termination. Similar measurements conducted at other axial locations would yield a different value. The maximum sound power error [3] in a non-anechoic duct relative to an anechoic duct is defined as a function of reflection coefficient magnitude  $\eta$  as

$$E_{\eta}^{max} = 20 \log \left( \frac{1 + \eta}{1 - \eta} \right) \quad [dB]. \quad (2.2.2)$$

Thus, the maximum error in sound power increases with reflection coefficient, i.e. as the duct termination becomes more reflective (see Table 2). Clearly, a less reflective anechoic termination is desirable for measurement of sound power of a fan in HVAC applications.

**Table 2** Maximum error in sound power level as a function of reflection coefficient from Eq. (2.2.2)

$ \eta $	Maximum Error [dB]
0.0	0.0
0.1	1.7
0.2	3.5
0.3	5.4
0.4	7.4

### 2.2.2. Transmission Loss Measurement

As a second example illustrating the need for an anechoic termination, consider transmission loss measurements of mufflers in the automotive industry. Equation (2.2.3) defines transmission loss (TL) as

$$TL = 10 \log \left( \frac{P_{Wi}}{P_{Wt}} \right) \quad [dB], \quad (2.2.3)$$

where  $P_{Wi}$  and  $P_{Wt}$ , defined by Eq. (2.2.1), are the incident and transmitted sound power, respectively. In-duct transmission loss measurements are commonly made using three microphones [5]. Figure 2 shows a schematic of this arrangement. Since a sound wave incident on the muffler partially reflects due to the expanding cross section, two microphones located upstream from the muffler must separate

the standing wave into its incident and reflected pressures. This is necessary in order to determine the incident sound power using Eq. (2.2.1). A third microphone downstream from the muffler measures the transmitted sound wave, assuming an anechoic termination. The absence of reflections downstream allows the transmitted sound power to be calculated by Eq. (2.2.1) using a single microphone. In the absence of a completely non-reflective anechoic termination, the transmitted sound power cannot be obtained using Eq. (2.2.1), creating inaccuracies in transmission loss [5]. However, anechoic terminations with better absorption characteristics can improve the measurement accuracy, as will be discussed in Section 2.4.

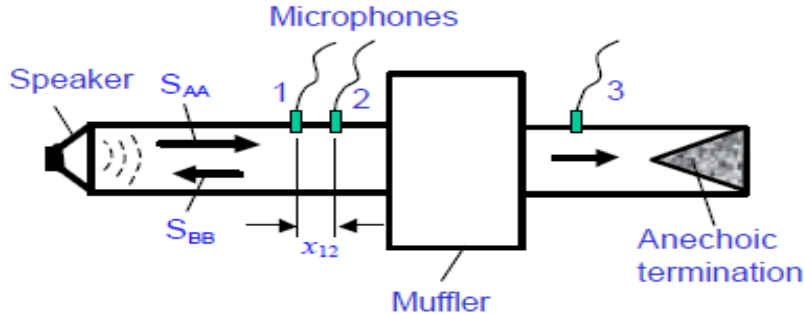


**Figure 2** A schematic of measuring muffler transmission loss using three microphones [5]. Microphones 1 and 2 are located upstream of the muffler and microphone 3 is downstream.<sup>4</sup>

<sup>4</sup> Reprinted with permission from SAE Paper No. 2003-01-1653 © 2003\* SAE International

### 2.3. Anechoic Terminations using Wedges

Beranek, *et al.* [6] in 1946, extensively studied the use of wedges to absorb sound inside anechoic chambers. The motivation for the study was to create a free field environment similar to the conditions high above the earth's surface for studying sound transmission problems. Beranek studied different shaped absorbing structures, including linear wedges, sheet layers, pyramids, exponentially tapered pyramids, exponentially tapered wedges, and blanket layers. Dozens of materials were studied which led to the selection of fiberglass for the final design. Experiments indicated that the linear wedge shape was superior to all other structures in terms of absorption and cost. For this reason, most anechoic chambers nowadays use the linear wedge shaped design. From experiment, Beranek presented design curves to determine the geometry of the wedge as a function of cutoff frequency<sup>5</sup>. The cutoff frequency for a particular anechoic chamber refers to the lowest frequency for which the acoustic field within the chamber is considered to be a free field (completely non-reflective). Watters [7] also designed a successful absorbing structure using columns arranged in steps as an approximation to Beranek's linear wedge design. The length of the column was selected to equal a quarter wavelength of the desired cutoff frequency. Watters then measured the reflection coefficient of his design and compared the results to Beranek's design.

---

<sup>5</sup> The frequency at which the reflection coefficient rises to 0.1, i.e. frequencies less than the cutoff have a reflection coefficient greater than 0.1.

The findings indicate that Beranek's linear wedge design produces slightly less reflection than the stepped wedge approximation, particularly at the frequency for which the wedge acts as a quarter-wavelength resonator.

The work of the two authors mentioned above has motivated the use of wedges to construct anechoic terminations. A properly designed wedge gives superior absorption above any cutoff frequency depending on the depth of the wedge. Wedges can be oriented in an in-duct arrangement such that the incoming wave strikes the wedge at normal incidence to give maximum absorption. In 1952, Beranek *et al.* [8] used the linear wedge design described in his previous paper [6] to construct an anechoic termination in order to measure acoustic power and spectra of fans in-duct. An exponential horn made the transition from the test duct to the absorbing termination. Suspended in the center of the termination were three fiberglass wedges. Fiberglass lined the outer walls of the absorbing termination. The end of the termination consisted of two perforated plates, one of which could be turned to control airflow through the system by changing the open area through the perforations.

Shenoda [9] studied designs similar to Beranek's along with several other variations. One of the most complete treatments on the subject, this paper focused specifically on anechoic termination performance. Many of the designs used conic transitions from test duct to wedge termination. Shenoda predicted

reflection coefficients for anechoic terminations that used conic transitions, but the predictions did not include the role of the wedges. Rather, it was assumed that the wedge section was completely absorptive, i.e. behaving as an infinite tube. In another paper, Holgersson [10] constructed a single wedge termination made of mineral wool for HVAC applications. He measured the reflection coefficient for different angle wedges and for wedges with multiple partitions of varying density. The experiments revealed that a single wedge could be effective at absorbing incident sound down to the cutoff frequency for small ducts. An analytical basis was absent from the paper.

To summarize the findings of this section, wedges create a non-reflective environment for frequencies at or above the cutoff. Experiments indicate that the degree of reflection from these surfaces is dependent on wedge shape and construction material.

#### 2.4. Anechoic Terminations using Absorbing Layers

A pipe stuffed with one layer (see Figure 3) or many different layers (see Figure 4) of absorbing material will partially reflect some incident sound energy at the air/material boundary and at boundaries between the different layers. The amount of reflection depends on the change in acoustic impedance  $Z$  across the boundary. The *acoustic impedance*  $Z$  at a boundary of area  $S$  is defined as [11]

$$Z = \frac{p}{U} , \tag{2.4.1}$$

where  $p$  is the complex acoustic pressure and  $U$  is the complex volume velocity. Acoustic impedance will be discussed in detail in Section 3.1, where knowledge of the impedance function will be necessary to compute the reflection coefficient of the anechoic termination. When impedance changes from  $Z_0$  to  $Z_1$  across a boundary, the difference in impedance is used to calculate the reflection coefficient at that boundary. The relationship between changes in impedance and reflection coefficient are given by [11],

$$\eta = \frac{Z_1 - Z_0}{Z_1 + Z_0} . \quad (2.4.2)$$

Thus, when the impedance is equal on both sides of the boundary, no reflection occurs. Figure 3 shows a schematic of a pipe anechoic termination stuffed with a single layer of material. An acoustic wave travelling to the right in the pipe suddenly meets the absorbing material at the air/material boundary. The wave will tend to reflect due to the impedance mismatch across the air/material boundary. A well-designed tube filled with absorbing material minimizes reflections at the boundary, while attenuating the transmitted acoustic pressure along the tube axis. This could be achieved, for example, by using a long pipe with material that has impedance at its surface similar to that of air. These types of anechoic terminations are ubiquitous in the automotive industry since mean airflow is absent in the duct when measuring transmission loss. They are less common among HVAC applications where fans generate mean airflow through

the duct. A pipe stuffed with absorption would impede airflow and generate noise.

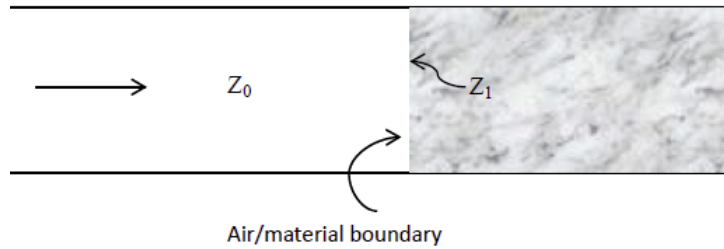


**Figure 3** A pipe anechoic termination stuffed with absorbing material. Sound traveling to the right in air meets the absorbing material at the boundary shown and partially reflects due to the change in impedance

When using a single material, it can be difficult to reduce reflections at the air/material boundary, while at the same time providing sufficient acoustic pressure attenuation axially throughout the material. An important factor in determining the impedance of a material is its flow resistivity.<sup>6</sup> Materials with low packing density generally have a small flow resistivity (shown in Section 0). Using a pipe stuffed with material having small flow resistivity reduces reflections at the air/material boundary because the surface impedance  $Z_1$  approaches the impedance of the air  $Z_0$ . However, a material with small flow resistivity will not provide sufficient acoustic pressure attenuation unless the absorbing section is very long. Choosing a material with larger flow resistivity

---

<sup>6</sup> A measure of airflow resistance per unit thickness of material. Flow resistivity is related to the inverse of permeability (see p. 235 in reference [35])



provides greater attenuation in a short distance along the pipe axis, but reflections at the air/material boundary increase due to the greater impedance mismatch. A problem like this requires use of multiple materials. The optimum solution minimizes reflection at the air/material boundary while at the same time, provides sufficient acoustic pressure attenuation within the absorbing material.

Zheng and Kleinfeld [12] designed an anechoic termination for transmission loss measurements in the form of a long, straight tube stuffed with glass wool. Their anechoic termination was limited to using only one material, so they selected the best variation of glass wool to minimize reflections. The authors selected various combinations of fiber diameter and packing density for the glass wool to minimize reflection at the air/material boundary. In addition, they considered a range of termination lengths as a third variable and found that longer terminations provided greater damping of the sound waves. Numerical simulations used these three variables (fiber diameter, packing density, termination length) to optimize for the best combination of parameters to yield the best termination. Of the seven cases considered, a 2-meter long termination packed with glass wool of density 25 grams/liter and 24- $\mu\text{m}$  fiber diameter gave the most accurate transmission loss measurements up to 3000 Hz. Huallpa, *et al.* [13] also used two different length anechoic terminations, both with a 55 mm diameter tube, to determine which one gives most accurate transmission loss measurements. Their first approach was to increase the occupied volume

with absorption material gradually along the 3-meter termination. The material the authors used was unclear, but they stated it was a common absorption material. Measurements indicated values no greater than 0.5 for the reflection coefficient for frequencies above 60 Hz. Above 170 Hz, the reflection coefficient did not exceed 0.1. In their second design, the authors used a shorter termination filled with foam. This termination proved to be more reflective than the longer termination. Around 170 Hz, the reflection coefficient was approximately 0.8. Consequently, experimentally measured values for the transmission loss of an expansion chamber showed better agreement with theoretical predictions when using the longer termination.

Another approach to construct an anechoic termination is to use multiple materials arranged in layers that have different acoustic properties, as shown in Figure 4. This approach is more effective over the single layer design because impedance  $Z$  at each boundary can be gradually increased from layer to layer, allowing sound to enter the material with minimal reflection and then be attenuated internally within the materials. The use of multiple layers has become more widespread recently since numerical computation can readily optimize for specific configurations. Dunn and Davern [14] were the first to explore the optimization of reflection coefficient using three layers having different acoustic properties and thicknesses lining a flat wall positioned normal to wave propagation direction. Dunn, *et al.* calculated the reflection coefficient of the

multi-layered lining by successively applying the single-layer impedance equation [15]  $N$  times for  $N$  layers. Optimization determined each layer thickness. The authors selected materials *a priori* and used empirical relationships [16] to determine the characteristic impedance and propagation constant for each layer. The contribution of this paper was to eliminate the need for trial and error optimization procedures by establishing an analytical means to calculate reflection coefficient for multi-layered linings.

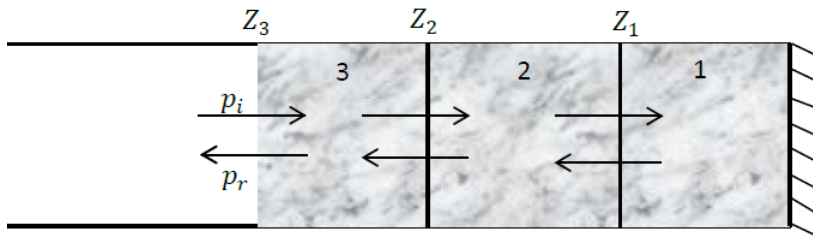


**Figure 4** Three material layers lining a flat wall in an impedance tube. Shown are incident and reflected components at each boundary with impedance  $Z_i$ . The three layers have different material characteristics.

Bracciali and Cascini [17] also used a multi-layered approach but instead performed their optimization at discrete frequencies using material acoustic properties and layer thicknesses as design variables. In contrast to Dunn and Davern, their calculation of reflection coefficient involved a transfer matrix between the first and last layer. The results indicated reflection coefficients of 0.45 at 125 Hz and 0.22 for frequencies higher than 210 Hz. Xu et al. [18] designed a multi-layered anechoic lining with the genetic algorithm toolbox in

MATLAB<sup>®</sup>. Using 16 different materials of fixed thickness, the algorithm constructed an optimum three layer lining by calculating the thicknesses of each layer in multiples of their fixed thicknesses. Although this research was conducted in order to construct an anechoic chamber without using traditional wedges, it could easily be applied to design a long pipe anechoic termination.

In summary, anechoic terminations can be built by inserting one or many different absorbing layers arranged in succession inside a pipe. This type of termination is used most commonly in automotive applications. By using numerical optimization, an anechoic termination can be designed to produce minimal reflection at the air/material boundary while providing sufficient acoustic pressure attenuation along the tube. Zwicker and Kosten's single layer impedance equation [15] can in general be applied to  $N$  layers, thus providing a firm analytical basis for numerical optimization.

## 2.5. Anechoic Terminations using Stepped Cross-Sections

A completely different approach to anechoic termination design than ones described previously is to use a pipe with step increases in cross-sectional area. Olson [19] describes acoustic wave propagation between step increases. As shown in Figure 5, a sudden step increase in area will create a reflected and transmitted wave, the former being out of phase with the incident wave since the area downstream is larger (the phase reversal is apparent from Eq. (3.2.18) for

$S_2 > S_1$ , disregarding the magnitude). The abrupt change in impedance from the smaller pipe to the larger pipe causes an increase in reflection coefficient.

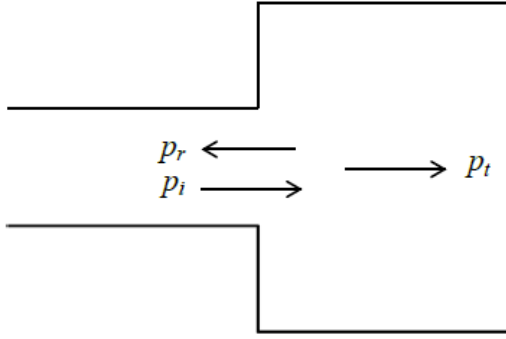


**Figure 5** An acoustic wave incident on the boundary between the two pipes will have reflected and transmitted pressure components

If multiple steps are used, the length of the sections can be adjusted such that the reflected waves at each boundary interact with each other and cancel out. An anechoic termination design motivated by this concept first appears in the literature by Bolton *et al.* [1], shown in Figure 6. Another example is found in the ISO 7235 [20], although the original source of the design is unknown. Bolton derived the equation for reflection coefficient of the six-stepped termination by considering incident and reflected waves at each boundary. Absorbing material lined the inner circumference of each step. For simplicity sake however, the theory did not account for the effect of the material, and an infinitely long tube represented the termination end. At certain frequencies, the measured reflection coefficient did not exceed values given by ISO 5136 in Table 1. The primary

motivation for this new design was to reduce the amount of material needed to construct an anechoic termination. The termination could also adapt to different diameter fans provided the steps were the same size as the fan and were removable.

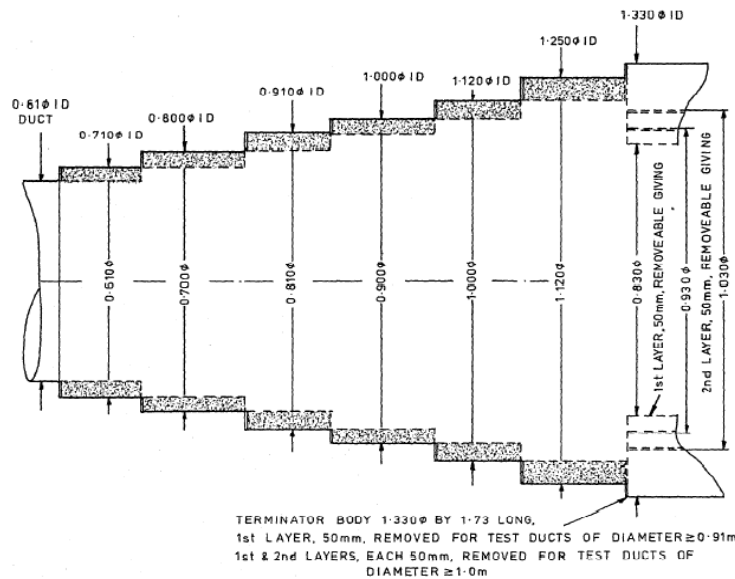


**Figure 6** A six stepped anechoic termination [1]. The incident wave travels to the right towards the terminator body at the far right

## 2.6. Anechoic Terminations using Horns and Cones

Anechoic terminations also use gradual transitions in the shape of horns or cones to transition from a smaller diameter test duct to an absorbing duct of larger diameter as was shown in Figure 1. A travelling sound wave that experiences an abrupt change in duct diameter will reflect at the discontinuity, as Figure 5 shows. This is understood in terms of a change in impedance between the two diameter pipes. Transitioning the two sections with a horn or cone can substantially reduce

reflections (this will be shown in Section 3.2.3). A proper horn flare and length will ensure that there is a gradual change in impedance from test duct to absorbing duct. Thus, the role of a horn in general is to act as an acoustical transformer between two different impedances [19].

The horn type anechoic termination is used more often in HVAC applications where airflow must be controlled. In 1972, Shenoda [9] conducted analytical and experimental research on horn type anechoic terminations. Many designs used exponential and conic transitions terminating into ducts assumed to be infinitely long. Theoretical predictions of reflection coefficient for these terminations were compared to experimental measurements. In the following year, Wollherr [21] studied centrifugal fans and developed an expanding anechoic termination. Neise [22] further developed this termination (see Figure 7). Its unique features included mineral wool lining the expanding sections, and pockets of empty space within the mineral wool. The absorbing material was arranged in the expansion such that a constant diameter cross section was formed for proper airflow.

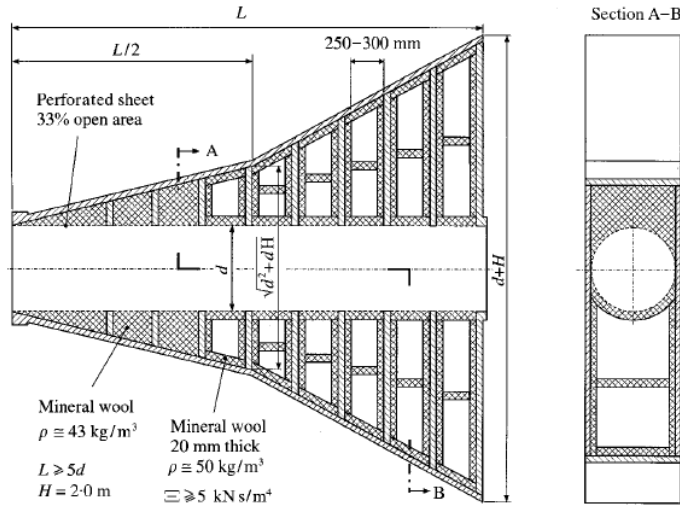


**Figure 7** Horn shaped anechoic termination developed by Wollherr and modified to its present form by Neise [22]

Bolleter et al. [3] made an exponential type termination filled partially with fiberglass to measure in-duct sound power of fans. The ISO 5136 standard [2] presented the details of this design. Experimental measurements determined the degree of reflection, but a theoretical method was absent. Myers [23] experimentally measured reflection coefficients for a variety of terminations that used conic and catenoidal transitions. These terminations were developed for use in a fan test facility at Carrier Corporation. The results showed that catenoidal horns lined with absorbing material near the mouth and connected to an absorbing tube yielded the smallest amount of reflection. This design performed better than a bare catenoid open to the air, and a catenoid open to the air with some absorbing material near the mouth. Overall, the work was experimental and lacked an analytical basis. Bolton *et al.* [1] then attempted to predict the reflection



coefficient of a catenoidal horn using an analytical model for an exponential horn terminating into an infinitely long tube. Although an analytical model for catenoidal horns existed in the literature [24], it appears to have been overlooked by Bolton. Sufficient agreement between theory and experiment led Bolton to conclude that predicting reflection coefficient using horn theory justified its use as a design tool.

To summarize the findings of Section 2.6, anechoic terminations using horns and absorbing pipes are well studied experimentally. Bolton used a simplified analytical method to model a catenoidal horn terminating into an infinitely long pipe. Simplified analytical models for horns proved effective at predicting the reflection coefficient of horn type anechoic terminations.

## 2.7. Anechoic Terminations using Active Cancellation

The category of active cancellation is reviewed briefly since HVAC and automotive industries give little attention to anechoic termination design using these methods. The anechoic terminations discussed so far are the passive type used for applications in these industries. These have the benefit of reduced complexity and cost, since they do not require additional microphones, data acquisition systems, etc. One-dimensional active cancellation in ducts is thoroughly covered in Ch.5 of Nelson and Elliott [25]. A literature review on the topic can also be found in this source. The general idea is to cancel the sound

waves emanating from a primary source at one end of the duct with a secondary sound source placed at the other duct end. The incident wave signal from the primary source is measured with a microphone at the secondary source location where a data acquisition system processes the signal and generates a wave that is out of phase with the incident. The two waves cancel, creating an absorbing termination at the location of the secondary source. However, if both sources continuously generate sound, the sound field would cancel in the section where sound power and transmission loss are measured. This would lead to erroneous measurements. Any anechoic termination using this approach would have to avoid interfering with the desired measurements. Whether or not this is possible is unknown to the author. Perhaps for this reason, little attention is given to active anechoic terminations used in experimental arrangements measuring sound power and transmission loss.

## 2.8. Research Motivation

The effectiveness of predicting the reflection coefficient of horn type anechoic terminations with analytical horn models has been demonstrated previously. However, these methods involved considerable simplifications to model the horn and the absorbing termination. In the 1980's, Bolton [1] used an exponential horn model to predict the reflection coefficient of a catenoidal anechoic termination. Perhaps unknown to Bolton, an analytical model for catenoidal horns had been developed in 1950 by Thiessen [24]. To the best of the

author's knowledge, no work thus far has used Thiessen's model to predict the reflection coefficient of anechoic terminations that use a catenoid. Further, although the effect of lined ducts on the attenuation of sound waves is well known [26], no analytical model has used these findings to account for the effects of the absorbing termination. All analytical models so far have idealized the absorbing termination to act like an infinite duct, without accounting for the properties of the absorbing material. Therefore, the purpose of this research is to account for the shape of the catenoidal horn and the material in the absorbing termination to predict the reflection coefficient of such an anechoic termination. The broader goal is to provide engineers with a means of predicting the effectiveness of this type of anechoic termination design. Such a model can then be used for optimization of the shape of a particular design in order to achieve the lowest reflection coefficient over a wide range of frequencies of interest. Chapter 3 will describe the mathematics of catenoidal horns, along with wave propagation through pipes lined with absorbing material, in order to develop the analytical model.

## CHAPTER 3

### ANALYTICAL MODEL DEVELOPMENT

The steps taken to derive an analytical model used to predict the reflection coefficient of a catenoidal horn terminating into a pipe lined with absorbing material are presented in this chapter. First, a derivation of the reflection coefficient will be given following a definition of acoustic impedance. Then, the acoustic pressure field in the catenoidal horn will be found by solution of Webster's one-dimensional horn equation [27]. This will be used to derive the impedance at the horn throat in terms of the impedance at the horn mouth (i.e. termination inlet). Next, the acoustic pressure field inside the termination will be described so that expressions for the specific acoustic impedance at the termination boundaries can be derived. The effect of the wall absorption is taken into account by imposing Morse's local reacting boundary condition [26]. In order to determine the impedance properties of the absorbing material, an empirical model of the material is used. This leads to the determination of the complex axial wavenumber through the absorbing tube. The impedance at the termination inlet can then be expressed in terms of the impedance at the termination end (for the open or closed end conditions). This chapter concludes with a procedural summary to compute the reflection coefficient of the anechoic termination.

### 3.1. Acoustic Impedance

In Section 2.4, a brief discussion of impedance was presented in order to understand the cause of reflection at discontinuities. A more detailed version is presented [11] in this section. *Acoustic impedance*  $Z$  at a boundary of cross-sectional area  $S$  is defined as

$$Z = \frac{p}{U} , \quad (3.1.1)$$

where  $p$  is the complex acoustic pressure averaged over the surface, and  $U$  is the complex volume velocity through it. The complex volume velocity is related to the particle velocity  $v$  by

$$U = vS . \quad (3.1.2)$$

Equation (3.1.1) can be expressed as

$$Z = \frac{p}{vS} . \quad (3.1.3)$$

Multiplying both sides by  $S$  yields the *specific acoustic impedance*,

$$z = \frac{p}{v} , \quad (3.1.4)$$

where  $z = ZS$ . The specific acoustic impedance is complex in general, where the real part is the *specific acoustic resistance* and the imaginary part is the *specific acoustic reactance*. The resistance term represents energy lost by the system whether by dissipative effects or energy flowing out. If the resistance term is zero, the specific acoustic impedance is purely imaginary, and all energy stays contained within the system (e.g. in the form of standing waves). An example of

this is resonance in a closed pipe (neglecting viscous effects). For a plane wave travelling in a frictionless, infinite medium, Eq. (3.1.4) reduces to a purely real constant,

$$z_0 = \pm \rho c , \quad (3.1.5)$$

where  $\rho$  is the equilibrium density of the medium, and  $c$  is the speed of sound in the medium (air in this case). A positive sign indicates a wave traveling in the +x direction (rightward in this thesis), and a negative sign indicates a wave traveling in the -x direction (leftward). Since both of these quantities are dependent on the medium, Eq. (3.1.5) is called the *characteristic impedance* because it is a unique property of the particular medium.

Equations (3.1.4) and (3.1.5) are used in the derivation of the reflection coefficient of the anechoic termination as follows: consider a hypothetical boundary between two different impedances  $z_0$  and  $z_1$ , shown in Figure 8. Assuming the acoustic pressure varies harmonically with time  $t$ , an incident wave travelling rightward in the +x direction will have reflected and transmitted acoustic pressure components [11] at the boundary  $x = 0$ ,

$$p_i = P_i e^{j(\omega t - k_0 x)} , \quad (3.1.6)$$

$$p_r = P_r e^{j(\omega t + k_0 x)} , \quad (3.1.7)$$

$$p_t = P_t e^{j(\omega t - k_1 x)} , \quad (3.1.8)$$

where  $p_i$ ,  $p_r$ , and  $p_t$  are the incident, reflected, and transmitted acoustic pressures,  $P_i$ ,  $P_r$ , and  $P_t$  are the respective complex acoustic pressure amplitudes,  $\omega$  is the angular frequency,  $k_1$  and  $k_2$  are the wavenumbers in mediums 0 and 1, and  $j = \sqrt{-1}$ . The wavenumber  $k$  is defined as

$$k = \frac{\omega}{c} = \frac{2\pi f}{c} , \quad (3.1.9)$$

where  $f$  is frequency in Hertz.

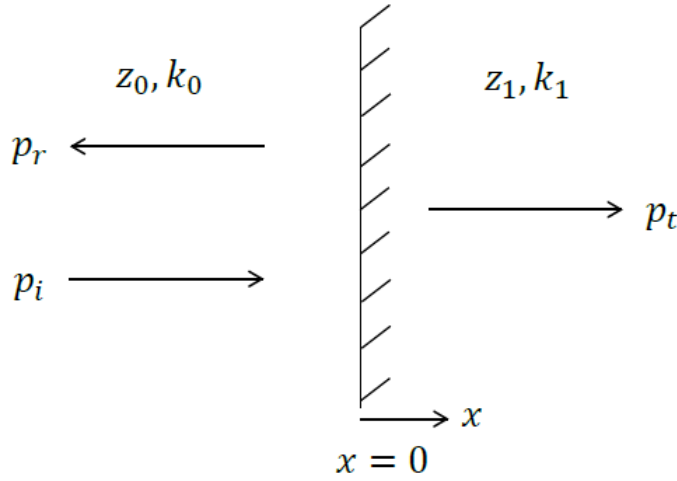


**Figure 8** Incident, reflected, and transmitted acoustic pressures at a boundary

At all times, the acoustic pressure and normal particle velocity must be continuous across the boundary since the medium itself must remain continuous.

That is, at  $x = 0$ ,

$$p_i + p_r = p_t , \quad (3.1.10)$$

$$v_i + v_r = v_t , \quad (3.1.11)$$

Dividing Eq. (3.1.10) by Eq. (3.1.11) gives

$$\frac{p_i + p_r}{v_i + v_r} = \frac{p_t}{v_t} . \quad (3.1.12)$$

With use of Eq. (3.1.4) and the definition of reflection coefficient in Eq. (1.2.1), some algebraic manipulation yields the reflection coefficient at the boundary,

$$\eta = \frac{z_1 - z_0}{z_1 + z_0} , \quad (3.1.13)$$

If a plane wave traveling to the right in medium 0 is assumed, then the specific acoustic impedance is just  $+\rho c$ , the characteristic impedance of Eq. (3.1.5).

Therefore, the magnitude of Eq. (3.1.13) becomes

$$|\eta| = \left| \frac{z_1 - \rho c}{z_1 + \rho c} \right| . \quad (3.1.14)$$

It is apparent that as  $z_1$  approaches the characteristic impedance of the plane wave, the magnitude of the reflection coefficient goes to zero, i.e. the reflected wave by Eq. (3.1.7) vanishes. Thus, for the case of an infinite tube (since there are no reflections), the reflection coefficient would be zero.

The specific acoustic impedance at the horn throat, labeled  $z_1$  in Figure 9, must be determined to calculate the reflection coefficient of the anechoic termination using Eq. (3.1.14). It is assumed that a plane wave travels to the right in the test tube from the sound source with characteristic impedance  $z_0 = \rho c$ . The wave meets the horn throat and encounters specific acoustic impedance  $z_1$ . The impedance at this boundary is a function of the impedance  $z_2$  at the horn



mouth. The specific acoustic impedance  $z_2$  at the horn mouth (or terminator inlet) is a function of the impedance  $z_3$  at the terminator end, and of  $z_w$ , the impedance normal to the surface of the absorbing material. Therefore, the throat impedance  $z_1$  must be expressed as a function of the mouth impedance  $z_2$ , and  $z_2$  expressed as a function of  $z_3$  and  $z_w$ . The expressions for the horn throat impedance and terminator inlet impedance are derived in Sections 3.2.2 and 3.3.6, respectively.

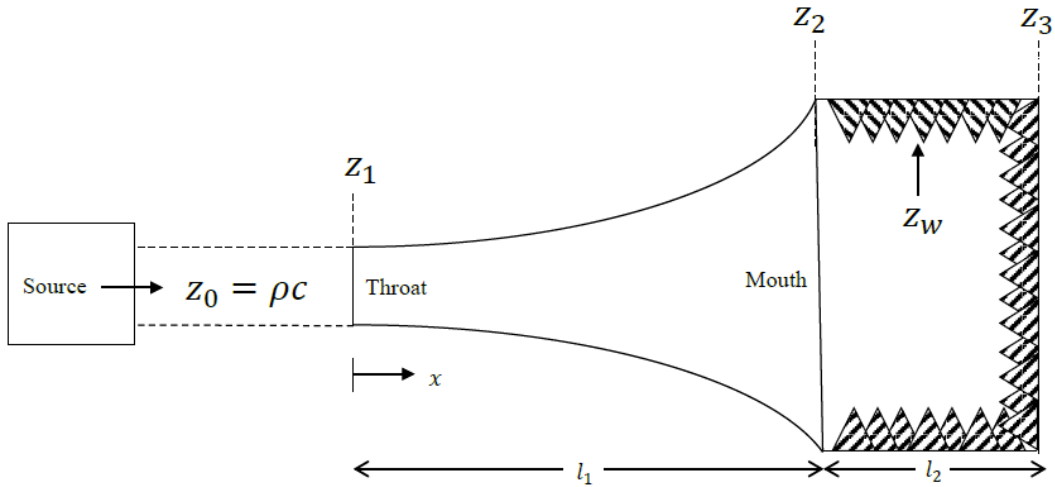


**Figure 9** A schematic of an anechoic termination with specific acoustic impedances shown at each boundary. A plane wave travels to the right in the test tube

### 3.2. The Catenoidal Horn

In the mid 1940's, Salmon studied the impedance characteristics of a family of infinitely long horns [28]. This family of horns was obtained by considering perturbations of the exponential profile. The range of shapes was

bound between a hyperbolic cosine profile and a conical horn, the exact shape depending on the value of the “family parameter.” The impedance characteristics of these horns were presented, and the hyperbolic cosine profile attracted attention for its potential applications in sound reproduction and amplification. The horn contour described by the hyperbolic cosine in Salmon’s paper was later called a catenoid by Morse [29]. This is because a hyperbolic cosine describes a catenary curve<sup>7</sup>, and revolution of a catenary about a central axis produces a catenoidal surface. Following Salmon’s paper, Thiessen [24] studied the impedance characteristics of a *finite* catenoid, and derived the relationship for the impedance at the horn throat as a function of the impedance at the mouth through solution of Webster’s one-dimensional horn equation [27]. In the next sections, Webster’s horn equation is discussed and the steps in Thiessen’s derivation for the impedance characteristics of a finite catenoid are shown.

### 3.2.1. Webster’s Horn Equation

A time harmonic wave travelling along axial direction  $x$  through a volume with cross-sectional area  $S = S(x)$  is described approximately<sup>8</sup> by the 2<sup>nd</sup> order, linear, homogenous differential equation [27]

$$\frac{d^2 p}{dx^2} + \frac{d}{dx}(\ln S) \frac{dp}{dx} + k^2 p = 0 \quad , \quad (3.2.1)$$

---

<sup>7</sup> A chain hanging between two supports follows a catenary curve

<sup>8</sup> As long as the diameter at any cross section in the horn is small compared to the acoustical wavelength, then the wave is approximately one dimensional [30]

where  $p = p(x)$  is the acoustic pressure and  $k$  is the angular wavenumber. This is Webster's horn equation. The solution to Equation (3.2.1) is a one-parameter wave, which in this case, is a plane wave whose properties depend only on the parameter  $x$ . A plane wave will have acoustic properties with constant amplitude and phase on plane surfaces perpendicular to the direction of wave propagation. Although this condition is not met inside a horn (the surfaces of constant phase are curved), it is approximately true for a horn whose contour does not flare out too rapidly [30]. Specifically, the rate of change of  $\sqrt{S}$  with  $x$  must be much smaller than one (i.e.  $d\sqrt{S}/dx \ll 1$ ).

Some authors [30] choose to express Eq. (3.2.1) in terms of the velocity potential  $\varphi = \varphi(x, t)$ , a scalar function associated with irrotational flow,

$$\frac{\partial^2 \varphi}{\partial t^2} - c^2 \frac{\partial(\ln S)}{\partial x} \frac{\partial \varphi}{\partial x} - c^2 \frac{\partial^2 \varphi}{\partial x^2} = 0 \quad . \quad (3.2.2)$$

The acoustic pressure and particle velocity along the x-axis are related to the velocity potential by [11]

$$p = -\rho \frac{\partial \varphi}{\partial t} \quad , \quad (3.2.3)$$

$$v = \frac{\partial \varphi}{\partial x} \quad , \quad (3.2.4)$$

Notice that for constant cross-sectional area, Eq. (3.2.2) reduces to the well-known one-dimensional wave equation.

### 3.2.2. Impedance at the Horn Mouth

The solution to Eq. (3.2.2) is presented for a catenoidal horn of length  $l_1$  subject to boundary conditions (refer to Figure 9)

$$\left. \frac{p}{v} \right|_{x=0} = z_1 , \quad (3.2.5)$$

$$\left. \frac{p}{v} \right|_{x=l_1} = z_2 , \quad (3.2.6)$$

The cross sectional area as function of axial distance  $x$  for a catenoid is

$$S(x) = S_0 \cosh^2(mx) , \quad (3.2.7)$$

where  $S_0 \equiv S(x = 0)$  is the area at the horn throat, and  $m$  is a flare constant determining the rate of flare of the horn contour. A flare constant of zero describes a cylinder. Inserting Eq. (3.2.7) into (3.2.2) yields

$$\frac{\partial^2 \varphi}{\partial t^2} - 2mc^2 \tanh(mx) \frac{\partial \varphi}{\partial x} - c^2 \frac{\partial^2 \varphi}{\partial x^2} = 0 . \quad (3.2.8)$$

The solution of Eq. (3.2.8) is given by Thiessen [24],

$$\varphi = \frac{e^{j\omega t}}{\cosh(mx)} [A \cos(bx) + B \sin(bx)] \quad (3.2.9)$$

where  $A$  and  $B$  are complex constants and  $b$  is defined as

$$b = \sqrt{k^2 - m^2} . \quad (3.2.10)$$

Equations (3.2.3) and (3.2.4) are used to calculate the acoustic pressure and velocity along the  $x$ -axis, yielding

$$p = \frac{-j\omega\rho}{\cosh(mx)} [A \cos(bx) + B \sin(bx)] e^{j\omega t} , \quad (3.2.11)$$

$$v = \frac{e^{j\omega t}}{\cosh(mx)} [-Ab \sin(bx) + Bb \cos(bx) + \dots - m \tanh(mx) (A \cos(bx) + B \sin(bx))]. \quad (3.2.12)$$

Using the two above expressions in Eq. (3.1.4), the specific acoustic impedance of the catenoidal horn is determined,

$$z(x) = \rho c j k \left[ \frac{A \cos(bx) + B \sin(bx)}{Ab \sin(bx) - Bb \cos(bx) + m \tanh(mx) (A \cos(bx) + B \sin(bx))} \right]. \quad (3.2.13)$$

More compactly [24],

$$\frac{1}{z(x)} = \frac{1}{\rho c} \left[ \frac{m \tanh(mx)}{jk} + \frac{b}{jk} \frac{A \sin(bx) - B \cos(bx)}{A \cos(bx) + B \sin(bx)} \right]. \quad (3.2.14)$$

The boundary conditions defined in Eqns. (3.2.5) and (3.2.6) are applied to Eq. (3.2.14) yielding,

$$\frac{1}{z_1} = \frac{1}{\rho c} \left[ -\frac{B}{A} \frac{b}{jk} \right], \quad (3.2.15)$$

$$\frac{1}{z_2} = \frac{1}{\rho c} \left[ \frac{m \tanh(ml_1)}{jk} + \frac{b}{jk} \frac{A \sin(bl_1) - B \cos(bl_1)}{A \cos(bl_1) + B \sin(bl_1)} \right]. \quad (3.2.16)$$

The complex constants can be eliminated, and after some rearranging, the specific acoustic impedance  $z_1$  of the throat is

$$z_1 = \rho c \frac{jk}{b} \left[ \frac{jk \frac{\rho c}{z_2} \tan(bl_1) - m \tanh(ml_1) \tan(bl_1) + b}{jk \frac{\rho c}{z_2} - m \tanh(ml_1) - b \tan(bl_1)} \right]. \quad (3.2.17)$$

The specific acoustic impedance at the horn throat depends on the specific acoustic impedance at the horn mouth, the geometry of the catenoidal horn, and on frequency (since  $b$  is frequency dependent). Also, note that the complex

constants,  $A$  and  $B$ , did not need to be explicitly determined since the relationship between the boundary conditions (i.e.  $z_1$  and  $z_2$ ) was desired.

To illustrate Eq. (3.2.17), assume a 1 in. throat diameter, 20 in. mouth diameter, and 64 in. horn length. The flare constant  $m$  for this horn is calculated from Eq. (3.2.7) to be  $0.0577 \text{ in}^{-1}$ . For simplicity's sake, assume that an infinitely long tube is connected to the mouth of the horn so that  $z_2 = \rho c$ . A plot of the real and imaginary parts of the specific acoustic impedance ratio  $\frac{z_1}{\rho c}$  (a dimensionless quantity) versus frequency is shown in Figure 10. The resonances of the horn are identified at frequencies where the specific acoustic reactance ratio (imaginary part) goes to zero and the specific acoustic resistance ratio (real part) reaches a local minimum [11]. Anti-resonances, regions where acoustic energy is inefficiently transmitted through the horn, are indicated where the reactance ratio (imaginary part) goes to zero and the resistance ratio (real part) peaks. The horn exhibits a strong anti-resonance around 150 Hz (the first peak) and the first resonance occurs at 171 Hz. A plot of the magnitude of the specific acoustic impedance ratio in Figure 11 also indicates anti-resonances where the plot peaks and resonances where the plot reaches a local minimum. As frequency increases, the impedance ratio approaches the real value of one, since the reactance ratio (imaginary part) approaches zero and the resistance ratio (real part) approaches

one. This indicates high frequencies travel efficiently through the horn into the infinitely long pipe with minimal reflection.

The assumption that the termination is infinitely long is an idealization and mathematically convenient since the specific acoustic impedance at the horn mouth is  $z_2 = \rho c$ . In Section 3.3, an expression for  $z_2$  is derived that accounts for the termination length, wall absorption and boundary condition at the terminator end. Discussed in the next section is the motivation for using a horn in an anechoic termination, and in particular, a catenoidal horn.

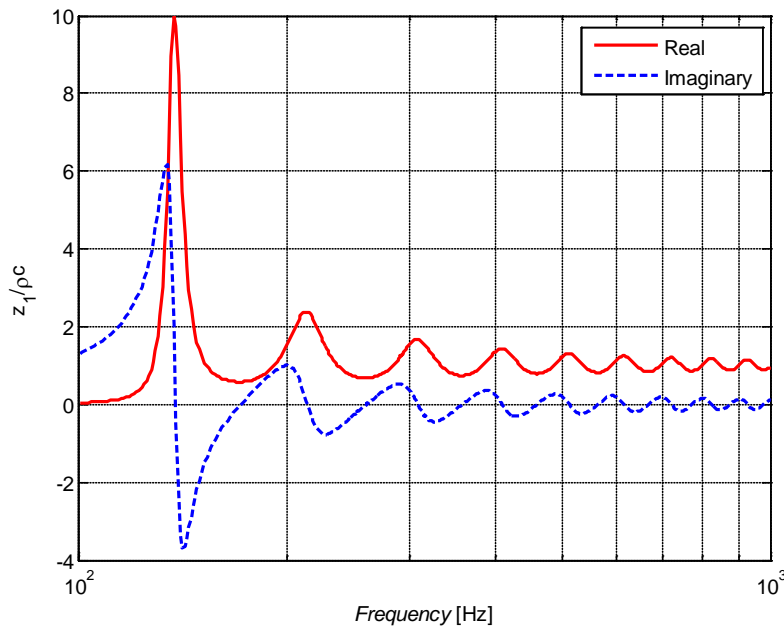


**Figure 10** Specific acoustic impedance ratio for a catenoidal horn of length 64 in. with throat and mouth diameters of 1 in. and 20 in. The horn terminates into an infinite tube

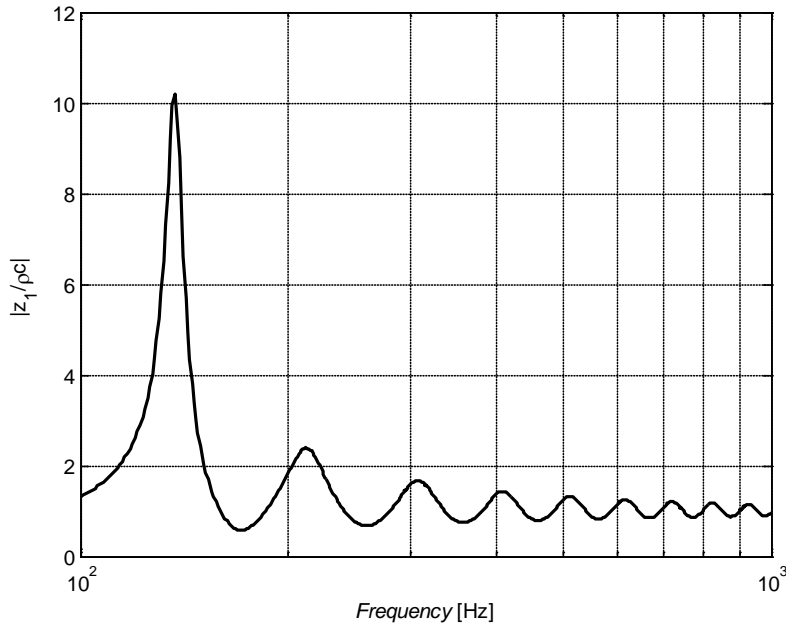


**Figure 11** Magnitude of the specific acoustic impedance ratio for the example horn

### 3.2.3. Motivation for Using a Catenoid

It is well known that open pipes radiating sound into the environment do so very inefficiently, especially when the opening is small compared to the acoustic wavelength (see [11], p. 414). A significant amount of sound energy is simply reflected back into the pipe as the sound wave meets the open end. Attaching a horn to the end of this pipe greatly increases the amount of energy radiated into the environment, thereby reducing reflections. Historically, this technique was used before electronic amplifiers were available to amplify sound generated by phonographs. In a similar manner, a horn is used in an anechoic termination to transmit sound efficiently from a small diameter test tube into the



environment where the wave will be absorbed (the environment in this case being an absorbing tube with a diameter equal to the horn mouth).

To illustrate the effectiveness of a using a horn to transition from two different diameter tubes, a comparison of reflection coefficient is made for two arrangements with and without a horn transition, as shown in Figure 12. Recall that in Section 2.5, it was stated that an abrupt change in diameter between two tubes causes reflection at the discontinuity, as Figure 5 showed. If the left tube has area  $S_1$  and the right tube area  $S_2$ , then the magnitude of the reflection coefficient when the pipes are connected (without a horn) is [19]

$$|\eta| = \left| \frac{S_1 - S_2}{S_1 + S_2} \right| , \quad (3.2.18)$$

where the reflection coefficient is independent of frequency because the pipes are assumed infinitely long. The reflection coefficient for the arrangement with the horn is found by insertion of Eq. (3.2.17) into (3.1.14), again assuming the horn terminates into an infinitely long pipe. A comparison of the reflection coefficient magnitude for the two arrangements shown in Figure 12 is shown in Figure 13. The area of the first tube,  $S_1$ , is equal to the throat area of the example horn in Section 3.2.2. The area of the second tube,  $S_2$ , is equal to the mouth area. For the two pipes connected to each other without a horn, 99.5% of the incident acoustic pressure at any frequency reflects back into the first pipe. Transitioning the two pipes with a 64-inch long catenoid reduces the reflections over a broad frequency

range, with the largest reduction at high frequencies. This example shows that a horn should be used to transition from the test duct to an absorbing duct of larger diameter when designing an anechoic termination.

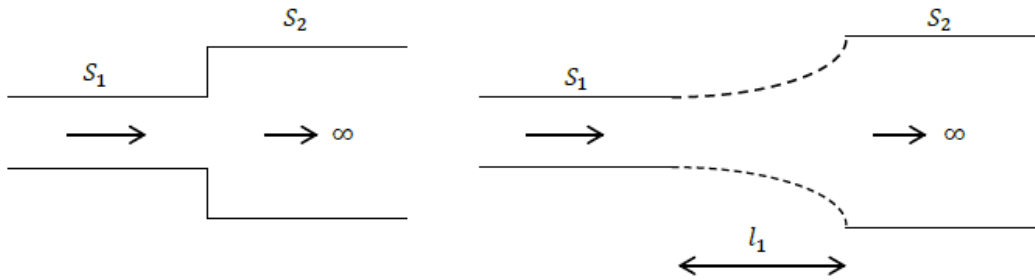


**Figure 12** On the left, two pipes of different area are connected to each other. On the right, a horn is used to transition the same two pipes. The wave travels from left to right

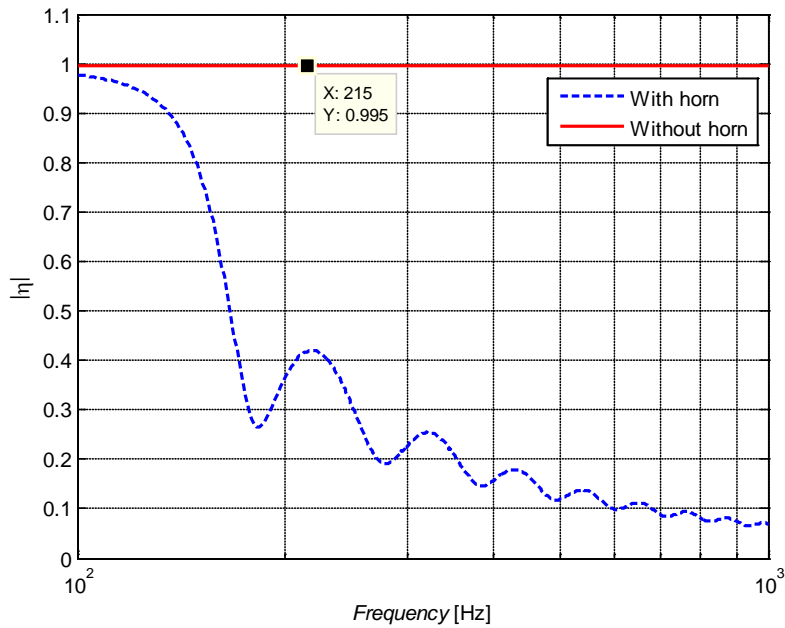


**Figure 13** Comparison of reflection coefficient between two pipes of different diameters with a horn transition and without

As an aside, if there existed an infinite amount of space to work with, an infinitely long straight tube would absorb every frequency without reflection since the acoustic wave would never meet a discontinuity in geometry. This would be a “perfect” anechoic termination. However, since space is limited in many practical cases, the horn design represents a practical solution to minimize reflections when given a finite amount of space.

Although any gradual transition between different diameter pipes would likely reduce reflections, the catenoidal horn gives the best performance. Section 2.6 described the widespread use of catenoidal horns by engineers to construct anechoic terminations. The focus on the catenoid in this thesis is motivated by the theoretical findings of Morse [29]. Morse demonstrated that for the same overall dimensions, infinitely long catenoidal horns have superior transmission characteristics over infinitely long exponential and conical horns. The transmission coefficient is defined as the ratio of power radiated from the horn to a diaphragm radiating into an infinite tube<sup>9</sup>. The diaphragm is equal in radius to the horn throat and moves at the same velocity as a diaphragm positioned at the horn throat. The transmission characteristics for an infinitely long catenoid are excellent above its cutoff frequency (no wave motion occurs below the cutoff, although this is an approximation due to the approximate nature of Eq. (3.2.1)).

---

<sup>9</sup> The transmission coefficient defined here is not an efficiency since it is a comparison to a standard case (a diaphragm radiating into an infinite tube), not an ideal case. Therefore, the coefficient can exceed one.

The exponential horn is the next best choice and both are superior to the conical horn, which exhibits relatively poor transmission characteristics. A comparison between catenoidal and exponential profiles shows that the catenoid transmits energy more efficiently at low frequencies, while at high frequencies the transmissions are indistinguishable. This makes a catenoid favorable since it will be demonstrated that low frequencies have the highest reflection coefficients. The catenoid also differs in shape near the throat from the exponential horn. A catenoid has zero slope at the throat and can connect to a test tube smoothly without presenting a slope discontinuity at the connection point. However, both exponential and conical horns have non-zero slope at their throats, creating reflections due to the sudden change in area. The subsequent focus on the catenoid in this thesis is justified by the reasoning presented.

### 3.3. The Absorbing Termination

The goal of this section is to derive a relationship for the specific acoustic impedance at the horn mouth  $z_2$ , in terms of the specific acoustic impedances of the absorbing wall and the termination end. This relationship will ultimately be used in Eq. (3.2.17) to describe the impedance presented to the test tube by the entire anechoic termination. This derivation will be presented in steps. First, the acoustic pressure field inside a cylinder will be presented for use in boundary

conditions <sup>10</sup>. Next, some simplifying assumptions will be gathered by considering the boundary condition for a rigid-wall cylinder. Then, absorption properties will be accounted for with a modified boundary condition involving the impedance at the lining surface. In Section 3.3.4, an empirical method for determining the specific acoustic impedance properties of the absorption is given. Finally, the expression for  $z_2$  is derived in Section 3.3.6.

### 3.3.1. Acoustic Pressure Field in a Cylinder

The acoustic wave equation is given by [11]

$$\nabla^2 p = \frac{1}{c^2} \frac{\partial^2 p}{\partial t^2} , \quad (3.3.1)$$

and by separation of variables <sup>11</sup>, its time-harmonic solution in cylindrical coordinates yields the acoustic pressure field of normal modes inside a cylinder, [31]

$$p(r, \theta, x, t) = J_q(k_r r) e^{jq\theta} [Ae^{-jk_x x} + Be^{jk_x x}] e^{j\omega t} . \quad (3.3.2)$$

The radial and axial wavenumbers are related by

$$k^2 = \left(\frac{\omega}{c}\right)^2 = k_r^2 + k_x^2 . \quad (3.3.3)$$

Acoustic pressure dependent on radial direction  $r$  is described by  $J_q(k_r r)$ , Bessel's function of the first kind of integer order  $q$ . The pressure variation

---

<sup>10</sup> Horns are commonly designed with a circular cross-section meant to fit the cylindrical impedance tube at its throat, and the cylinder at its mouth. Hence, only circular cross-sections are treated here.

<sup>11</sup> See Appendix B for a complete derivation of Eq. (3.3.2)

around the azimuthal angle  $\theta$  is described by the term  $e^{jq\theta}$ . The term in brackets of Eq. (3.3.2) represents a wave travelling left and right along the axis  $x$ .

### 3.3.2. Rigid Wall Boundary Condition

First, consider the case where the outer walls are rigid. Although this is not the actual case (the walls have absorption), it will lead to two important conclusions. If the outer walls of the cylinder are rigid, then Eq. (3.3.2) must satisfy

$$\left. \frac{\partial p}{\partial r} \right|_{r=a} = 0 , \quad (3.3.4)$$

since the particle velocity is zero at the cylinder radius  $a$ . This implies

$$J'_q(k_r a) = 0 , \quad (3.3.5)$$

where the prime denotes the derivative with respect to  $r$ . The solutions to Eq. (3.3.5) are the  $n^{\text{th}}$  roots of  $J'_q(k_r a)$  so that  $n = 1$  represents the first root,  $n = 2$  represents the second root, etc. As an example, for  $(q, n) = (0, 1)$ , the first root of  $J'_0$  occurs at  $k_r a = 0$ ; for  $(q, n) = (0, 2)$ , the second root of  $J'_0$  occurs at  $k_r a = 3.83$ ; for  $(q, n) = (1, 1)$ , the first root of  $J'_1$  occurs at  $k_r a = 1.84$ ; and for  $(q, n) = (1, 2)$ , the second root of  $J'_1$  occurs at  $k_r a = 5.33$ . A particular mode shape corresponds to each combination of  $(q, n)$ . Some of these shapes are shown in Figure 14. In this figure,  $q$  is the number of radial nodal lines (places with zero acoustic pressure), and  $n$  is the number of nodal circles. The signs indicate vibration out of phase with each other.

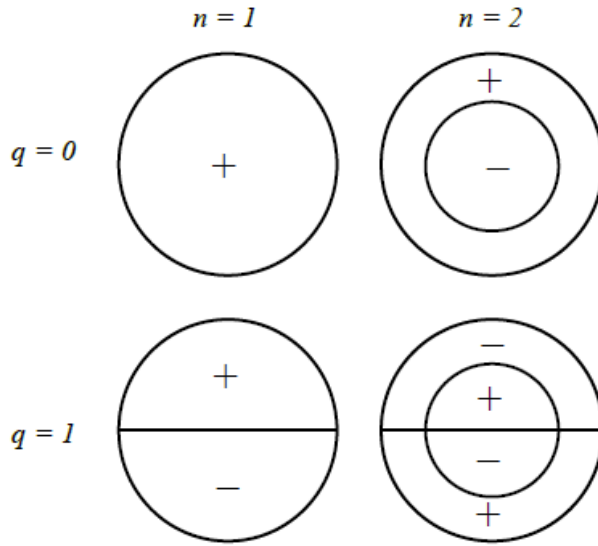


**Figure 14** Normal mode shapes at a cross section of the cylindrical cavity

The reason for considering the rigid-wall case is two-fold:

1. For simplicity sake, only the  $(q, n) = (0, 1)$  plane mode will be considered when applying Morse's boundary condition at the absorbing walls, and
2. The range of frequencies for which plane waves occur in the duct can now be determined.

The first point simplifies the analysis since higher order modes are neglected. Therefore, the acoustic pressure is described completely by the  $(q, n) = (0, 1)$  plane mode of Eq. (3.3.2). This assumption is consistent with Morse [26] and is reasonable if very high frequencies are not of interest. It is also mathematically necessary so that the impedance can be defined uniformly over a plane in the

horn. The second point is that the plane wave region, i.e.  $0 < ka < 1.84$  gives the frequency range for a duct of radius  $a$  over which this assumption is valid,

$$0 < f < \frac{1.84c}{2\pi a} . \quad (3.3.6)$$

Focusing the analysis inside the range defined by Eq. (3.3.6) allows higher modes to be neglected since those modes will not form in this frequency range.

Notice that if only plane waves are considered and absorption is not accounted for,  $k_r = 0$  and  $k_x = k$  since the first root of  $J'_0(k_r a)$  is zero. Then Eq. (3.3.2) reduces to the solution of the one-dimensional wave equation,

$$p(x, t) = [Ae^{-jkx} + Be^{jkx}]e^{j\omega t} . \quad (3.3.7)$$

Equation (3.3.7) shows that acoustic pressure has no radial dependence since  $J_0(k_r r) = J_0(0) = 1$  for all  $r$  in Eq. (3.3.2). However, the presence of absorption in the tube modifies these findings. In the next section, it will be shown that adding an absorption lining to the outer termination walls yields acoustic pressure dependence on the radial direction, even in the frequency range defined by Eq. (3.3.6). The presence of the absorption creates complex radial and axial wavenumbers in the “plane wave” region.



### 3.3.3. Absorbing Wall Boundary Condition

For a termination that contains absorption lining the inner circumference, it is assumed here that the material is “local-reacting.”<sup>12</sup> Morse’s local-reacting assumption [26] is a good approximation for densely packed materials and low frequencies.<sup>13</sup> The boundary condition at the absorbing surface located at  $r_0$  (see Figure 15) is finite such that [31]

$$\left. \frac{p}{v_r} \right|_{r=r_0} = z_w , \quad (3.3.8)$$

where  $z_w$  is the specific acoustic impedance normal to the wall surface and  $v_r$  is the particle velocity normal to the surface (acting in the radial direction).

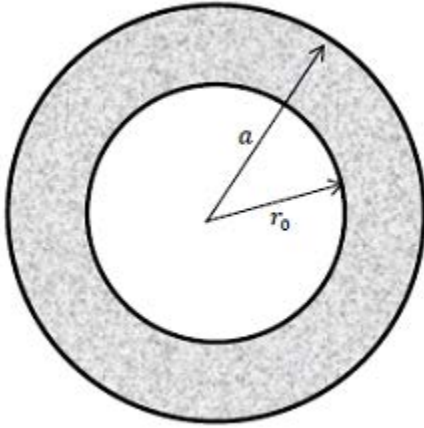


**Figure 15** Cross-section of the absorbing termination with absorbing material of thickness  $a - r_0$  around the wall

---

<sup>12</sup> i.e. particle velocity at the lining surface depends only on the local acoustic pressure and acoustic impedance. Further, axial wave propagation through the material is neglected.

<sup>13</sup> For other materials, the local reacting assumption may lead to erroneous predictions. See reference [40] for a comparison between the local-reacting and “bulk-reacting” approach, which accounts for propagation through the lining.

The radial velocity is calculated by assuming a time-harmonic dependence in Euler's linear equation [11],

$$v_r = -\frac{1}{j\omega\rho} \frac{\partial p}{\partial r} . \quad (3.3.9)$$

The pressure in the absorbing duct, assuming axisymmetric modes (i.e.  $m = 0$ ), must be of the form

$$p(r, x, t) = J_0(k_r r) [Ae^{-jk_x x} + Be^{jk_x x}]e^{j\omega t} , \quad (3.3.10)$$

since the finite impedance at the absorbing wall implies  $\frac{\partial p}{\partial r}$  is non-zero. This gives rise to the acoustic pressure having radial dependence. Using Eqns. (3.3.9) and (3.3.10), Eq. (3.3.8) becomes the characteristic equation [31]

$$\frac{(k_r r_0)J_1(k_r r_0)}{J_0(k_r r_0)} = jkr_0 \frac{\rho c}{z_w} , \quad (3.3.11)$$

where the relationship  $J'_0(k_r r_0) = -J_1(k_r r_0)$  was used. The condition in Eq. (3.3.11) is a transcendental function whose roots are discrete values of  $k_r r_0$  that satisfy the equation for each frequency dependent  $z_w$ . It applies only to modes for which  $m = 0$ . Since the specific acoustic impedance  $z_w$  at the wall is complex, the roots will also be complex. Therefore, both radial and axial wavenumbers are complex quantities. This is to be expected since the imaginary part of the complex axial wavenumber is the attenuation constant of the duct.

Determining the complex roots of Eq. (3.3.11) is not trivial. This was first treated by Molloy *et al.* [32] with nomograms. Using this method in the current

analysis is impractical since the nomogram would have to be used for every single frequency corresponding to its unique  $z_w$ . Furthermore, since  $z_w$  is dependent on the absorption material properties (discussed in the next section), the procedure would have to be repeated if a different material was used. A practical approach to obtaining the roots over a particular frequency range is to implement an approximate formula<sup>14</sup>, since it is readily programmable into a computer. According to Mechel [33], the roots of Eq. (3.3.11) are approximately

$$(k_r r_0)^2 \approx \frac{96 + 36jQ \pm \sqrt{9216 + 2304jQ - 912Q^2}}{12 + jQ} , \quad (3.3.12)$$

where

$$Q \equiv kr_0 \frac{\rho c}{z_w} . \quad (3.3.13)$$

The complex radial wavenumber  $k_r$  is found by dividing the value of  $k_r r_0$  by  $r_0$ . Equation (3.3.12) gives two complex roots for  $k_r r_0$  due to the two signs in front of the radical. Next, each of these  $k_r$  are inserted into

$$k_x = \sqrt{k^2 - k_r^2} , \quad (3.3.14)$$

---

<sup>14</sup> Alternatively, the roots could be found with a numerical routine. Using the “fsolve” command in MATLAB<sup>®</sup> to call the function defined by Eq. (3.3.11), the roots can be numerically calculated for each impedance. The results show that Eq. (3.3.12) is an excellent root approximation over the frequency range of interest (100 – 1000 Hz) in this thesis, and thus justifies its use.

yielding two  $k_x$  values. The axial wavenumber  $k_x$  of interest in Eq. (3.3.14) corresponds to the one with the smallest absolute value of the imaginary part (i.e. the least attenuation).

#### 3.3.4. Normal Specific Acoustic Impedance, $z_w$

The problem now is to determine the specific acoustic impedance  $z_w$  normal to the lining. This is accomplished experimentally with an impedance tube using a sample of the material [34]. However, if measuring the impedance is not possible, the impedance characteristics can be estimated using empirical methods. The latter method is described below because it is conveniently applied to a wide range of materials. In this thesis, an empirical model for polyester fiber is given since this material was used in the anechoic termination prototype. The experimental verification of the empirical estimates can be found in Appendix E.

First, assume the walls of the cylinder are very rigid and that there is no air gap between the wall and the absorbing material. Then the specific acoustic impedance normal to the layer surface is given by [35]

$$z_w = -jz_c \cot(k_w d) \quad , \quad (3.3.15)$$

where  $z_c$  is the characteristic impedance of the absorbing material,  $k_w$  is the propagation constant of the absorbing material, and  $d$  is the layer thickness. Equation (3.3.15) takes into account incident and reflected waves within the absorbing material. If the material is very thick,  $\cot k_w d \rightarrow j$ , and the impedance

normal to the surface is the same as the characteristic impedance. This is expected because a thick sample behaves as an “infinite” medium where reflections are absent.

The material characteristic impedance and propagation constant are determined by empirical methods. Delany and Bazley [16] were the first to do this for fibrous materials using regression analysis conducted on experimentally measured data. Their empirical equations expressed as a function of a non-dimensional parameter  $E$  are of the form [35]

$$\frac{Z_c}{\rho c} = (1 + c_1 E^{c_2}) - j c_3 E^{c_4} , \quad (3.3.16)$$

$$\frac{k_w}{k} = (1 + c_5 E^{c_6}) - j c_7 E^{c_8} , \quad (3.3.17)$$

where the regression constants  $c_i$  are dependent on the material (e.g. rock wool, glass wool, polyester fiber, etc.). The non-dimensional parameter  $E$  is defined as

$$E = \frac{R}{\rho f} . \quad (3.3.18)$$

The flow resistivity  $R$  is also determined by empirical methods and has the form

$$R = \frac{c_9 \rho_A^{c_{10}}}{D^2} , \quad (3.3.19)$$

where  $D$  is the mean fiber diameter of the material, and  $\rho_A$  is the bulk density of the material (found by dividing the mass of a sample by its total volume). Thus, the bulk density determines the flow resistivity of a particular class of materials

(assuming a uniform fiber diameter across each sample). When the flow resistivity is known, the material properties are estimated using Eqns. (3.3.16) and (3.3.17). Then, the material thickness is used in Eq. (3.3.15) to determine the specific acoustic impedance  $z_w$  normal to the material surface. In short, only two parameters, the bulk density  $\rho_A$  and material thickness  $d$ , must be known *a priori* in order to estimate  $z_w$ .

For polyester fiber, the characteristic impedance, propagation constant and flow resistivity is estimated using Garai and Pompoli's [36] empirical relationships,

$$\frac{z_c}{\rho c} = (1 + 0.078E^{0.623}) - j0.074E^{0.660} , \quad (3.3.20)$$

$$\frac{k_w}{k} = (1 + 0.121E^{0.530}) - j0.159E^{0.571} , \quad (3.3.21)$$

$$R = 25.989\rho_A^{1.404} , \quad (3.3.22)$$

where  $E$  is defined as in Eq. (3.3.18). The polyester fiber used in the anechoic termination prototype is manufactured by Technicon Acoustics [37] and has a bulk density and thickness of  $24 \text{ kg/m}^3$  and 44 mm (1.75 inches). See Appendix C for a complete listing of material specifications. Using these values, a plot of the real and imaginary parts of the characteristic impedance ratio (Eq. (3.3.20)) is shown in Figure 16. A plot of the real and imaginary parts of the propagation

constant  $k_w$  is shown in Figure 17. Finally, the specific acoustic impedance normal to the absorbing surface is plotted in Figure 18.

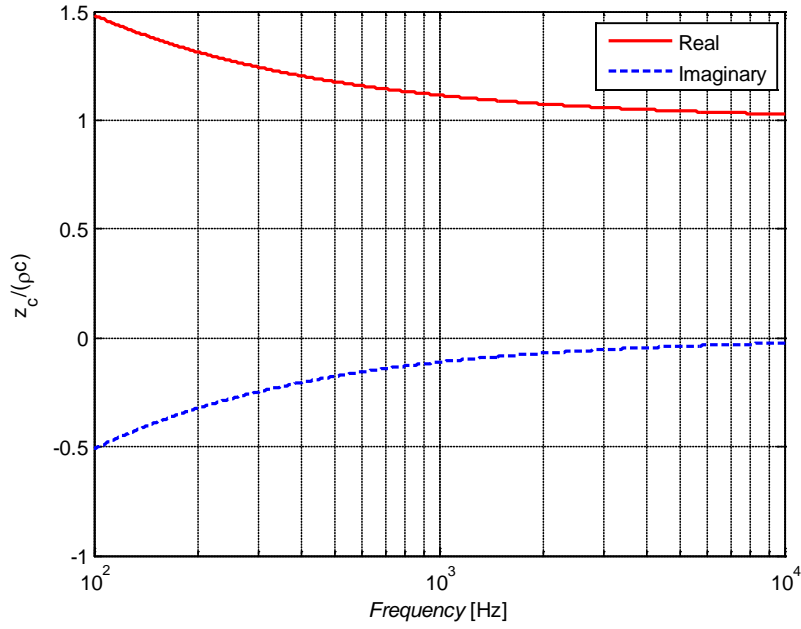


**Figure 16** Characteristic impedance ratio of the polyester fiber

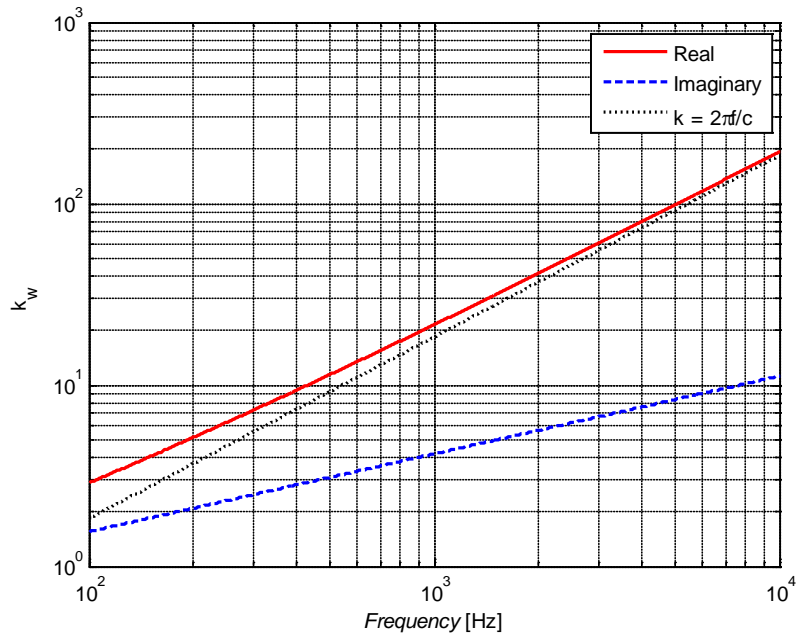


**Figure 17** Propagation constant of the polyester fiber (absolute value of imaginary part) plotted with the wavenumber in air

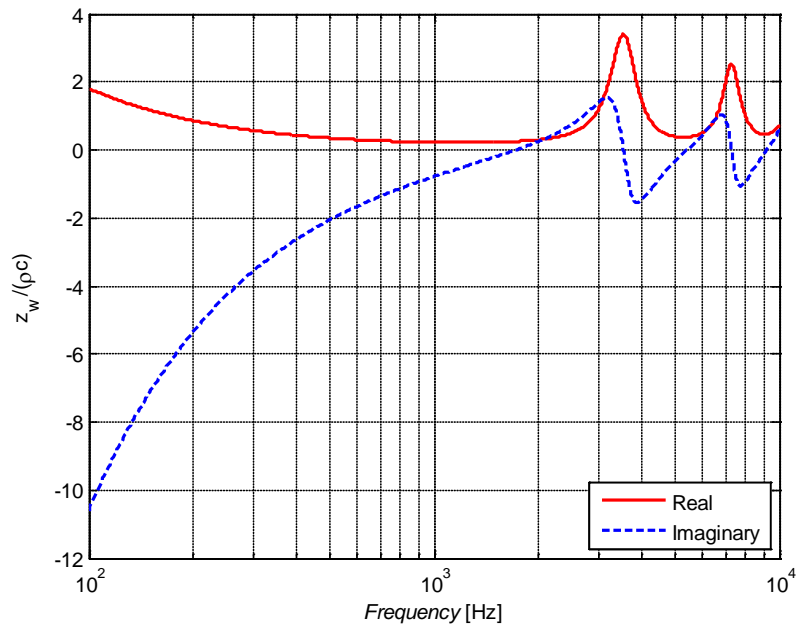


**Figure 18** Specific acoustic impedance normal to the polyester fiber surface (normalized with the characteristic impedance of air)



As shown in Figure 16, the characteristic impedance of the material at high frequencies approaches the real value of the characteristic impedance of the air (since the imaginary part approaches zero). For thick materials, this implies that high frequencies are absorbed with minimal reflection. The imaginary part of the propagation constant in Figure 17 (representing the attenuation constant within the material, plotted as the absolute value of the imaginary part) increases, indicating that high frequencies have greater acoustic pressure attenuation within the absorbing material than low frequencies. In Figure 18 the real and imaginary parts of the specific acoustic impedance of the polyester fiber (normalized with  $\rho c$ ) is plotted by using Eq. (3.3.15). The peaks and valleys in the real part at high frequencies indicate anti-resonances and resonances within the material sample.

### 3.3.5. Complex Axial Wavenumber, $k_x$

The complex radial wavenumber  $k_r$  of the absorbing termination is determined by using the specific acoustic impedance normal to the lining  $z_w$  in Eq. (3.3.12). Then, the complex radial wavenumber is inserted into Eq. (3.3.14) to calculate the complex axial wavenumber,  $k_x$ .

A plot of the real and imaginary parts of  $k_x$  is shown in Figure 19. Also shown is the wavenumber in air. The imaginary part of the axial wavenumber is the attenuation constant of the absorbing duct. The behavior of the attenuation

constant in Figure 19 is consistent with round silencers, where the attenuation of acoustic pressure increases with frequency (up to the formation of non-planar modes, where the attenuation begins to decrease) [35]. In the special case for termination walls with no absorption, the real part of the axial wavenumber and the wavenumber in air are identical since the attenuation constant is zero. This was discussed at the end of Section 3.3.2.

Figure 19 assumes the radius to the absorbing surface is 108 mm (4.25 inches) since for the prototype, the absorbing duct radius is 6 inches and the material thickness is 1.75 inches. Therefore, from Eq. (3.3.6), the first cross mode inside the duct should form around 1000 Hz (this is an approximation for lined ducts since the equation assumes rigid walls). After 1000 Hz, the estimated wavenumber is no longer valid since Eq. (3.3.11) is valid only for planar modes.

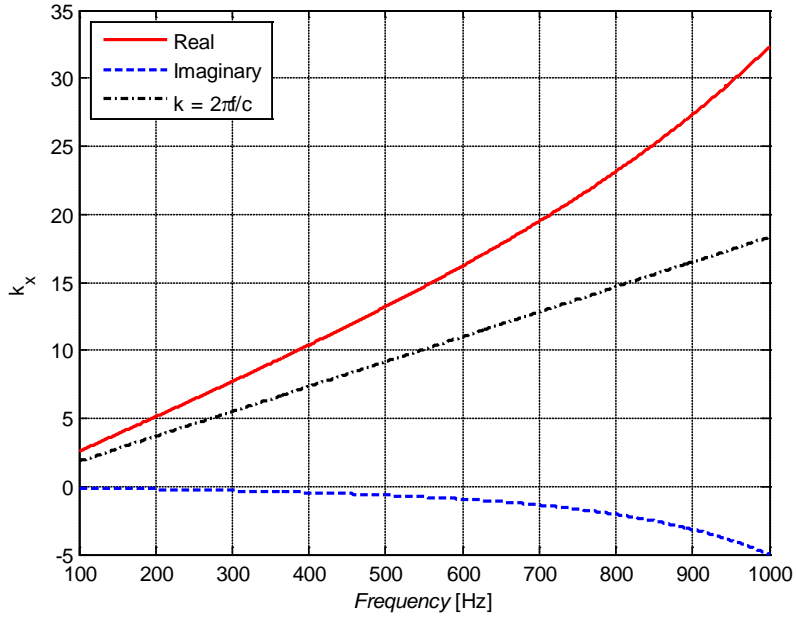


**Figure 19** Real and imaginary components of the axial wavenumber. Also shown is the wavenumber in air

### 3.3.6. Impedance at Termination Inlet

The relationship between the specific acoustic impedance at the horn mouth (terminator inlet)  $z_2$  and the specific acoustic impedance at the terminator end,  $z_3$  is derived in this section. Referring to Figure 9, the boundary conditions are

$$\left. \frac{p}{v} \right|_{x=l_1} = z_2 \quad , \quad (3.3.23)$$

$$\left. \frac{p}{v} \right|_{x=l_1+l_2} = z_3 \quad . \quad (3.3.24)$$

The boundary condition in Eq. (3.3.23) is identical to the horn mouth boundary condition in Eq. (3.2.6). The acoustic pressure in the duct is given by Eq. (3.3.10). The particle velocity along the x-axis is given by [11],

$$v = -\frac{1}{j\omega\rho} \frac{\partial p}{\partial x} . \quad (3.3.25)$$

Taking the ratio of pressure to particle velocity yields the specific acoustic impedance at any plane in the duct,

$$z(x) = \frac{k}{k_x} \rho c \left[ \frac{Ae^{-jk_x x} + Be^{jk_x x}}{Ae^{-jk_x x} - Be^{jk_x x}} \right] , \quad (3.3.26)$$

where the constants  $A$  and  $B$  will be eliminated similar to Section 3.2.2. Applying boundary conditions at the termination inlet and outlet yields,

$$z_2 = \frac{k}{k_x} \rho c \left[ \frac{Ae^{-jk_x l_1} + Be^{jk_x l_1}}{Ae^{-jk_x l_1} - Be^{jk_x l_1}} \right] , \quad (3.3.27)$$

$$z_3 = \frac{k}{k_x} \rho c \left[ \frac{Ae^{-jk_x(l_1+l_2)} + Be^{jk_x(l_1+l_2)}}{Ae^{-jk_x(l_1+l_2)} - Be^{jk_x(l_1+l_2)}} \right] \quad (3.3.28)$$

Using Euler's identity, the expression for the specific acoustic impedance at the termination inlet is,

$$z_2 = \rho c \frac{\frac{z_3}{\rho c} + j \frac{k}{k_x} \tan(k_x l_2)}{1 + j \frac{k_x}{k} \frac{z_3}{\rho c} \tan(k_x l_2)} . \quad (3.3.29)$$

It is seen from Eq. (3.3.29) that the impedance at the termination inlet is dependent on the impedance at the termination end,  $z_3$ , the termination length,  $l_2$ , and the axial wavenumber,  $k_x$ , itself a function of the material lining the duct.

Equation (3.3.29) is identical in form to the impedance presented to a piston vibrating inside a rigid walled pipe<sup>15</sup>, with the addition of the wavenumber ratio. This ratio approaches a value of one for a pipe with no absorption along its walls.

### 3.4. Summary of Analytical Model

All of the equations necessary to predict the reflection coefficient of the anechoic termination have been presented thus far. The steps needed to carry out this procedure are summarized below.

1. Express the specific acoustic impedance at the horn throat in terms of the impedance at the horn mouth using Eq. (3.2.17).

$$z_1 = \rho c \frac{jk}{b} \left[ \frac{jk \frac{\rho c}{z_2} \tan bl_1 - m \tanh ml_1 \tan bl_1 + b}{jk \frac{\rho c}{z_2} - m \tanh ml_1 - b \tan bl_1} \right]$$

where,

$\rho$  is the density of air

$c$  is the speed of sound in air

$k = 2\pi f/c$ , the wavenumber in air,  $f$  is the frequency

$b = \sqrt{k^2 - m^2}$ , where  $m$  is the horn flare by Eq. (3.2.7)

$z_2$  is the specific acoustic impedance at the horn mouth

$l_1$  is the horn length

2. The specific acoustic impedance at the horn mouth is given by Eq. (3.3.29) and substituted in step 1,

---

<sup>15</sup> See pg. 273 in Reference [11]

$$z_2 = \rho c \frac{\frac{z_3}{\rho c} + j \frac{k}{k_x} \tan k_x l_2}{1 + j \frac{k_x}{k} \frac{z_3}{\rho c} \tan k_x l_2}$$

where,

$z_3$  is the specific acoustic impedance at the termination end

$k_x$  is the axial wavenumber in the termination

$l_2$  is the length of the termination

Steps 3 – 6 estimate the axial wavenumber  $k_x$ , and step 7 gives expressions for  $z_3$ .

3. Estimate the characteristic impedance and propagation constant of polyester fiber by Eq. (3.3.20) and (3.3.21),

$$\frac{z_c}{\rho c} = (1 + 0.078E^{0.623}) - j0.074E^{0.660}$$

$$\frac{k_w}{k} = (1 + 0.121E^{0.530}) - j0.159E^{0.571}$$

where,

$E = \frac{R}{\rho f}$ , a non-dimensional parameter

$R = 25.989\rho_A^{1.404}$ , the flow resistivity of polyester fiber

$\rho_A$  is the bulk density of the material

4. Calculate the specific acoustic impedance normal to the wall by Eq. (3.3.15), assuming material thickness  $d$ ,

$$z_w = -jz_c \cot(k_w d)$$

5. Compute the radial wavenumber with Eq. (3.3.12),

$$(k_r r_0)^2 \approx \frac{96 + 36jQ \pm \sqrt{9216 + 2304jQ - 912Q^2}}{12 + jQ}$$

where,

$$Q = kr_0 \frac{\rho c}{Z_w}$$

$r_0$  is the distance from the duct center to the absorbing surface

6. With the radial wavenumber, the axial wavenumber is

$$k_x = \sqrt{k^2 - k_r^2}$$

The value of  $k_x$  corresponds to the  $k_r$  that gives least attenuation, i.e. the smallest imaginary part of  $k_x$ .

7. Determine the specific acoustic impedance at the termination end depending on the following scenarios:

- a. Termination closed with a rigid cap,

$$Z_3 = \infty$$

- b. Termination closed with a rigid cap lined with absorption, assuming the same layer thickness throughout the duct,

$$Z_3 = Z_w$$

- c. Termination open to the air, assuming the radiation into the air is a baffled circular piston of radius  $a$  [11],

$$Z_3 = \rho c [R_1(2ka) + jX_1(2ka)] \quad (3.4.1)$$

where,

$$R_1(2ka) = 1 - \frac{2J_1(2ka)}{2ka} \text{ is the piston resistance function}$$

$J_1(2ka)$  is a bessel function of the first kind, order 1

$X_1(2ka) = \frac{2H_1(2ka)}{2ka}$  is the piston reactance function  
 $H_1(2ka)$  is a first order Struve function<sup>16</sup>

d. Reflections are neglected at the termination end,

$$z_3 = \rho c$$

8. Calculate the reflection coefficient magnitude of the anechoic termination by Eq. (3.1.3)

$$|\eta| = \left| \frac{z_1 - \rho c}{z_1 + \rho c} \right|$$

Alternatively, the power absorption coefficient can be calculated by [35],

$$\alpha = 1 - |\eta|^2 \quad . \quad (3.4.2)$$

This represents the amount of incident sound energy absorbed by the anechoic termination.

---

<sup>16</sup> See Aarts and Janssen [41] for a numerical approximation to the first order Struve function. It is useful since the function is not available in MATLAB<sup>®</sup>



## CHAPTER 4

### EXPERIMENTAL VALIDATION

In this chapter, reflection coefficient predictions made using the analytical model presented in Ch. 3 are compared against experimentally measured reflection coefficient of an anechoic termination prototype. All measurements were conducted at Western Michigan University's Noise and Vibration Laboratory following the ASTM E1050 standard [38]. Comparisons are made against experiment for the variety of termination boundary conditions. A comparison of the analytical model developed in Ch. 3 against existing analytical models will conclude the chapter.

#### 4.1. Description of the Prototype

The anechoic termination consisting of the catenoidal horn (white) and absorbing termination (black) of length 0.914 m (36 in.) and diameter 0.305 m (12 in.) is shown in Figure 20. Experimental measurements were also conducted using a termination 3.28 m (129 in.) in length, pictured in Figure 21. All horn and absorbing termination dimensions are given in Table 3. The catenoid was constructed by gluing multiple parts fabricated by selective laser sintering (SLS). The horn prototype was drawn in AutoCAD in order to generate a stereolithograph (.stl) output file of the geometry for input into the 3D prototyping machine. The absorbing termination is made of polyethylene pipe used for

outdoor drainage. Its interior walls are smooth so the layer of polyester fiber lining the circumference fits tightly against the walls (see Figure 22).



**Figure 20** Anechoic termination prototype with catenoidal horn (white) and absorbing termination (black) of length 0.91 m (36 in.) and diameter 0.305 m (12 in.)



**Figure 21** An absorbing termination 3.28 m (129 in.) in length and diameter 0.305 m (12 in.). The mouth of the horn connects to the end shown on the left

**Table 3** Dimensions of each component of the anechoic termination prototype

Catenoid horn length	0.914 m	(36 in.)
Catenoid throat diameter	0.0191 m	(0.75 in.)
Catenoid mouth diameter	0.305 m	(12 in.)
Short absorbing termination length	0.914 m	(36 in.)
Long absorbing termination length	3.28 m	(129 in.)
Absorbing termination diameter (both)	0.305 m	(12 in.)
Polyester fiber layer thickness	0.0445 m	(1.75 in.)

Figure 22 shows the inlet of the absorbing termination with the horn unattached. A layer of polyester fiber of thickness 44 mm (1.75 in.) lines the termination around the circumference throughout the entire length (see Appendix C for material properties provided by the manufacturer. Note the measured thickness is slightly less than specified). With reference to Figure 15, this makes a 108 mm (4.25 in.) radius measured to the surface of the absorbing material. Surrounding the termination inlet is medium density fiberboard (MDF) to facilitate a tight connection to the horn mouth. As shown in Figure 23, the mouth of the horn is fastened to the absorbing termination by clamping the mouth lip to the MDF. A smooth transition is made in the interior since the inner diameters of the horn mouth and termination are both 0.305 m (12 in.).



**Figure 22** Inlet of the absorbing termination with the horn unattached to the medium density fiberboard. A layer of polyester fiber lines the circumference throughout the termination

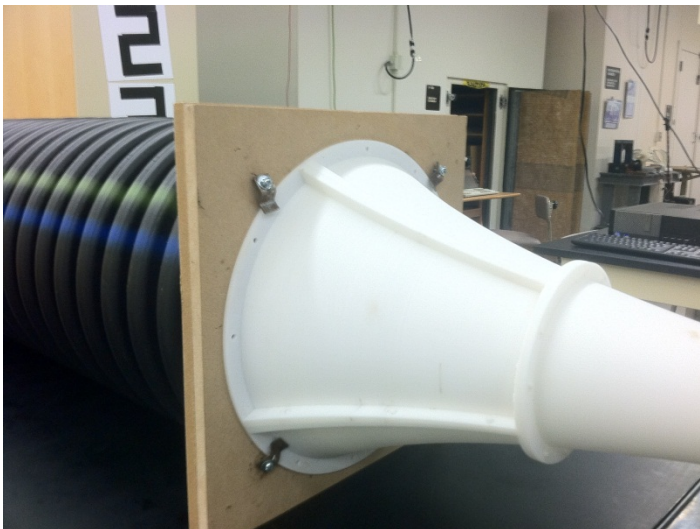


**Figure 23** Connection of the horn mouth to the absorbing termination inlet

The end of the absorbing termination opposite the horn mouth can be either open or closed with an end cap made of MDF. Experiments were conducted with the termination end open (Figure 24), closed with a bare cap (Figure 25a) and closed with a lined cap (Figure 25b).

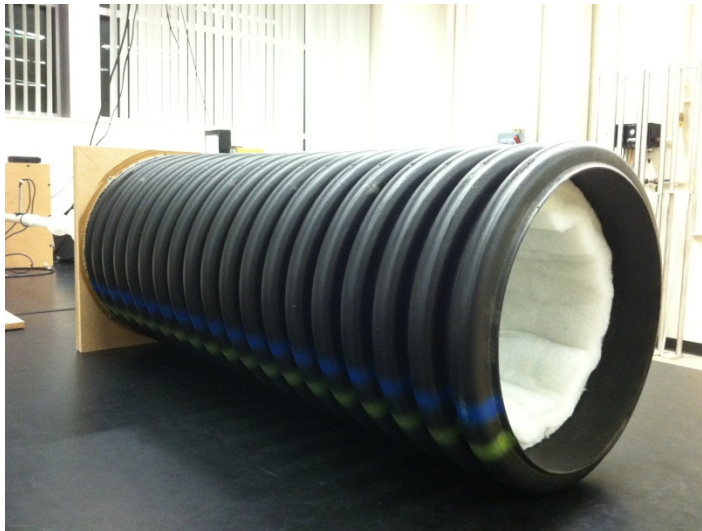


**Figure 24** Absorbing termination with open end. Horn is partially visible on the far left



(a)



(b)

**Figure 25** A bare cap (a) and the same cap with a layer of polyester fiber (b) is used to close the termination end shown in Figure 24



Analytical predictions are made for each of these cases by considering the specific acoustic impedance created by the termination end (referred to as  $z_3$  in Ch. 3).

#### 4.2. Experimental Setup

The entire experimental arrangement is pictured in Figure 26. On the far right of the figure is the sound source enclosure. Between the enclosure and the horn throat is the impedance tube, where the data acquisition system measures the reflection coefficient of the anechoic termination. Connected to the impedance tube is the catenoid, and following the catenoid is the absorbing termination. A schematic of the data acquisition system is shown in Figure 29.



**Figure 26** Experimental arrangement with sound source, impedance tube, catenoid, absorbing termination, and data acquisition system

#### 4.2.1. Sound Source and Impedance Tube

The sound source (RadioShack speaker of diameter 0.152 m (6 in.)) is housed in a 0.381 m x 0.381 m x 0.203 m (15 in. x 15 in. x 8 in.) MDF enclosure (Figure 27a) to prevent any flanking sound transmission to the microphones, as required by ASTM E1050 [38]. A 19 mm (0.75 in.) diameter opening is fabricated for connection to the same size impedance tube. The sound source is mounted inside the enclosure on the front wall (Figure 27b). The enclosure contains a layer of polyester fiber lining the interior walls in order to damp any resonances within the cavity.

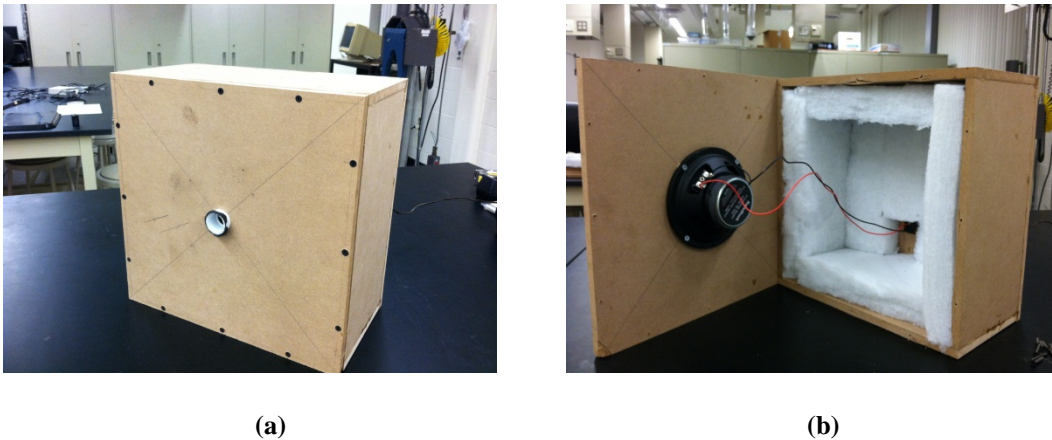
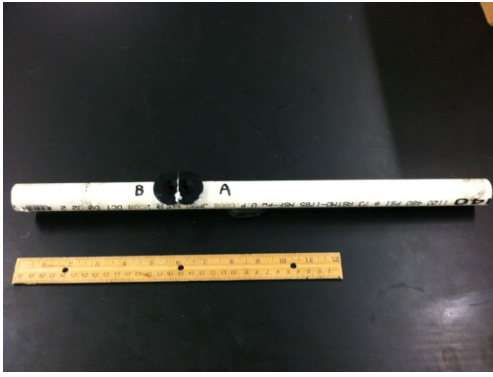


**Figure 27** Enclosure for sound source (a) and front wall open (b) with speaker mounted

Shown in Figure 28a is the impedance tube. This connects to the sound enclosure at its opening. Microphone position A is the closest microphone to the sound source. The impedance tube is made of 19 mm (0.75 in.) diameter PVC pipe. Acoustical measurements are made in the impedance tube with two 6.4 mm

(0.25 in.) microphones mounted such that their diaphragms are flush with the interior wall (Figure 28b). The microphone diameter  $d_m$  allows valid measurements to be made up to 11 kHz, found using [38]

$$f_u < \frac{0.2c}{d_m} . \quad (4.2.1)$$



(a)



(b)

**Figure 28** Impedance tube (left) and close-up of microphone mounts (right)

The dimensions of the impedance tube and microphones are given in Table 4. The diameter of the impedance tube ensures that only plane waves will propagate through the tube up to 9800 Hz. This upper limit is calculated using Eq. (3.3.6). The frequency range for which measurements are valid in this setup is limited by the microphone spacing,  $s$ . This range is approximately 235 – 9400 Hz, determined using [38],

$$\frac{0.01c}{s} < f < \frac{0.8c}{2s} . \quad (4.2.2)$$



**Table 4** Impedance tube specifications

Inner Diameter	0.0191 m	(0.75 in.)
Length	0.464 m	(18.25 in.)
Center to center microphone spacing	0.0146 m	(0.575 in.)
Source to Mic A distance	0.298 m	(11.75 in.)
Mic B to horn throat distance	0.149 m	(5.87 in.)

The distance from the source to the first microphone (microphone A) is chosen to be larger than three tube diameters to avoid measuring non-planar waves in the near field of the source. The distance between the second microphone (microphone B) and the horn throat is larger than two tube diameters. This way, higher order modes created by reflections from the horn throat have a sufficient distance to decay before they reach the second microphone.

#### 4.2.2. Data Acquisition System

A schematic of the data collection system is shown in Figure 29. The signal generator generates white noise, which is amplified by the stereo amplifier. This signal is fed into the speaker. The white noise, generated by the speaker, travels through the impedance tube in the direction towards the horn and then into the absorbing termination.

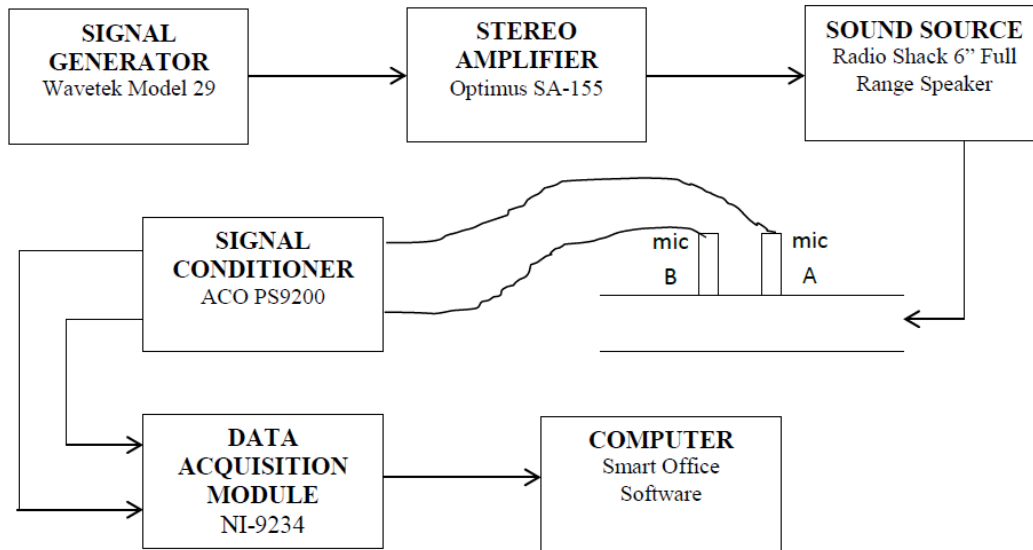


**Figure 29** Schematic of the signal flow for data collection

Two ACO Type 7016  $\frac{1}{4}$ -inch phase-matched microphones mounted on the impedance tube (see Figure 28b) measure a transfer function so that the reflection coefficient of the anechoic termination can be calculated (described in the next section). Each of the microphone signals are amplified by the ACO PS9200 signal conditioner and collected by the NI-9234 data acquisition (DAQ) module. The DAQ module is connected via USB port to a computer running Smart Office software [39].

The data is collected with a sampling rate of 25.6 kHz, useful bandwidth of 10 kHz, and a spectral resolution equal to 3200 lines. One-hundred blocks are used to compute the linear average, with a Hanning window applied to each block. The total acquisition time is 32 seconds. The level of the white noise

exceeds the background noise measured in the impedance tube by more than 20 dB to ensure an adequate signal to noise ratio. Measurements were made at different source levels and the results indicated that source level had no effect on the reflection coefficient.

#### 4.3. Experimental Measurement Procedure

The procedure to measure the reflection coefficient of the anechoic termination follows the two-microphone technique outlined in ASTM E1050 [38]. The procedure is valid only for plane waves within the impedance tube.

##### 4.3.1. Complex Reflection Coefficient

This two-microphone technique involves measuring a frequency dependent transfer function defined as

$$\bar{H} = \frac{G_{12}}{G_{11}} \quad , \quad (4.3.1)$$

where  $G_{12}$  is the cross-power spectrum and  $G_{11}$  is the input auto-power spectrum (measured by the microphone at location A closest to the source). This transfer function is measured for each experimental arrangement (e.g. open horn, horn with absorbing termination, etc.) To correct for a phase mismatch between the two microphones, a correction factor is computed by

$$\bar{H}_c = (\bar{H}^I \times \bar{H}^{II})^{1/2} \quad , \quad (4.3.2)$$

where  $\bar{H}^I$  is the calibration transfer function measured when microphone 1 occupies location A and microphone 2 occupies location B, and  $\bar{H}^{II}$  is the calibration transfer function measured when microphone 1 occupies location B and microphone 2 occupies location A. This correction factor needs to be computed only once. The transfer function with the correction factor applied to it becomes

$$H = \frac{\bar{H}}{\bar{H}_c} . \quad (4.3.3)$$

Then, the complex reflection coefficient is

$$\eta = \frac{H - e^{-j\bar{k}s}}{e^{j\bar{k}s} - H} e^{2j\bar{k}(l+s)} , \quad (4.3.4)$$

where  $l$  is the distance from the horn throat to the nearest microphone (location B in this case), and  $s$  is the center to center spacing between the microphones (see Table 4). The wavenumber  $\bar{k}$  in Eq. (4.3.4) accounts for acoustic pressure attenuation in the impedance tube and is defined as

$$\bar{k} = k - jk' , \quad (4.3.5)$$

where  $k$  is the wavenumber defined as in Eq. (3.1.9) and  $k'$  is the attenuation constant in the impedance tube of diameter  $d'$  and is empirically estimated [38] as

$$k' = 0.02203 \frac{\sqrt{f}}{cd'} . \quad (4.3.6)$$

#### 4.3.2. Benchmark for Experimental Measurements

To validate the experimental measurement procedure, a benchmark case is considered (Figure 30).

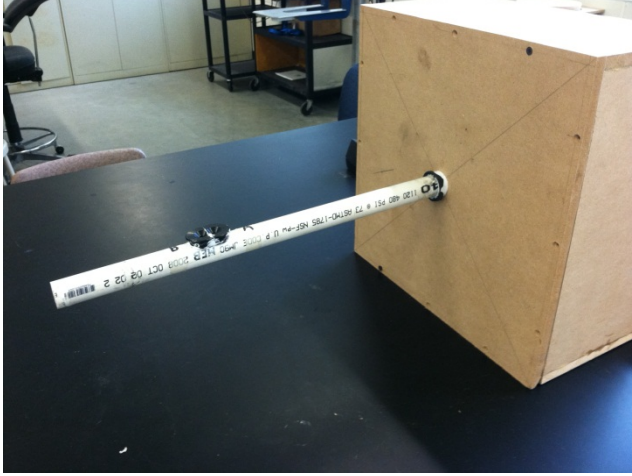


**Figure 30** Open impedance tube used as a benchmark arrangement to validate experimental procedure

The reflection coefficient is measured for the open impedance tube and compared to the theoretical reflection coefficient for an open tube whose end condition can be assumed to act as a baffled piston [11]. A schematic showing a side and front view of this baffled piston arrangement is shown in Figure 31. The specific acoustic impedance  $z_D$  of the driven (by the loudspeaker) end of the impedance tube of length  $l$  is given in terms of the specific acoustic impedance of the piston  $z_P$ ,

$$z_D = \rho c \frac{z_P \cos(kl) + j\rho c \sin(kl)}{jz_P \sin(kl) + \rho c \cos(kl)} , \quad (4.3.7)$$

The specific acoustic impedance of the baffled piston radiating into the environment is given by Eq. (3.4.1). The reflection coefficient of the open tube is given by Eq. (3.1.14), after replacing  $z_1$  with  $z_D$ .

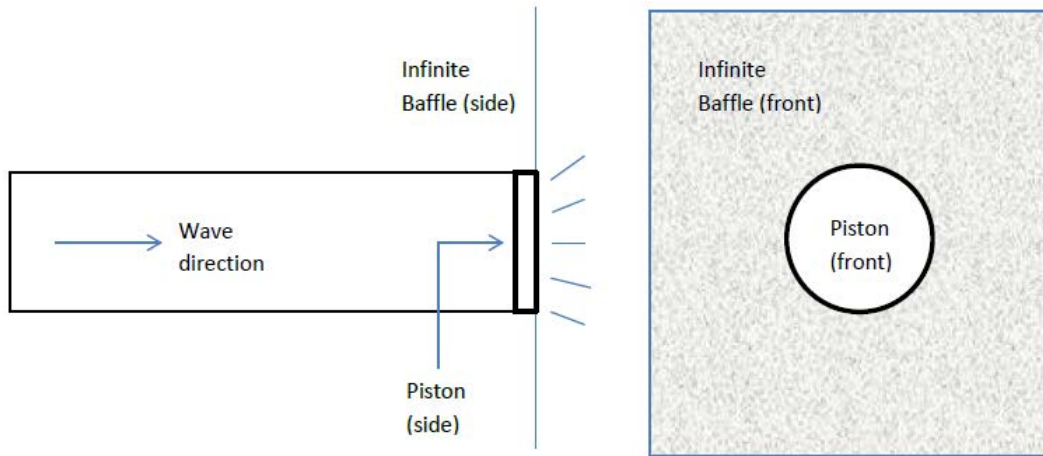


**Figure 31** Side and front view of a baffled piston representing the open end of a tube

As illustrated in Figure 32, the agreement between theoretical and experimentally measured reflection coefficient is very good. The abrupt decrease in the measured reflection coefficient at 5000 Hz is due to a poor sound source response at this frequency (observed experimentally), possibly caused by a resonance within the enclosure. Around 9800 Hz, cross modes begin to form within the impedance tube. As the figure indicates, the measurement accuracy decreases in this region because the measurement technique is limited to plane waves.

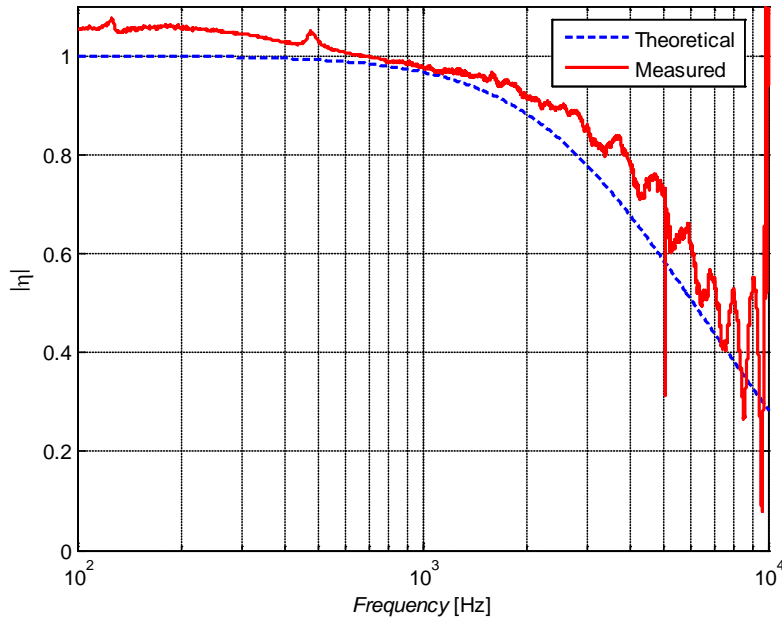


**Figure 32** Experimental measurement of reflection coefficient for an open tube compared to theoretical predictions made using Eq. (4.3.7)

#### 4.4. Experimental Results vs. Analytical Predictions

Shown in the following sections are comparisons of experimental results with predictions made by the analytical model described in the previous chapter for a variety of termination configurations. The experimental measurements of reflection coefficient follow the procedure outlined in Section 4.3.1, and the corresponding analytical predictions follow the summary in Section 3.4. The frequency range spans from 100 - 1000 Hz in the plots since the first cross mode forms in the absorbing termination around 1000 Hz. The experimental data is plotted starting at approximately 235 Hz since the small microphone spacing in the experimental setup imposed this lower limit.

#### 4.4.1. Open Horn, No Termination

In the first test configuration, measurements are taken on the horn prototype only, so that the mouth of the horn is open to the air.

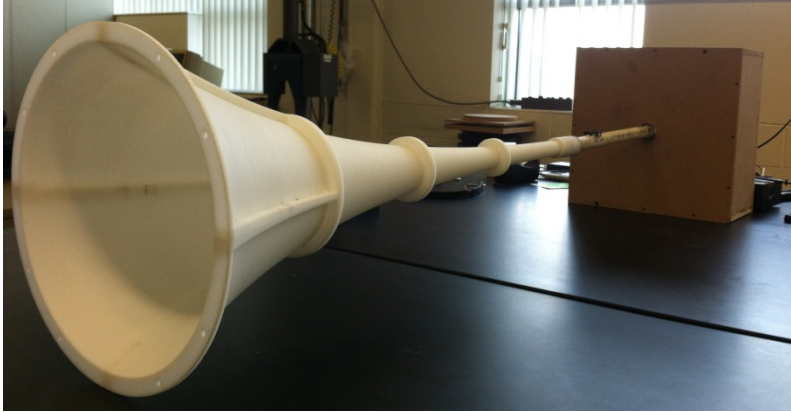


**Figure 33** Horn prototype open to the air

Shown in Figure 34 is a plot of the reflection coefficient magnitude versus frequency. The mouth of the open horn radiates sound into the air and is modeled as a piston in an infinite baffle. The impedance of the baffled piston, given by Eq. (3.4.1), is used in place of the mouth specific acoustic impedance  $z_2$  in Eq. (3.2.17).



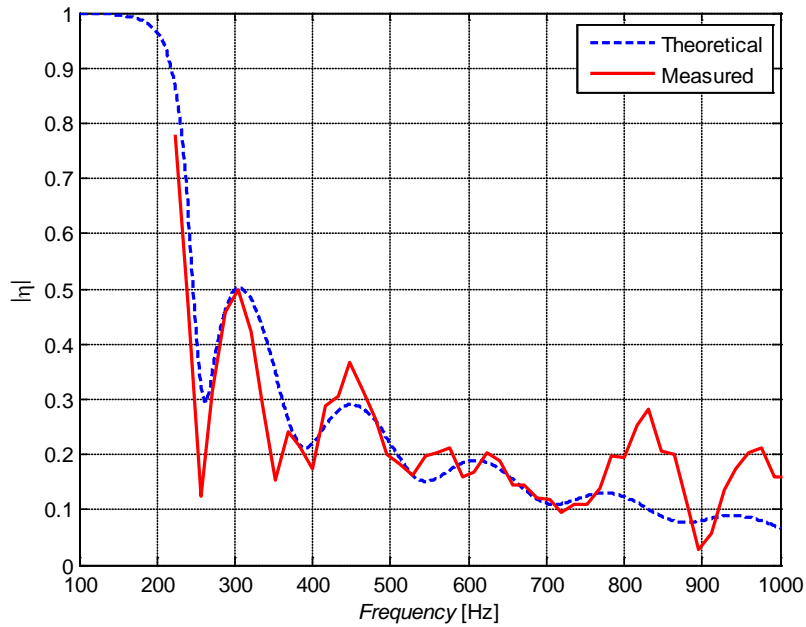


**Figure 34** Measured and predicted reflection coefficient for open catenoid

The experimental results show excellent agreement with the theoretical predictions. The first local minimum around 260 Hz corresponds to the first resonant frequency of the catenoid. At frequencies of about 460 Hz and greater, the reflection coefficient is smaller than 0.3 (i.e. 30 percent of the incident energy is reflected by the horn back into the impedance tube).

Alternatively, the power absorption coefficient of the horn is plotted using Eq. (3.4.2). In Figure 35, the power absorption coefficient,  $\alpha$ , is compared between experiment and theory. The figure indicates that if the horn alone were used as an anechoic termination, 90 percent of the incident sound energy would be absorbed for frequencies greater than about 460 Hz. The figure also

underscores the fact that the lowest frequencies are most difficult for the horn to absorb (or transmit into open space).

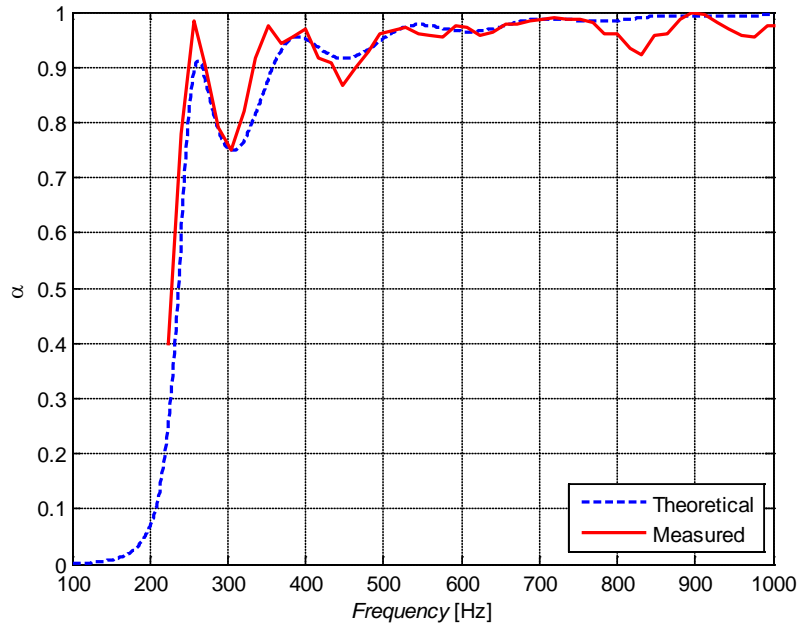


**Figure 35** Plot of power absorption coefficient for the open catenoid

#### 4.4.2. Horn with Open Termination

The plots in this section represent the case where each absorbing tube is connected to the mouth of the horn and the opposite end of the tube is open to the air. Figure 36 shows this arrangement for the 36 in. length absorbing tube.

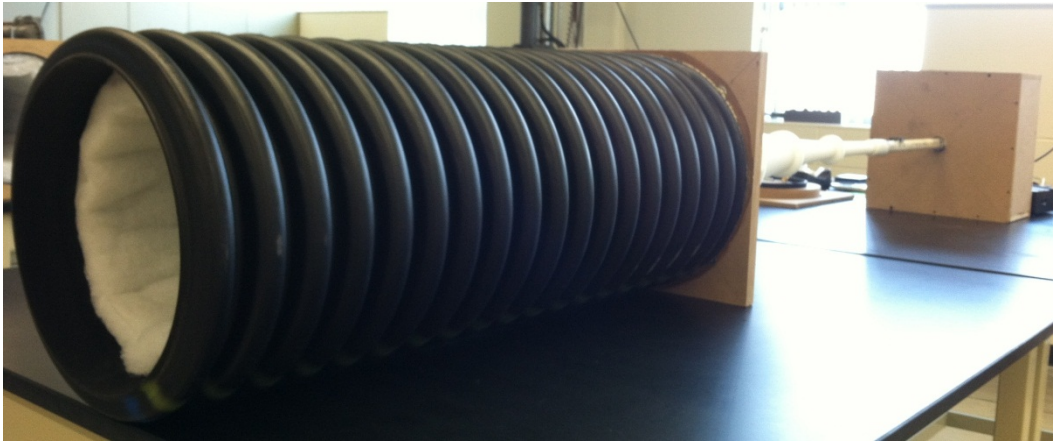


**Figure 36** Horn (partially shown) and absorbing termination open to the air (picture, far left)

The specific acoustic impedance at the open end of the absorbing tube is modeled as a piston in an infinite baffle, like the open horn in the previous section. Shown in Figure 37 is the theoretical reflection coefficient magnitude for this case compared to experimentally measured values. In Figure 38, the corresponding plot is made for the power absorption coefficient. These measurements are made using the 0.914 m (36 in.) long absorbing termination.

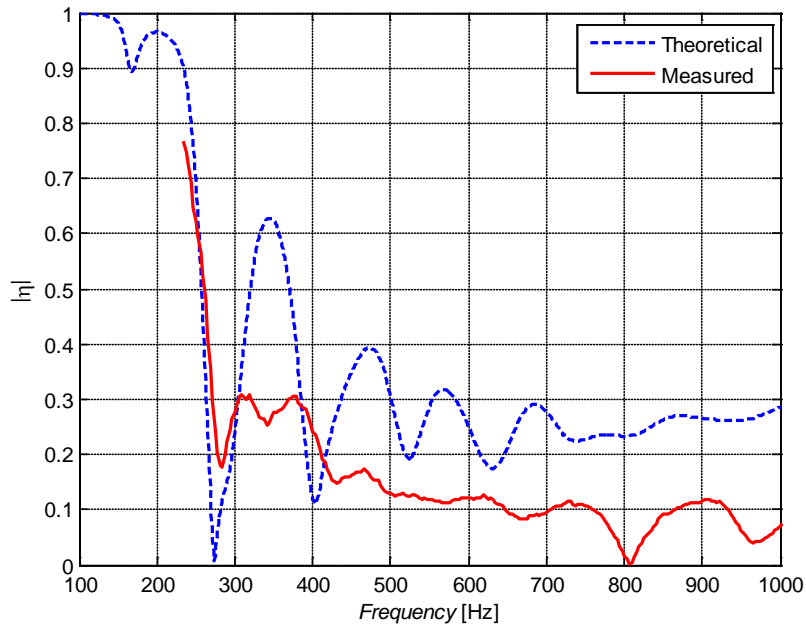


**Figure 37** Reflection coefficient magnitude for the horn and absorbing termination (length = 36 in.) open to the air

The theoretical prediction captures the rapid decrease in experimentally measured reflection coefficient between 200 and 300 Hz very well. After 300 Hz, the prediction tends to overestimate the reflection coefficient. This error is less pronounced when viewing the absorption coefficient plot in Figure 38. With the exception of the region around 350 Hz, the experimentally measured power absorption coefficient matches theoretical predictions to within 10 % error.

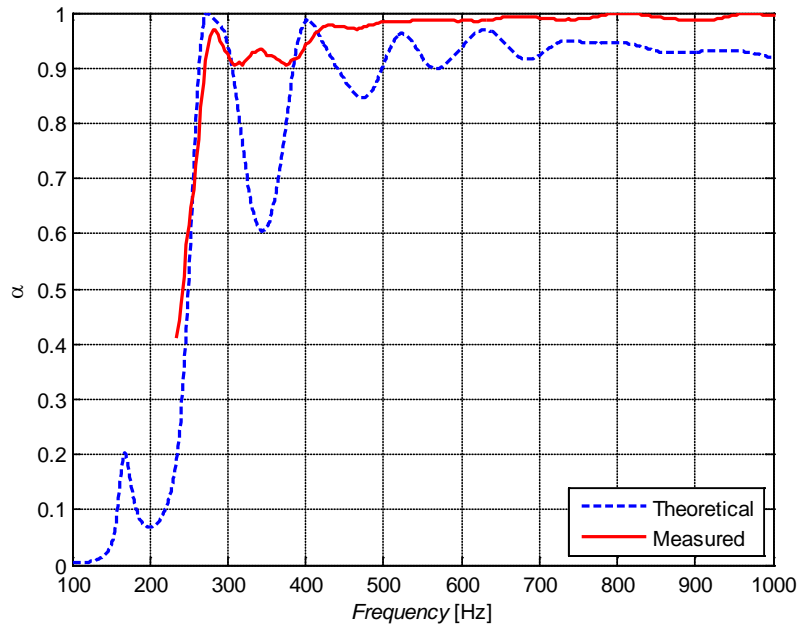


**Figure 38** Power absorption coefficient for horn and absorbing termination (length = 36 in.) open to the air

Similar plots for reflection coefficient magnitude and power absorption coefficient are presented in Figure 39 and Figure 40 for the longer 3.28 m (129 in.) absorbing termination. Notably, the analytical model using the longer termination predicts less reflection at the local maximum around 350 Hz, and the result is closer to the experimentally measured value. This is likely due to increased acoustic pressure attenuation since the wave travels through a longer absorbing duct. A further analysis of the effect that the length of the absorbing termination has on reflection coefficient will be presented in Chapter 5.

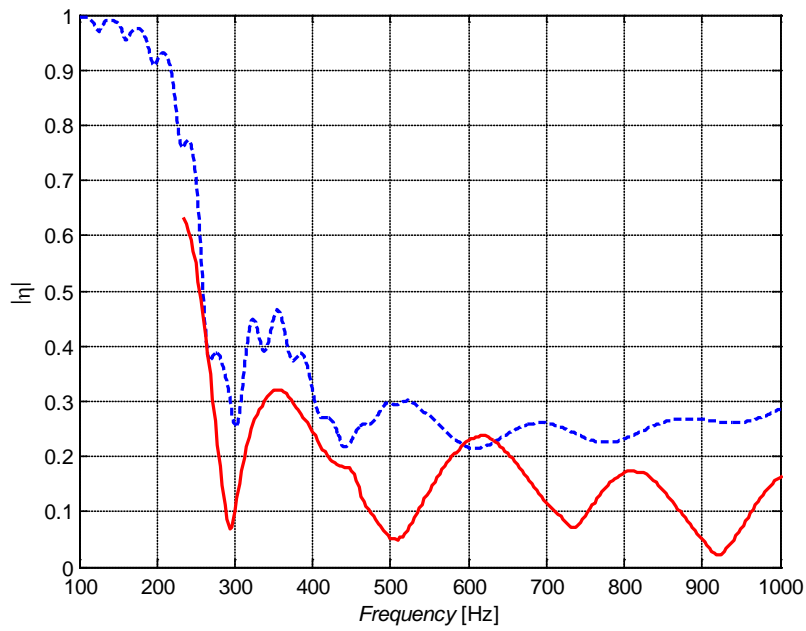


**Figure 39** Reflection coefficient magnitude for the horn and absorbing termination (length = 129 in.) open to the air

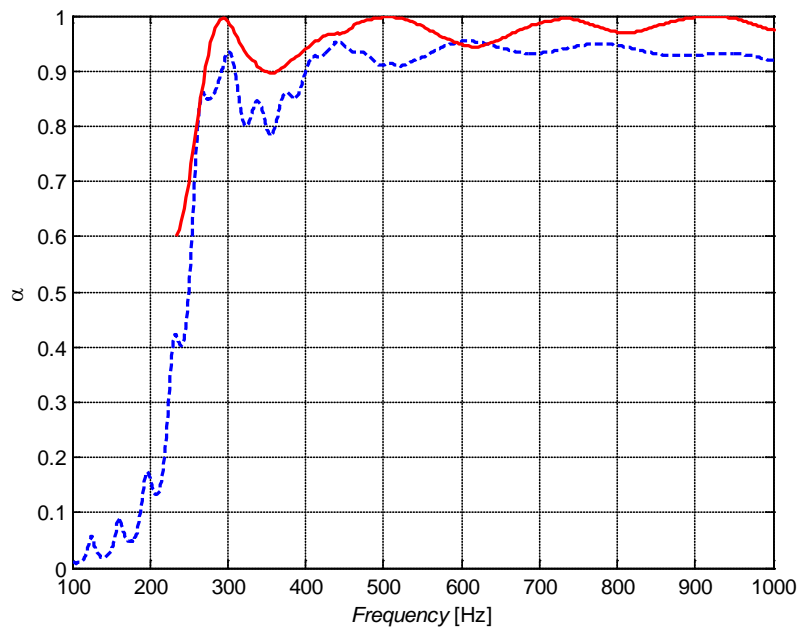


**Figure 40** Absorption coefficient for horn and absorbing termination (length = 129 in.) open to the air

#### 4.4.3. Horn with Closed Termination (Rigid Cap)

The plots in this section represent the case where the horn and absorbing tube are connected, with the absorbing tube closed to the environment using a rigid cap (see Figure 25a). The rigid cap is attached to the end of the absorbing termination as shown on the left in Figure 41.

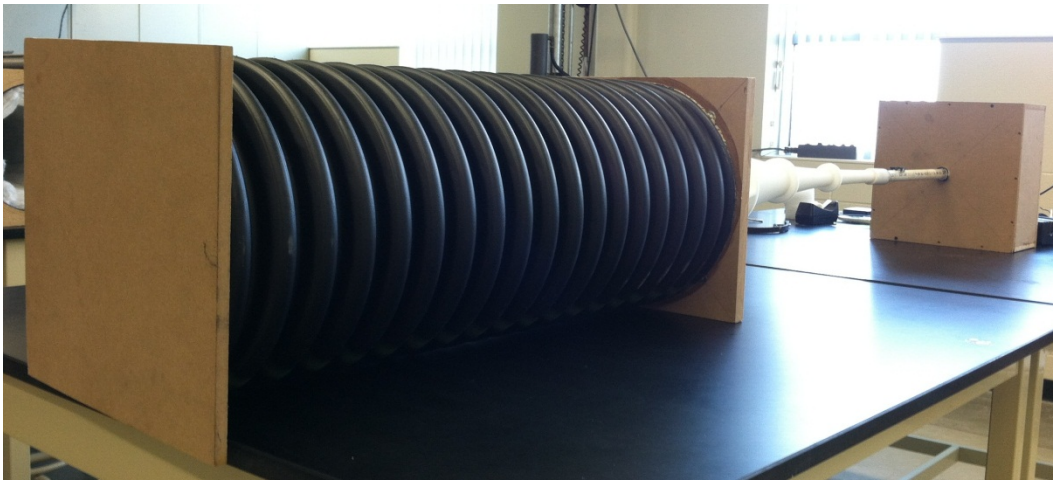


**Figure 41** Horn (partially shown) and absorbing termination with rigid cap attached (picture, far left)

The reflection coefficient magnitude and power absorption coefficient (Figure 42 and Figure 43) is plotted for the 0.914 m (36 in.) absorbing termination and for the 3.28 m (129 in.) absorbing termination (Figure 44 and Figure 45).

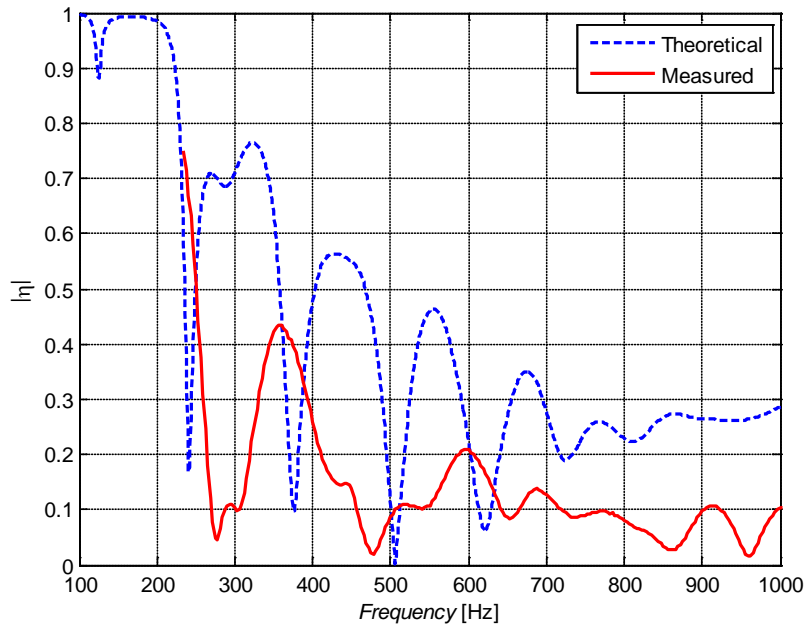


**Figure 42** Reflection coefficient magnitude for the horn and absorbing termination (length = 36 in.) closed with a rigid cap

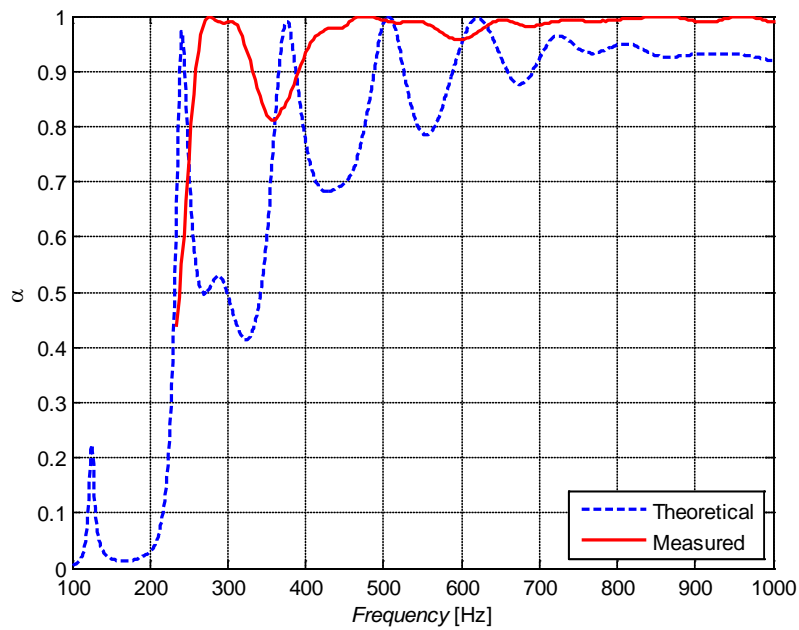


**Figure 43** Absorption coefficient for horn and absorbing termination (length = 36 in.) closed with a rigid cap



With reference to Figure 42, the theoretical reflection coefficient for the 36 in. long absorbing termination shows large variation between successive local minima and maxima. This is observed experimentally also. This is likely due to the rigid cap creating resonances within the anechoic termination. Conversely, this variation is less prevalent when using the 129 in. long termination (see Figure 44). This indicates the end boundary condition may have a negligible influence when longer absorbing terminations are used. When the sound wave reaches the absorbing tube end, the acoustic pressure amplitude is attenuated more in the longer absorbing duct than the shorter. Therefore, the influence of resonances on the reflection coefficient is diminished.

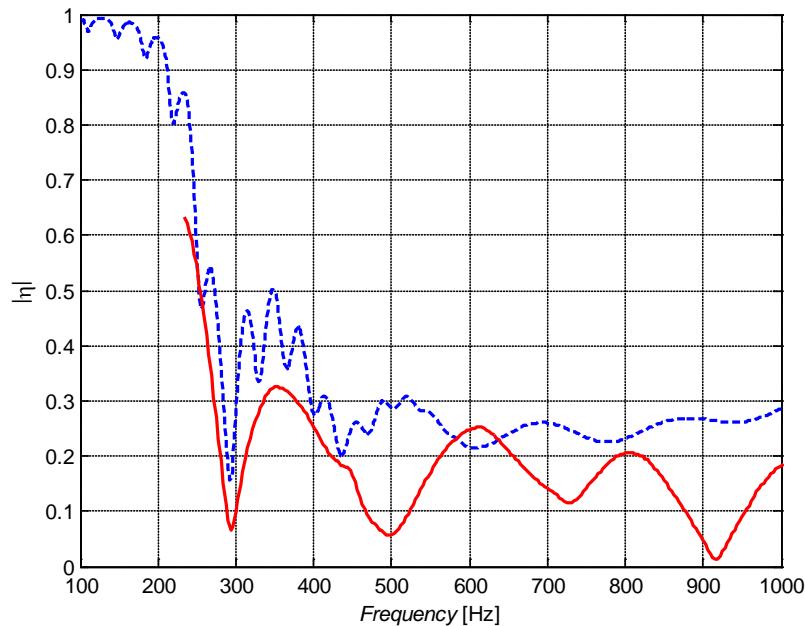


**Figure 44** Reflection coefficient magnitude for the horn and absorbing termination (length = 129 in.) closed with a rigid cap

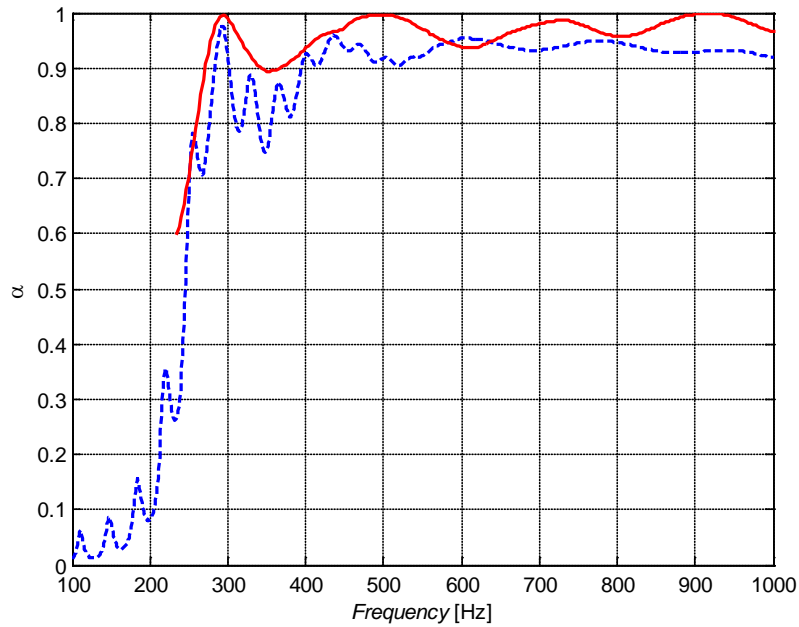


**Figure 45** Absorption coefficient for horn and absorbing termination (length = 129 in.) closed with a rigid cap

#### 4.4.4. Horn with Closed Termination (Layered Rigid Cap)

Next, a 1.75 in. thick layer of polyester fiber is added to the rigid cap (see Figure 25b) and the absorbing termination is closed in a similar manner to the previous section (see Figure 41). The findings are negligibly different from Figures 45 – 48, the case of the absorbing termination closed with a non-layered rigid cap. Presumably, this means the addition of the polyester fiber to the rigid cap has a negligible influence on the reflection and power absorption coefficients. The next section will show an experimental comparison between the various experimental arrangements.

#### 4.4.5. Comparison between Experimental Arrangements

Figure 46 shows a relative comparison of reflection coefficient magnitude between the various anechoic termination arrangements. In this figure, the plots are made for the open horn and for each of the end boundary conditions on the 36 in. long absorbing termination. Figure 47 shows the corresponding absorption coefficients. Three observations can be made from these figures: 1) the addition of the absorbing termination increases the first natural frequency from the open horn case (see annotations), 2) the addition of the absorbing termination lowers the reflection coefficient at higher frequencies, and 3) the absorbing termination with rigid and layered cap are nearly indistinguishable at low frequencies.

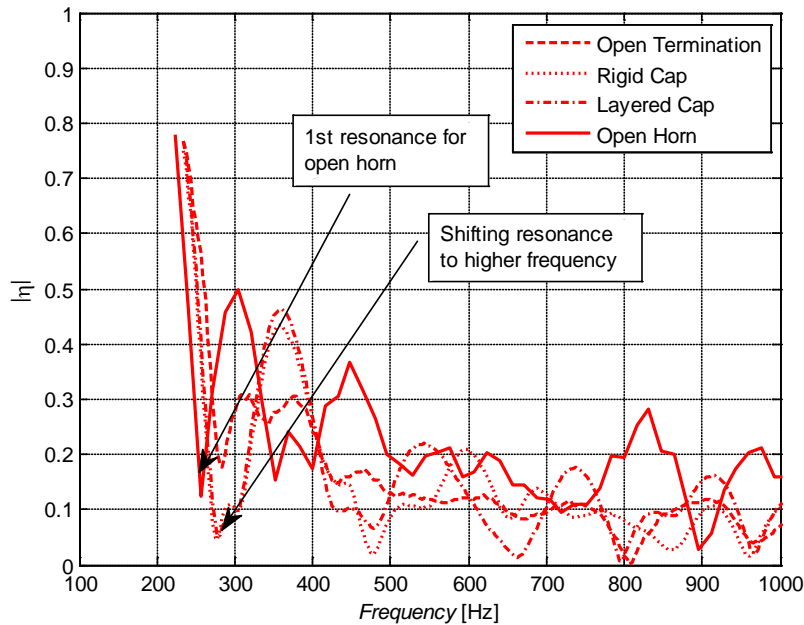


**Figure 46** Experimentally measured reflection coefficient for each boundary condition (36 in. absorbing termination)

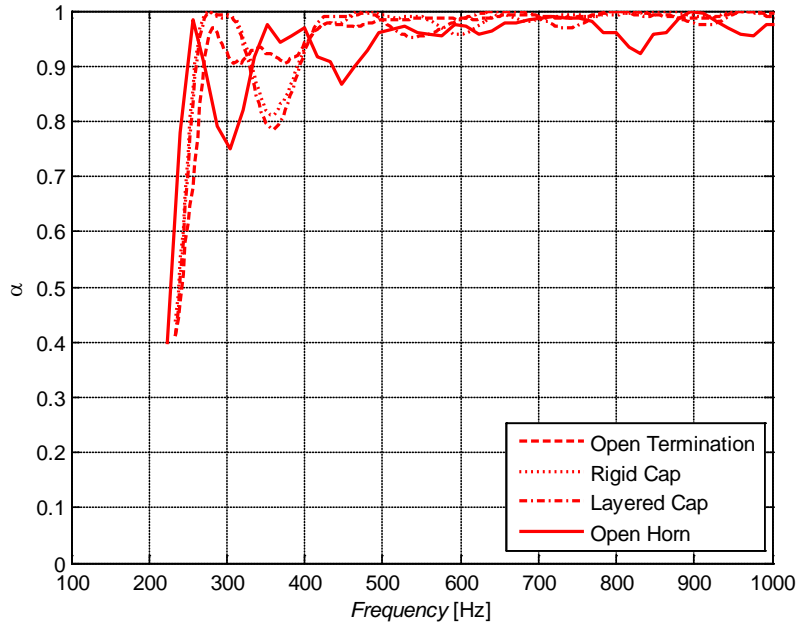


**Figure 47** Experimentally measured power absorption coefficient for each boundary condition (36 in. absorbing termination)

Further, it is difficult to make any conclusions from experiment as to which case (e.g. open termination vs. closed with rigid/layered cap) is “better” based on the objective of attaining a small reflection coefficient (or absorption coefficient near one) over a certain frequency range. In Chapter 5, we present a cost function to evaluate how “good” these anechoic terminations are relative to each other with the goal of optimizing the design of the anechoic termination in order to achieve small reflection coefficient.

In Figure 48, the experimentally measured reflection coefficient magnitude is plotted for the open horn and for each of the end boundary

conditions for the absorbing termination of length 3.28 m (129 in.). Figure 49 shows the corresponding power absorption coefficients.

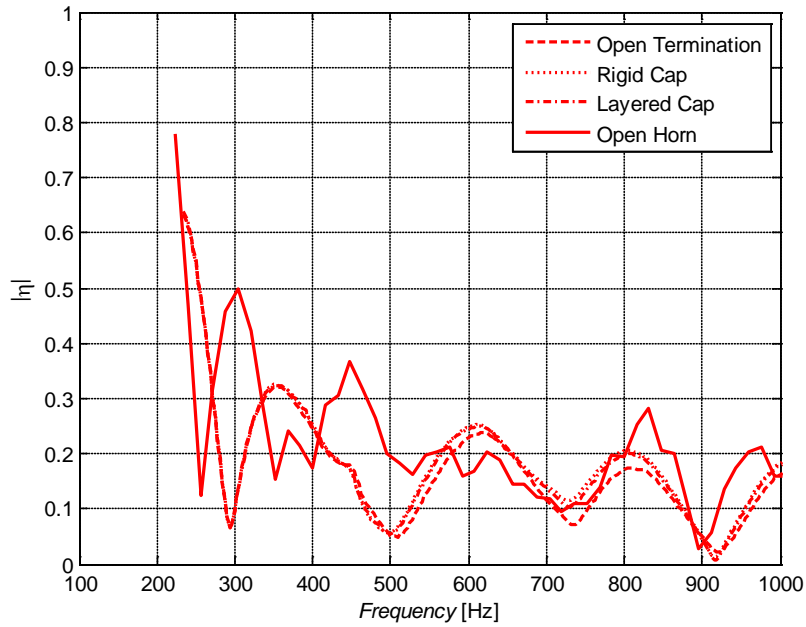


**Figure 48** Experimentally measured reflection coefficient for each boundary condition (129 in. absorbing termination)

These figures indicate that when using a longer absorbing termination, the reflection (and power absorption) coefficient is less sensitive to changes in the boundary condition at the termination end (e.g. open termination, closed with rigid and layered cap).

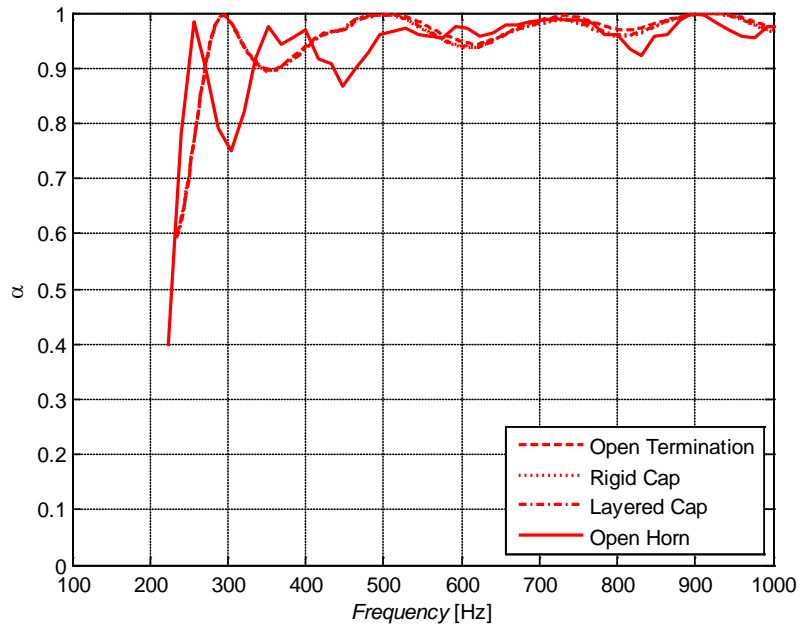


**Figure 49** Experimentally measured power absorption coefficient for each boundary condition (129 in. absorbing termination)

In Figure 50, the experimentally obtained reflection coefficient is compared between the two absorbing terminations of different length when their ends are open. As the figure indicates, replacing the 0.914 m (36 in.) termination with the longer 3.28 m (129 in.) termination does not have a significant effect on the reflection coefficient magnitude. The effect is even less pronounced in Figure 51 when examining the power absorption coefficient. This suggests there may be a limit to the influence a longer termination can have on the absorption (and reflection) coefficient of anechoic terminations.

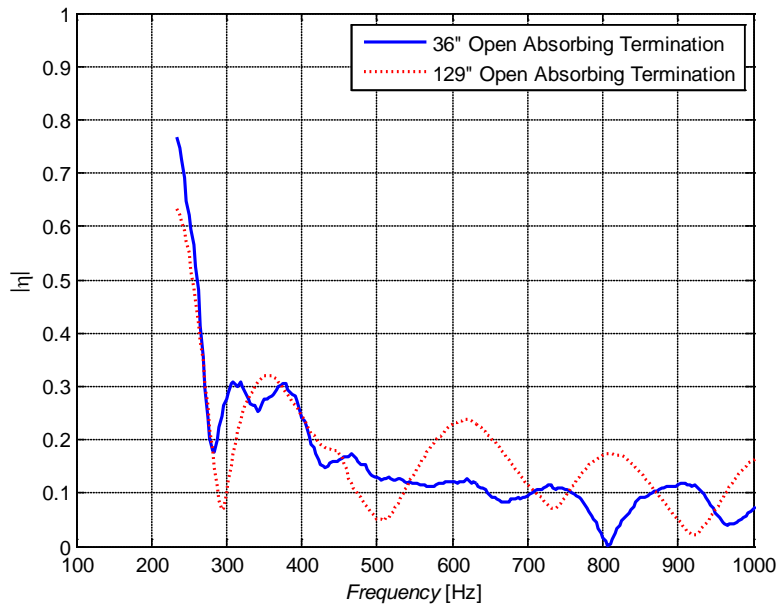


**Figure 50** A relative comparison of experimentally measured reflection coefficient between two different length absorbing terminations (when both are open)

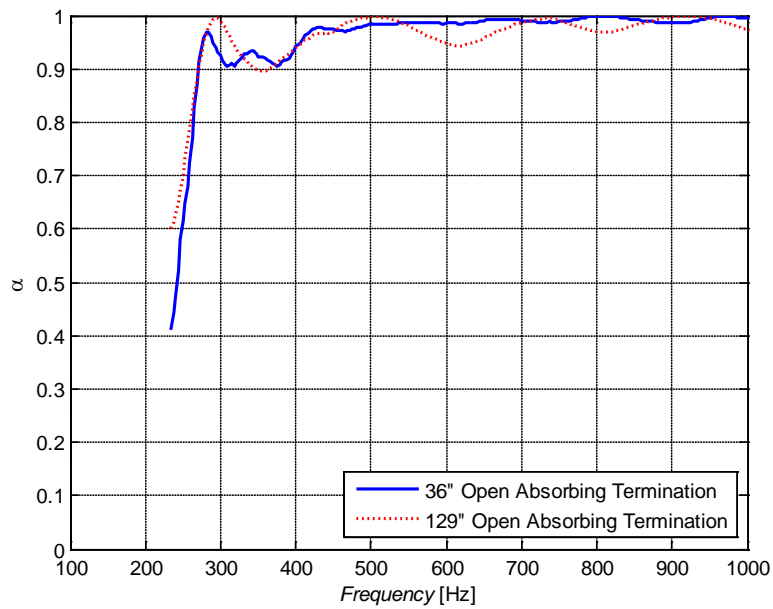


**Figure 51** A relative comparison of experimentally measured absorption coefficient between two different length absorbing terminations (when both are open)

#### 4.4.6. Analytical Model Compared to Bolton's Model

Effort has been applied to the analytical model outlined in this thesis to account for the shape of the catenoid and the effect of the absorbing termination. An analytical model developed by Bolton [1] did not account for the catenoid shape (he approximated it as an exponential horn) and modeled the absorbing tube as if it were infinitely long (no account for absorbing material). Does the analytical model presented in this thesis yield an improvement over Bolton's model to predict the reflection coefficient of the anechoic termination prototype? To answer this, the experimentally measured reflection coefficient for the anechoic termination prototype (catenoid connected to 36 in. long absorbing termination, open at the end) is plotted and compared against predictions from the analytical model presented in Ch. 3. To predict the reflection coefficient of a catenoidal horn connected to an absorbing termination, Bolton mathematically modeled the arrangement as an exponential horn connected to an infinitely long tube. For an exponential horn, the area of a cross section as a function of axial distance  $x$  is [1]

$$S_e(x) = S_{oe} \exp(m_e x), \quad (4.4.1)$$

where  $S_{oe}$  is the area at the exponential horn throat and  $m_e$  is the horn flare. Assuming the horn terminates into an infinitely long tube, the specific acoustic impedance at the throat of the exponential horn is



$$z_{1e} = \rho c \frac{\cos(b_e l_e + \theta_e) + j \sin(b_e l_e)}{\cos(b_e l_e - \theta_e) + j \sin(b_e l_e)} , \quad (4.4.2)$$

where  $l_e$  is the length of the exponential horn, and the parameters  $b_e$  and  $\theta_e$  are defined in terms of the wavenumber  $k$  in air as,

$$b_e = 0.5 \sqrt{4k^2 - m_e^2} , \quad (4.4.3)$$

$$\theta_e = \tan^{-1} \left( \frac{m_e}{2b_e} \right) . \quad (4.4.4)$$

Equation (4.4.2) is used in place of  $z_1$  in Eq. (3.1.14) to predict the reflection coefficient created by this arrangement. Bolton's analytical model is plotted in Figure 52 and compared against the reflection coefficient predictions of the analytical model presented in this thesis. The predictions are compared against experimental measurements of the prototype consisting of the catenoidal horn and open absorbing termination of length 129 inches. The power absorption coefficient is plotted in Figure 53.

These figures show that the current model better estimates the reflection coefficient magnitude than Bolton's model at lower frequencies. This makes the analytical model particularly useful to HVAC applications. Measurement error due to large reflections at lower frequencies is of particular interest when measuring sound power radiated by fans into ducts (refer to Table 2 in Ch. 1). Bolton's model tends to underestimate the reflection coefficient (or power absorption coefficient) over the broad spectrum. This implies measurement errors

would be understated. Since the analytical model presented in this thesis tends to overestimate the reflection coefficient, a more conservative estimate of the measurement errors will be given.

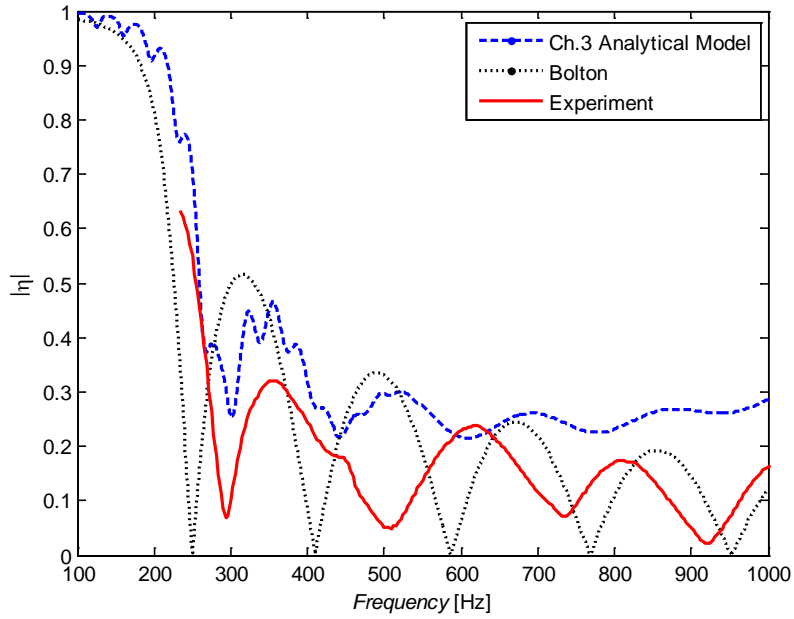


**Figure 52** Bolton's model vs. the present analytical model (catenoid and 129" open absorbing termination) compared to experimentally measured reflection coefficient

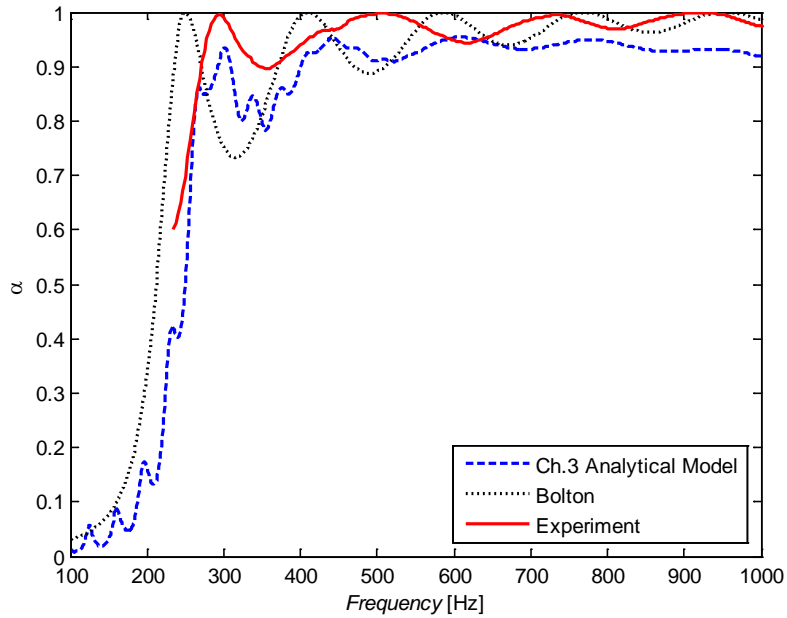


**Figure 53** Bolton's model vs. the present analytical model (catenoid and 129" open absorbing termination) compared to experimentally measured absorption coefficient

In the next chapter, an analytical investigation will be conducted on the analytical model in order to understand how various changes in geometry affect the reflection coefficient. Optimization examples will be given. The goal is to design the best termination possible.

## CHAPTER 5

### OPTIMUM DESIGN OF A TERMINATION

In this chapter, the use of the analytical model presented in this thesis is studied to gain insight into the physics described by the equations. In addition, particular emphasis is given on using the model to construct an optimum anechoic termination designed for minimum reflection coefficient over a prescribed frequency range. Optimization can be applied to the horn geometry, the absorbing termination, or both. An example of an optimized anechoic termination is presented.

#### 5.1. Parametric Study of Horn Geometry

In contrast to other models, the analytical model presented in this thesis does not assume the absorbing termination to be an infinitely long tube but instead, accounts for its finite length. It is for this reason that it is unique in its ability to optimize for minimum reflection coefficient. As the next section will show through a parametric study of various horn flares, using the model of an infinitely long tube connected to a catenoid gives erroneous optimization results.

##### 5.1.1. An Infinitely Long Absorbing Termination

An infinitely long tube attached to a catenoidal horn (or any horn in general) can be considered as a model but not fabricated in the real world.

Furthermore, such a model cannot be used to optimize the horn geometry for minimum reflection coefficient. To illustrate, consider Eq. (3.2.17) with the specific acoustic impedance at the mouth  $z_2$  assumed as  $\rho c$  (this is the specific acoustic impedance of an infinitely long tube). Equation (3.2.17) becomes

$$z_1 = \rho c \frac{jk}{b} \left[ \frac{jk \tan(bl_1) - m \tanh(ml_1) \tan(bl_1) + b}{jk - m \tanh(ml_1) - b \tan(bl_1)} \right]. \quad (5.1.1)$$

For a catenoid horn of 1 meter in length, the reflection coefficient magnitude is plotted in Figure 54 for several flare values,  $m$ , where each curve represents a different flare. As flare (shown next to each curve) decreases, the reflection coefficient gets smaller over the frequency range until it reaches zero for a flare of zero. This corresponds to having a straight tube instead of a horn connecting the test tube to the termination section, which is also a straight, infinitely long tube. Any horn placed between two infinitely long tubes presents an area discontinuity. The discontinuity, no matter how small, will partially reflect the incident sound wave. The “zero flare” solution effectively eliminates the discontinuity (i.e. the horn) and results in no reflections. This leads to the erroneous conclusion that to minimize the reflection coefficient over a certain frequency range, no horn is necessary. The conclusion follows from the oversimplified model that assumes the termination as infinitely long.

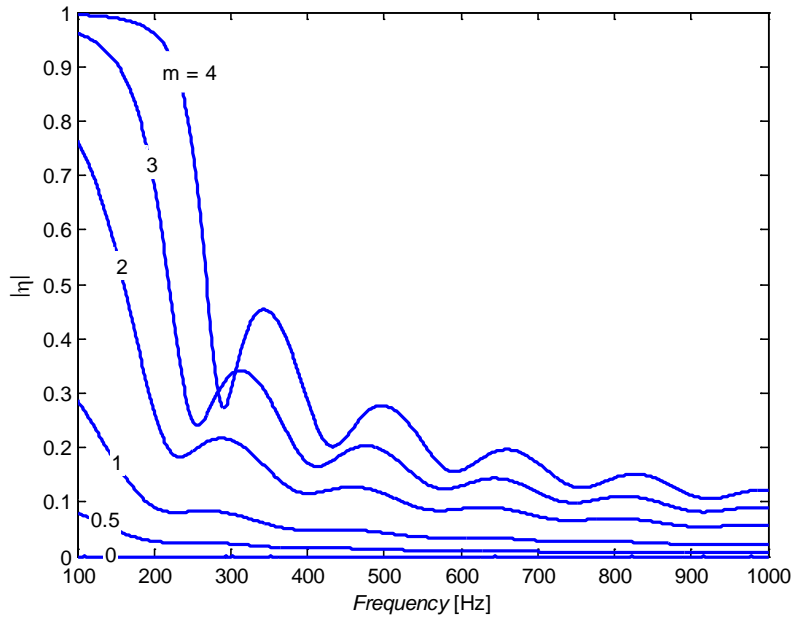


**Figure 54** Reflection coefficient of a catenoid 1 meter in length connected to an infinitely long tube for several flare values

### 5.1.2. An Open Catenoid

In practice, the horn plays a significant role in reducing the reflection coefficient. To see this, a realistic boundary condition at the horn mouth must be assumed. In this section, the horn mouth is open to the environment and is modeled as a piston in an infinite baffle. The mathematical modeling for the open catenoid is described by Eqns. (3.2.17) and (3.4.1). Through a parametric study of various horn mouth diameters, it is shown that an optimum horn geometry exists.

Consider a catenoidal horn whose throat diameter is fixed at 6 inches and length is fixed at 36 inches. The mouth diameter is allowed to change. The reflection coefficient for various mouth diameters is plotted in Figure 55. For comparison, an open tube of diameter 6 inches is also plotted. The open tube has the highest reflection coefficient for any frequency. Any horn represented by the curves in the plot shows smaller reflection coefficients than the straight tube. This motivates the need for a horn in order to reduce the reflection coefficient over a certain range of frequencies. As the mouth diameter is increased, the reflection coefficient gets smaller over the frequency range until the diameter reaches 24 inches. When the mouth diameter is changed from 24 to 48 inches, the reflection coefficient increases for the majority of frequencies<sup>17</sup>. This means there must be an optimum horn geometry that minimizes the reflection coefficient over the entire range. To find this optimum, a cost function must be defined.

---

<sup>17</sup> Physically speaking, when the mouth diameter becomes very large, the horn flares too rapidly, and the geometry suddenly changes, similar to Figure 12. This creates a large reflection coefficient.

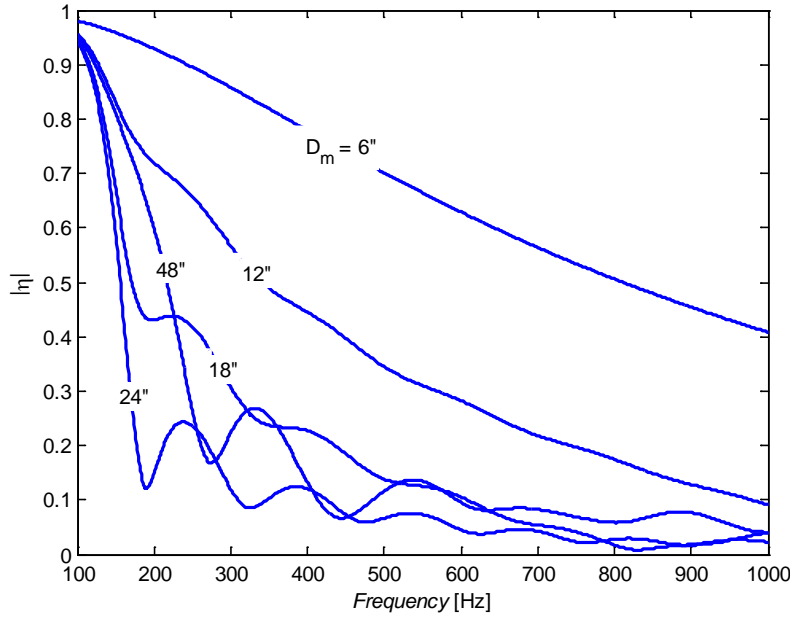


**Figure 55** Comparison of reflection coefficient for an open catenoid (6 in. throat diameter, 36 in. length) of various mouth diameters

## 5.2. Optimization Cost Function

Referring to Figure 55, an anechoic termination is better when the reflection coefficient measured at all frequencies for that termination is smaller than another termination. In practice, a comparison between any two terminations may show one having smaller reflection coefficient in some frequency ranges, and higher in others. The experimental results plotted in Figure 46 illustrated this behavior. How can it be determined which termination is “better?” A cost function  $\Omega$  is proposed as

$$\Omega = \frac{1}{\Delta f} \int_{f_l}^{f_u} |\eta| df , \quad (5.2.1)$$



where  $f_l$  and  $f_u$  are the lower and upper frequencies in the range of optimization, and  $\Delta f = f_u - f_l$ . Equation (5.2.1) is the normalized area bounded by the reflection coefficient magnitude and the abscissa between the lower and upper frequencies<sup>18</sup> (see Figure 56). As such,  $0 < \Omega < 1$ , where zero indicates the reflection coefficient is zero for every frequency in the frequency range, and one indicates the reflection coefficient is one for every frequency in the frequency range. The “best” anechoic termination for a given frequency range is one which has the smallest value of the cost function  $\Omega$ .

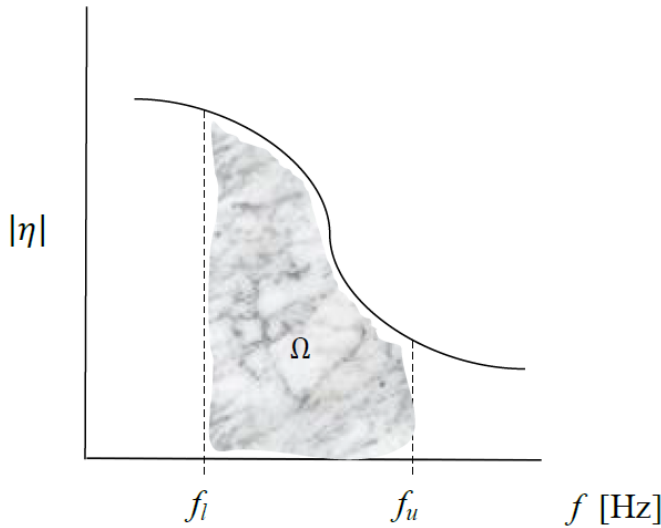


**Figure 56** The cost function is the normalized area under the reflection coefficient magnitude bounded between lower and upper frequencies

<sup>18</sup> The integral can be evaluated numerically using the “trapz” function in MATLAB®

### 5.3. Example of an Optimum Anechoic Termination

An anechoic termination consisting of a catenoid and absorbing termination is optimized for minimum reflection coefficient. The absorbing termination contains a layer of polyester fiber 1.75 inches thick around the inner circumference and the end opposite the horn mouth is open to the air. The optimization problem is defined as follows:

- Minimize  $\Omega$  over the range 50 – 500 Hz subject to
  - Horn throat diameter = 0.75 inches
  - 1 inch < Horn mouth diameter < 24 inches
  - 1 inch < Horn length < 200 inches
  - Horn length + Absorbing termination length = 200 inches

An exhaustive search method [40] is used to find the optimum design within the given constraints using step sizes of 1 inch for each variable. The optimization program stops when the cost function is found to have a global minimum in the feasible design space (see Appendix A for program listing). The horn throat diameter is fixed because in practice, it must fit to an existing impedance tube. The combined length of the horn and absorbing termination is also fixed because of hypothetical space constraints. The results of the optimization are summarized below. In this example, the optimized anechoic termination had the largest mouth diameter permitted. The horn length is approximately five times the mouth diameter and the termination length is about three times the mouth diameter. The

reflection coefficient for the optimized anechoic termination is plotted in Figure 57.

**Table 5** Optimized anechoic termination dimensions

Optimum Design	
Throat Diameter (in.)	0.75
Mouth Diameter (in.)	24
Horn Length (in.)	125
Termination Length (in.)	75
Cost Function $\Omega$	0.3216

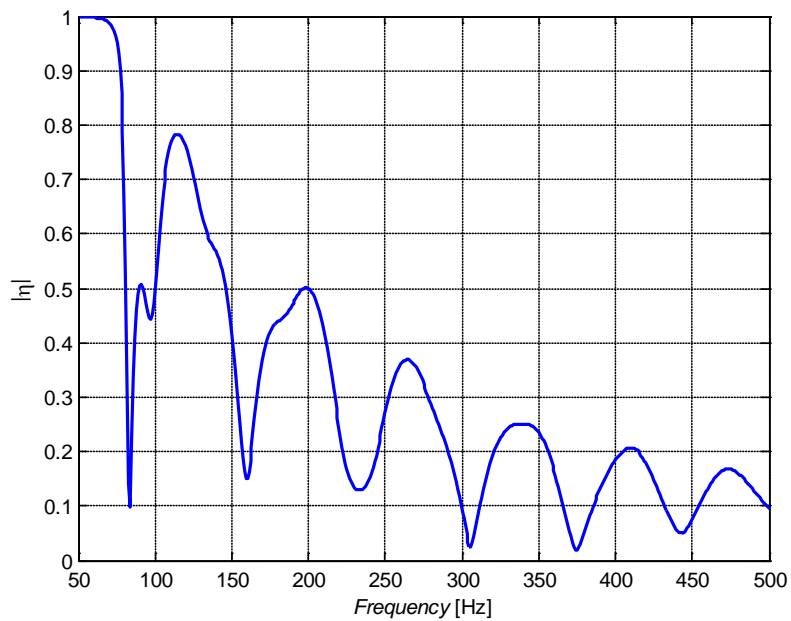


**Figure 57** Reflection coefficient magnitude of optimized anechoic termination

The results of this optimization example should not be interpreted to mean that the maximum mouth diameter should always be selected. Rules of thumb for designing an optimum anechoic termination are difficult to make and thus, optimization should be carried out on a case-by-case basis.

## CHAPTER 6

### CONCLUSION AND RECOMMENDATIONS

The goal of this thesis was to develop a new analytical model that could predict with accuracy the reflection coefficient of anechoic terminations that use catenoidal horns and tubes lined with absorbing material. The findings in Ch. 4 indicate that the predictions for reflection coefficient correlate well with experimental measurements, especially at low frequencies and for long absorbing terminations. By considering the impedance characteristics of each component (i.e. horn, tube, and absorbing material), a model could be constructed in order to calculate the reflection (or absorption) coefficient of the entire anechoic termination. The impedance characteristics of the catenoid were modeled using the theoretical developments of Thiessen [24]. To account for the effect of the finite length absorbing tube, the author provided a derivation (in Section 3.3.6) of the specific acoustic impedance at the inlet in terms of the axial wavenumber and impedance at the outlet. The axial wavenumber was computed by assuming that the material was locally reacting, according to Morse's model [26]. An empirical model was also used to determine the transmission characteristics of the absorbing material [36]. To the best of the author's knowledge, this was the first time these developments were applied to design of an anechoic termination.

The analytical model was also used to optimize the geometry of the horn and absorbing tube. The performance of the anechoic termination was quantified by introducing a cost function to assess the effect that each change in geometry had on the reflection coefficient. The cost function was a measure of the area under the reflection coefficient curve, bounded between a lower and upper frequency. An optimum design sought to minimize the cost function (i.e. the reflection coefficient across a certain frequency range).

This work could prove useful for engineers who seek to design anechoic terminations for automotive and HVAC applications. It is hoped that this work provides a general framework to assess the reflection characteristics of various types of anechoic terminations. The method of using impedances to develop the analytical model is by no means limited to the type of catenoidal anechoic termination described in this thesis. In general, this method can be used for any type of horn or cone whose impedance can be represented analytically. This is accomplished by replacing the impedance of the catenoid horn throat (Eq. (3.2.17)) with the impedance at the throat of the desired horn or cone. The analysis would then proceed as the summary in Section 3.4 outlined. Furthermore, by using any of the available empirical models for different types of absorbing materials, their effect on the transmission properties of the absorbing tube can be assessed. Polyester fiber was chosen for use in the prototype because of its widespread availability.

Further research should address some of the limitations of the model, namely, the tendency to overestimate the reflection coefficient at higher frequencies when taking into account the absorbing termination. The discrepancy between the predicted and experimentally measured reflection coefficient was largest for the shorter length absorbing termination. Better agreement was observed when the absorbing termination length was increased. In this case, the longer termination will provide increased acoustic attenuation of the sound wave. This suggests that the analytical model predicts the experimentally measured reflection coefficient more accurately when increased acoustic attenuation is accounted for. It is plausible that the analytical model used in this thesis underestimates the effect the absorbing termination has on attenuating the acoustic pressure of the sound wave. Lining the termination with absorbing material tends to compress the material, resulting in increased bulk density. An increase in bulk density would tend to increase the acoustic pressure attenuation within the material. This change in density is unknown, but if found to be large, this could significantly alter the predictions for reflection coefficient.

Another reason for the discrepancy may be the assumption that the lining is locally reacting (i.e. wave propagation through the lining is neglected). The theory developed by Scott [41] accounts for wave flow through the lining (i.e. bulk reacting model) and the results presented in the paper for duct attenuation were found in better agreement with experiment than the local reacting model,

especially when the absorbing material was “loosely packed.” Polyester fiber may be a material for which the bulk reacting assumption should be applied. If true, this may improve analytical predictions for reflection coefficient.



## REFERENCES

- [1] A. Bolton and E. Margetts, "Anechoic terminations for in-duct fan noise measurement," in *International Conference on Fan Design and Applications*, Sept. 7-9, Guildford, England, 1982.
- [2] "Acoustics - Determination of sound power radiated into a duct by fans and other air moving devices - in-duct method," *ISO 5136: 2003(E)*.
- [3] U. Bolleter, R. Cohen and J. Wang, "Design considerations for an in-duct sound measuring system," *Journal of Sound and Vibration*, vol. 28, no. 4, pp. 669-685, 1973.
- [4] P. Baade, "Effects of acoustic loading on axial flow fan noise generation," *Noise Control Engineering*, vol. 8, no. 1, 1977.
- [5] Z. Tao and A. Seybert, "A review of current techniques for measuring muffler transmission loss," *SAE International*, Vols. 2003-01-1653, 2003.
- [6] L. L. Beranek and H. P. Sleeper, "The design and construction of anechoic sound chambers," *J. Acoust. Soc. Am.*, vol. 18, no. 1, pp. 140-150, July 1946.
- [7] B. G. Watters, "Design of wedges for anechoic chambers," *Noise Control*, pp. 368-373, Nov. 1958.
- [8] L. L. Beranek, J. L. Reynolds and K. E. Wilson, "Apparatus and procedures for predicting ventilation system noise," *J. Acoust. Soc. Am.*, vol. 25, no. 2, pp. 313-321, March 1953.
- [9] F. B. Shenoda, *Reflexionsarme Abschlüsse für Durchstromte Kanäle, Akustik und Schwingungstechnik*, Berlin: VDE-Verlag GmbH, 1972.
- [10] S. Holgersson, "Development of an anechoic termination for fan noise measurements," *ASHRAE Trans.*, Vols. 74, Part I, Part No. 2069, 1968.

- [11] L. Kinsler, A. Frey, A. Coppens and J. Sanders, *Fundamentals of Acoustics*, 4th ed., New York: John Wiley & Sons, Inc., 2000.
- [12] S. Zheng and C. Kleinfeld, "Transmission loss measurements with and without an anechoic termination," *SAE International*, 2009.
- [13] B. Huallpa, S. Prati and F. Ferraz, "Development of a rig test to measure transmission loss of air intake systems," *SAE International*, 2005.
- [14] I. Dunn and W. Davern, "Calculation of acoustic impedance of multi-layer absorbers," *Applied Acoustics*, vol. 19, pp. 321-334, 1986.
- [15] C. Zwicker and C. Kosten, *Sound absorbing materials*, Amsterdam: Elsevier, 1949.
- [16] M. Delany and E. Bazley, "Acoustical properties of fibrous absorbent materials," *Applied Acoustics*, vol. 3, pp. 105-116, 1970.
- [17] A. Bracciali and G. Cascini, "Measurement of the lateral noise emission of an UIC 60 rail with a custom device," *Journal of Sound and Vibration*, vol. 231, no. 3, pp. 653-665, 2000.
- [18] J. Xu, J. M. Buchholz and F. R. Fricke, "Flat-walled multilayered anechoic linings: Optimization and application," *J. Acoust. Soc. Am.*, vol. 118, no. 5, pp. 3104-3109, 2005.
- [19] H. F. Olson, *Elements of acoustical engineering*, 2nd ed., New York: D. Van Nostrand Company, Inc., 1947.
- [20] "Laboratory measurement procedures for ducted silencers and air-terminal units," *DIN EN ISO 7235: 2003*.
- [21] H. Wollherr, "Akustische Untersuchungen an Radialventilatoren unter Verwendung der Vierpoltheorie," *Dissertation, Technische Universitat Berlin, Germany*, 1973.
- [22] W. Neise and F. Arnold, "On sound power determination in flow ducts,"

- Journal of Sound and Vibration*, vol. 244, no. 3, 2001.
- [23] G. H. Myers, "Development of an anechoic termination design for an in-duct fan sound test facility," *ASHRAE Transactions*, vol. 82, pp. 172-183, 1976.
  - [24] G. Thiessen, "Resonance characteristics of a finite catenoidal horn," *J. Acoust. Soc. Am.*, vol. 22, no. 5, pp. 558-562, 1950.
  - [25] P. Nelson and S. Elliott, *Active Control of Sound*, San Diego: Academic Press Inc., 1992.
  - [26] P. Morse, "The transmission of sound inside pipes," *J. Acoust. Soc. Am.*, vol. 11, pp. 205-210, 1939.
  - [27] A. Webster, "Acoustical impedance, and the theory of horns and of the phonograph," in *American Physical Society*, Philadelphia, 1914.
  - [28] V. Salmon, "A new family of horns," *J. Acoust. Soc. Am.*, vol. 17, no. 3, pp. 212-218, 1946.
  - [29] P. M. Morse, *Vibration and Sound*, 2nd ed., New York: McGraw-Hill Book Company, Inc., 1948.
  - [30] P. Morse and H. Feshbach, *Methods of Theoretical Physics*, vol. II, New York: McGraw-Hill Book Company, Inc., 1953.
  - [31] M. Munjal, *Acoustics of Ducts and Mufflers*, New York: Wiley-Interscience, 1987.
  - [32] C. Molloy and E. Honigman, "Attenuation of sound in lined circular ducts," *J. Acoust. Soc. Am.*, vol. 16, no. 4, pp. 267-272, 1945.
  - [33] F. Mechel, *Formulas of Acoustics*, 2nd ed., Springer, 2008.
  - [34] "Standard Test Method for Impedance and Absorption of Acoustical Materials by Impedance Tube Method," *ASTM C384 – 04*, 2004.

- [35] I. L. Ver and L. L. Beranek, in *Noise and Vibration Control Engineering*, 2nd ed., John Wiley & Sons, Inc., 2006.
- [36] M. Garai and F. Pompoli, "A simple empirical model of polyester fibre materials for acoustical applications," *Applied Acoustics*, vol. 66, pp. 1383-1398, 2005.
- [37] Technicon Acoustics, [Online]. Available: <http://www.tcnind.com/>. [Accessed 15 November 2011].
- [38] "Standard Test Method for Impedance and Absorption of Acoustical Materials Using a Tube, Two Microphones and a Digital Frequency Analysis System," *ASTM E1050-10*, 2010.
- [39] "Vibration testing, dynamic signal analysis and measurement data acquisition: m+p international," [Online]. Available: <http://www.mpihome.com/>. [Accessed 7 December 2011].
- [40] S. S. Rao, *Engineering Optimization: Theory and Practice*, 4th ed., Wiley, 2009, pp. 256-257.
- [41] R. Scott, "The propagation of sound between walls of porous material," *Proceedings of the Physical Society*, vol. 58, p. 358–368, 1946.
- [42] R. M. Aarts and A. J. E. M. Janssen, "Approximation of the Struve function  $H_1$  occurring in impedance calculations," *J. Acoust. Soc. Am.*, vol. 113, no. 5, pp. 2635-2637, 2003.

Appendix A  
MATLAB® Files

```

% This program calculates the reflection and power absorption
coefficient for a catenoidal anechoic termination

clear all
clc
close all
% global c rho r_0 zw k index

f      = 100:1:1000;           % frequency range [Hz\
Dt      = in2m(0.75);         % horn throat diameter [m]
Dm      = in2m(12);           % horn mouth diameter [m]
L1      = in2m(36);           % horn length [m]
L2      = in2m(36);           % termination length [m]
d       = in2m(1.75);         % thickness of layer [m]
r_0     = Dm/2 - d;           % radius to absorbing surface (6"-2")
rho_A   = 24;                 % packing density [kg/m^3]
c       = 343;                % speed of sound [m/s]
k       = 2*pi*f./c;           % wavenumber in air [m^-1]
rho     = 1.2041;             % air density [kg/m^3]
R       = 25.989*rho_A^1.404; % flow resistivity of layer (Garai, Pompoli)
E       = R./(rho*f);          % non-dimensional parameter

% Garai/Pompoli model
zc_GP = rho*c*((1+0.078*E.^0.623) - 1i*0.074*E.^0.660);
kw_GP = k.*( (1+0.121*E.^0.530) - 1i*0.159*E.^0.571);
zw_GP = -1i*zc_GP.*cot(kw_GP*d);

figure(1);
semilogx(f,real(zw_GP)./(rho*c),'r',f,imag(zw_GP)./(rho*c),'--b',...
'LineWidth',2); grid on
ylabel('z_w/(\rhoc)'); xlabel('{\itFrequency} [Hz]');
xlim([f(1) f(end)])
legend('Real','Imaginary',4)
title('Empirical Model for Polyester Fiber (---) and JCI Data (+)')

figure(11);
semilogx(f,real(zc_GP)./(rho*c),'r',f,imag(zc_GP)./(rho*c),'--b',...
'LineWidth',2); grid on
ylabel('z_c/(\rhoc)'); xlabel('{\itFrequency} [Hz]')
xlim([f(1) f(end)])
legend('Real','Imaginary')

figure(111);
semilogx(f,real(kw_GP),'r',f,-imag(kw_GP),'--b',f,k,':k',...
'LineWidth',2); grid on
ylabel('k_w'); xlabel('{\itFrequency} [Hz]')
xlim([f(1) f(end)])
legend('Real','Imaginary','k = 2\pif/c')

```

```

figure(1111); hold on
alpha_GP =
4*real(zw_GP)*rho*c./(abs(zw_GP).^2+2*rho*c*real(zw_GP)+(rho*c)^2);
plot(f,alpha_GP,'b','LineWidth',2)
xlim([f(1) f(end)]);grid on
xlabel('\itFrequency [Hz]');ylabel('Normal Absorption Coefficient, \alpha_n')
title('Empirical Model for Polyester Fiber (---) and JCI Data (+)')

% Activate this line to simulate a rigid-walled cylinder
% zw_GP = 1e8*ones(1,length(f));

Q = k*r_0*rho*c./zw_GP;
[kx,kr] = besselloots(Q,r_0,k,f);

% Check of root approximation using fsolve command

% zw = zw_GP;
% initial = [0.01;0.01];
% kr_times_r0 = zeros(length(f),1);
% kr = zeros(length(f),1);
% kx = zeros(length(f),1);
% for index = 1:length(f)
%     [z fval] = fsolve(@Morse,initial);
%     kr_times_r0(index,1) = z(1)+li*z(2);
%     kr(index,1) = kr_times_r0(index)/r_0;
%     kx(index,1) = sqrt(k(index).^2-kr(index).^2);
%     initial = [real(kr_times_r0(index));imag(kr_times_r0(index))];
% end
% kx = kx.';

figure(22)
plot(f,real(kx),'r',f,imag(kx),'--b',f,k,'-.k','LineWidth',2); grid on
xlim([f(1) f(end)])
legend('Real','Imaginary','k = 2\pif/c',2)
ylabel('k_x'); xlabel('\itFrequency [Hz]')

% BC's for termination end

% 1. Open end
x = 2*k*(Dm/2);
rA = 1-2*besselj(1,x)./x;
xA = 2*H1(x)./x;
z3 = rho*c*(rA+li*xA);

% 2. Lined cap
% z3 = zw_GP;

```

```

% 3. Hard cap
% z3 = 1e9;

% 4. Reflections are neglected at cap
% z3 = rho*c;

TOPz2 = z3./(rho*c) + 1i*k./kx .* tan(kx*L2);
BOTz2 = 1 + 1i*kx./k .* z3./(rho*c) .* tan(kx*L2);
z2     = rho*c*TOPz2./BOTz2;

% Thiessen
m       = flare_catenoid(L1,Dm,Dt);
b       = sqrt(k.^2-m^2);
TOPz1 = 1i*k*rho*c./z2.*tan(b*L1)+b-m*tanh(m*L1)*tan(b*L1);
BOTz1 = 1i*k*rho*c./z2-b.*tan(b*L1)-m*tanh(m*L1);
z1     = rho*c*1i*k./b .* TOPz1./BOTz1;

eta     = (z1-rho*c)./(z1+rho*c);

figure(50)
plot(f,abs(eta),'b','LineWidth',2)
xlabel('\itFrequency [Hz]');ylabel('\eta|')
axis([f(1) f(end) 0 1]);grid on

figure(60)
plot(f,1-abs(eta).^2,'--b','LineWidth',2)
axis([f(1) f(end) 0 1]);grid on
ylabel('\alpha')
xlabel('\itFrequency [Hz]')

```



```

% This program optimizes the horn and absorbing termination geometry
for minimum reflection coefficient over the specified frequency range

clear all
clc
close all

f      = 50:1:500;
c      = 343;                % speed of sound [m/s]
k      = 2*pi*f./c;          % wavenumber in air [m^-1]
rho    = 1.2041;             % air density [kg/m^3]
d      = in2m(1.75);         % thickness of layer [m]
Dt     = in2m(0.75);         % horn throat diameter [m]

rho_A  = 24;                  % packing density [kg/m^3]
R      = 25.989*rho_A^1.404; % flow resistivity of layer (Garai,
Pompoli)
E      = R./(rho*f);          % non-dimensional parameter

% Garai/Pompoli model
zc_GP = rho*c*((1+0.078*E.^0.623) - 1i*0.074*E.^0.660);
kw_GP = k.*( (1+0.121*E.^0.530) - 1i*0.159*E.^0.571);
zw_GP = -1i*zc_GP.*cot(kw_GP*d);

count = 1;
for Dm = in2m(1:24);
    for L1 = in2m(1:200);
        for L2 = in2m(200)-L1;

            r_0    = Dm/2 - d; % radius to absorbing surface

            Q      = k*r_0*rho*c./zw_GP;
            [kx,~] = besselfroots2(Q,r_0,k,f);

            % Open end
            x      = 2*k*(Dm/2);
            rA     = 1-2*besselj(1,x)./x;
            xA     = 2*H1(x)./x;
            z3     = rho*c*(rA+1i*xA);

            TOPz2 = z3./(rho*c) + 1i*k./kx .* tan(kx*L2);
            BOTz2 = 1 + 1i*kx./k .* z3./(rho*c) .* tan(kx*L2);
            z2     = rho*c*TOPz2./BOTz2;

            % Thiessen
            m      = flare_catenoid(L1,Dm,Dt);
            b      = sqrt(k.^2-m^2);
            TOPz1 = 1i*k*rho*c./z2.*tan(b*L1)+b-m*tanh(m*L1)*tan(b*L1);

```

```

BOTz1 = li*k*rho*c./z2-b.*tan(b*L1)-m*tanh(m*L1);
z1     = rho*c*li*k./b .* TOPz1./BOTz1;

eta     = (z1-rho*c)./(z1+rho*c);

I       = 1/(f(end)-f(1))*trapz(abs(eta));

mat(count,1) = Dm;
mat(count,2) = L1;
mat(count,3) = L2;
mat(count,4) = I;

count = count + 1;
end
end
end

clearvars -except mat Dt

[cost,loc] = min(mat(:,4));

Dm = mat(loc,1);
L1 = mat(loc,2);
L2 = mat(loc,3);
I  = mat(loc,4)

disp(['Dt_opt = ',num2str(Dt/0.0254)])
disp(['Dm_opt = ',num2str(Dm/0.0254)])
disp(['L_horn_opt = ',num2str(L1/0.0254)])
disp(['L_term_opt = ',num2str(L2/0.0254)])

```

```

function F = Morse(X)

    global c rho r_0 zw k index

    % Create complex value from real and imaginary parts
    x = X(1, :) + 1i*X(2, :);

    % Evaluate complex function
    constant = rho*c*k(index)*r_0;
    fun = x*besselj(1,x)./besselj(0,x) - 1i*constant./zw(index);

    % Separate real and imaginary parts
    F = [real(fun); imag(fun)];

function [kx] = besselroots(Q,r_0,k,f)

% 4th order polynomial to approximate the complex roots of the
% characteristic equation. See Mechel "Formulas of Acoustic" p.562-563

for n = 1:length(f)
    kr(n,:) = (1/r_0)*roots([- (12+1i*Q(n)) 0 24*(8+3*1i*Q(n)) 0 -
384*1i*Q(n)]);
    kx1 = sqrt(k(n)^2 - kr(n,1)^2);
    kx2 = sqrt(k(n)^2 - kr(n,2)^2);
    kx3 = sqrt(k(n)^2 - kr(n,3)^2);
    kx4 = sqrt(k(n)^2 - kr(n,4)^2);
    kxmat = [kx1 kx2 kx3 kx4];
    [~,I] = max(imag(kxmat),[],2);
    kx(n) = kxmat(I);
end

function m = flare_catenoid(x,d2,d1)

% FLARE_CATENOID computes the flare constant of a catenoid

% Inputs
% x : horn length
% d2 : mouth diameter
% d1 : throat diameter

% Output
% m : flare constant

m = (1/x)*acosh(d2/d1);

```

```

function y = H1(x)

% verified with Handbook of Mathematical Functions: Abramowitz, Stegun
% defines 1st order Struve function
% From Aarts, Janssen: Approximation of the Struve function H1
% occurring in impedance calculations - JASA May 2003

y = (2/pi)-besselj(0,x)+((16/pi)-5)*sin(x)./(x)...
    +(12-(36/pi))*(1-cos(x))./(x.^2);

```

## Appendix B

### Derivation of Acoustic Pressure in Cylindrical Coordinates

The acoustic pressure  $p(r, \theta, x, t)$  at any point and time in a cylinder, shown in Figure B.1 is described by the 3-dimensional wave equation [11],

$$\nabla^2 p = \frac{1}{c^2} \frac{\partial^2 p}{\partial t^2} \quad (\text{B.1})$$

where  $c$  is the speed of sound in air. The Laplace operator,  $\nabla^2$ , is defined in cylindrical coordinates as

$$\nabla^2 = \frac{1}{r} \frac{\partial}{\partial r} \left( r \frac{\partial}{\partial r} \right) + \frac{1}{r^2} \frac{\partial^2}{\partial \theta^2} + \frac{\partial^2}{\partial x^2} . \quad (\text{B.2})$$

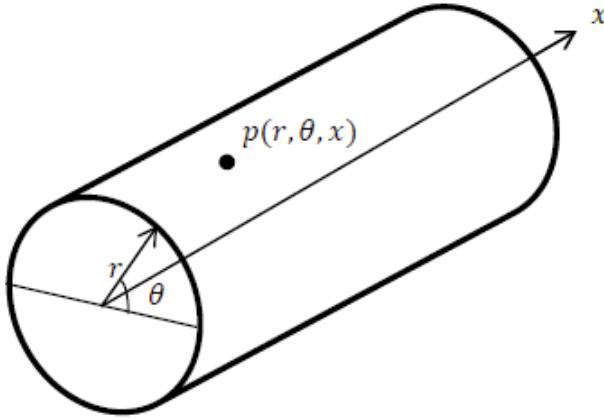


**Figure B.1** Acoustic pressure at a point in a cylinder expressed in cylindrical coordinates

Assume the time harmonic solution to Eq. (B.1) is of the form

$$p(r, \theta, x, t) = P(r, \theta, x) e^{j\omega t} , \quad (\text{B.3})$$

where  $P(r, \theta, x)$  is the acoustic pressure amplitude and  $\omega = 2\pi f$  is the angular frequency. Equation (B.3) is assumed separable such that

$$P(r, \theta, x) = R(r)\Theta(\theta)X(x) , \quad (\text{B.4})$$

where  $R$ ,  $\Theta$ , and  $X$  represent the functions for acoustic pressure, dependent on their respective coordinates. Inserting Eq. (B.3) with Eq. (B.4) into Eq. (B.1) and rearranging yields,

$$\frac{r^2}{R} \frac{\partial^2 R}{\partial r^2} + \frac{r}{R} \frac{\partial R}{\partial r} + \frac{r^2}{X} \frac{\partial^2 X}{\partial x^2} + k^2 r^2 = -\frac{1}{\Theta} \frac{\partial^2 \Theta}{\partial \theta^2} \quad (\text{B.5})$$

where  $k = \frac{\omega}{c}$ . The left side is a function of  $r$  and  $x$ , and the right side a function of  $\theta$ . The right side is a constant since the equation must hold for all  $r, \theta$ , and  $x$ .

Therefore, let

$$-\frac{1}{\Theta} \frac{\partial^2 \Theta}{\partial \theta^2} = q^2 \quad , \quad (\text{B.6})$$

so that Eq. (B.5) becomes

$$\frac{r^2}{R} \frac{\partial^2 R}{\partial r^2} + \frac{r}{R} \frac{\partial R}{\partial r} + k_r^2 r^2 + r^2 \left( \frac{1}{X} \frac{\partial^2 X}{\partial x^2} + k_x^2 \right) = q^2 \quad . \quad (\text{B.7})$$

The radial and axial wavenumbers are related by

$$k^2 = k_r^2 + k_x^2 \quad . \quad (\text{B.8})$$

The constant  $q$  must be an integer, since the pressure function  $\Theta(\theta)$  must be continuous after an azimuthal rotation of  $2\pi$ . Again, Eq. (B.7) must be true for all  $r$  and  $x$ . It follows that

$$\frac{1}{X} \frac{\partial^2 X}{\partial x^2} + k_x^2 = 0 \quad , \quad (\text{B.9})$$

since the 4<sup>th</sup> term in Eq. (B.7) is dependent on both  $r$  and  $x$ . Furthermore,

$$\frac{r^2}{R} \frac{\partial^2 R}{\partial r^2} + \frac{r}{R} \frac{\partial R}{\partial r} + k_r^2 r^2 = q^2 \quad . \quad (\text{B.10})$$

Equation (B.10) rewritten as

$$r^2 \frac{\partial^2 R}{\partial r^2} + r \frac{\partial R}{\partial r} + (k_r^2 r^2 - q^2) R = 0 \quad (\text{B.11})$$

is recognized as Bessel's equation of order  $q$ . Equations (B.6), (B.9), and (B.11) are the separated equations implied by Eq. (B.4). Their respective general solutions are

$$\Theta(\theta) = C e^{-jq\theta} + D e^{jq\theta} , \quad (\text{B.12})$$

$$X(x) = A e^{-jk_x x} + B e^{jk_x x} , \quad (\text{B.13})$$

$$R(r) = E J_q(k_r r) + F Y_q(k_r r) . \quad (\text{B.14})$$

where  $A$ ,  $B$ ,  $C$ ,  $D$ ,  $E$ , and  $F$  are complex constants. In Eq. (B.12), let  $C = 0$  since only one term is needed to describe wave propagation around the azimuth. Both terms are needed in Eq. (B.13) to describe incident and reflected waves axially through the termination. In Eq. (B.14),  $J_q$  and  $Y_q$  are Bessel functions of the first and second kind with order  $q$  and argument  $k_r r$ . For  $r = 0$ ,  $Y_q(k_r r)$  goes to negative infinity. Therefore,  $F = 0$  since the acoustic pressure on the  $x$ -axis must be finite. The acoustic pressure for a normal mode of the cylindrical cavity is therefore,

$$p(r, \theta, x, t) = J_q(k_r r) e^{jq\theta} [A e^{-jk_x x} + B e^{jk_x x}] e^{j\omega t} , \quad (\text{B.15})$$

where the complex constants  $D$  and  $E$  have been absorbed in  $A$  and  $B$ .



Appendix C

Polyester Fiber Specifications

**PRODUCT:** PF-012-80-00-00

**REV062509**

**PRODUCT DESCRIPTION:** 2" thick polyester fiber

### POLYESTER FIBER

Physical Property	Description - Value	Tolerance	Test Standard
Material	Polyester Fiber		
Thickness	1 inch	+/- 10%	
Color	White		
Density	3.5 oz/ft <sup>3</sup>	+/- 5%	
Flammability	HBF		UL94-HF
Flammability	SE		MVSS302
Flammability	Pass		California 117
Fungal Resistance	No Growth Observed		ASTM G21
Bacterial Resistance	No Growth Observed		ASTM G22
K Factor	0.3 Btu-in/hr-ft <sup>2</sup> -°F		ASTM C518
R Value	6.66 hr-ft <sup>2</sup> -°F/Btu		ASTM C518
Thermal Resistance	5.95 (m <sup>2</sup> K)/W for 2 inch	+/- 0.05	ASTM C518

### ABSORPTION COEFFICIENT AND NRC to ASTM C423 for PF-012-80-HR-00

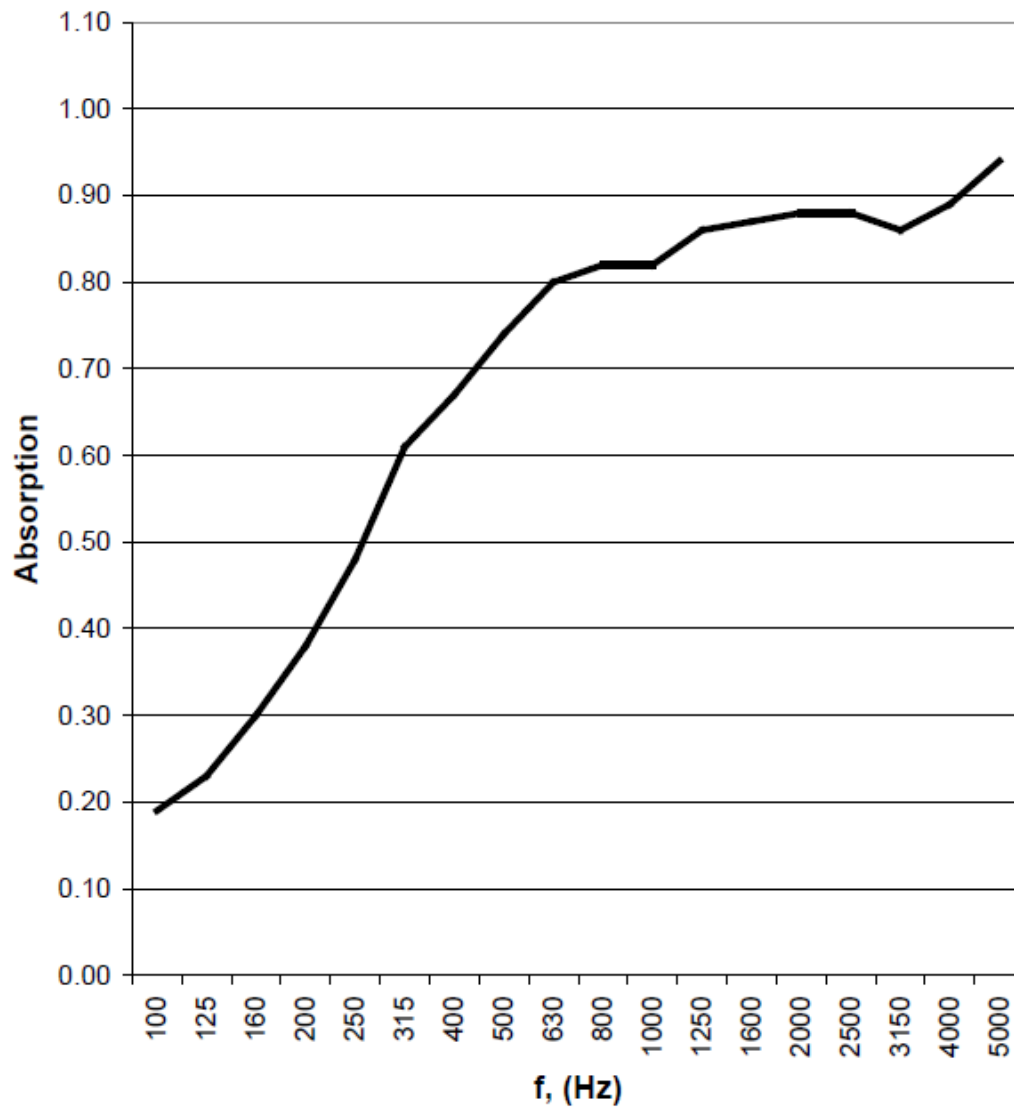
Test Lab	Test ID	Octave	125 Hz	250 Hz	500 Hz	1000 Hz	2000 Hz	4000 Hz	NRC
JohnsManville	500-2203	Absorp Coef	0.23	0.48	0.74	0.82	0.88	0.89	0.75

### AVAILABLE SIZES

Roll	55" X 50'
Sheet	As Specified

THE VALUES PRESENTED ARE TYPICAL AND ARE NOT INTENDED FOR SPECIFICATION PURPOSES. This information is provided without warranty, representation, inducement or license of any kind. INCLUDING BUT NOT LIMITED TO THE IMPLIED WARRANTIES OF MERCHANTABILITY AND FITNESS FOR A PARTICULAR USE OR PURPOSE, except that it is accurate to the best of Technicon Industries' knowledge or obtained from sources believed by Technicon Industries to be accurate, and Technicon Industries does not assume any legal responsibility for the use or reliance upon same. Customers are encouraged to conduct their own tests for suitability and conformance.

**ASTM C423**  
**Random Incidence Absorption**  
**Technicon Industries**  
**PF-012-80-HR-00**



Appendix D

Figure Copyright Documentation

## ELSEVIER LICENSE TERMS AND CONDITIONS

Oct 26, 2011

---

This is a License Agreement between Kyle R Myers ("You") and Elsevier ("Elsevier") provided by Copyright Clearance Center ("CCC"). The license consists of your order details, the terms and conditions provided by Elsevier, and the payment terms and conditions.

**All payments must be made in full to CCC. For payment instructions, please see information listed at the bottom of this form.**

Supplier	Elsevier Limited The Boulevard, Langford Lane Kidlington, Oxford, OX5 1GB, UK
Registered Company Number	1982084
Customer name	Kyle R Myers
Customer address	MAE Dept. Kalamazoo, MI 49008
License number	2776741053026
License date	Oct 26, 2011
Licensed content publisher	Elsevier
Licensed content publication	Journal of Sound and Vibration
Licensed content title	ON SOUND POWER DETERMINATION IN FLOW DUCTS
Licensed content author	W NEISE, F ARNOLD
Licensed content date	12 July 2001
Licensed content volume number	244
Licensed content issue number	3
Number of pages	23
Start Page	481
End Page	503
Type of Use	reuse in a thesis/dissertation

Intended publisher of new work	other
Portion	figures/tables/illustrations
Number of figures/tables/illustrations	1
Format	both print and electronic
Are you the author of this Elsevier article?	No
Will you be translating?	No
Order reference number	
Title of your thesis/dissertation	DESIGN OF A CATENOIDAL SHAPED ANECHOIC TERMINATION
Expected completion date	Dec 2011
Estimated size (number of pages)	120
Elsevier VAT number	GB 494 6272 12
Permissions price	0.00 USD
VAT/Local Sales Tax	0.0 USD / 0.0 GBP
Total	0.00 USD
Terms and Conditions	

Dear Kyle,

Thank you for your correspondence requesting permission to reprint figure 1 from SAE paper 2003-01-1653 – in your thesis titled “Design of a Catenoidal Shaped Anechoic Termination” for your degree of Master in Science in Mechanical Engineering from Western Michigan University.

Permission is hereby granted, and subject to the following conditions:

- Permission is for this one time use only. New requests are required for further use or distribution of the SAE material.
- The following credit statement must appear below the figure: “Reprinted with permission from SAE Paper No. 2003-01-1653 © 2003\* SAE International.”

Again, thank you for contacting SAE for this permission.

Regards,

Terri Kelly

Intellectual Property Rights Administrator

**SAE International**

Phone: 001.724.772.4095; Fax: 001.724.776.9765

E-mail: [terri@sae.org](mailto:terri@sae.org)

October 26, 2011

BHR Group (A trading name for VirtuaPiE Limited)  
Cranfield,  
Bedfordshire  
MK43 0AJ  
United Kingdom

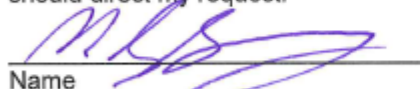
To Whom it may Concern,

I would like to request your permission to include an excerpt from the following item in my thesis:

Bolton and E. Margetts, "Anechoic terminations for in-duct fan noise measurement," in International Conference on Fan Design and Applications, Sept. 7-9, Guildford, England, 1982. (Figure 11, p. 329)

The reason I am using this figure is to describe the use of expanding cross sections to construct an anechoic termination as part of an experimental arrangement measuring fan sound power in-duct. The figure will be used in my thesis for a literature review of work that has been done relating to anechoic termination design. My thesis titled "Analytical and Experimental Analysis of a Catenoidal Shaped Anechoic Termination" will be used as partial fulfillment for my degree of Master in Science in Mechanical Engineering from Western Michigan University on December 16, 2011. My thesis will be available in both electronic and physical formats. The source will receive full credit in the manuscript.

For your convenience, I am including a space for your signature to indicate your permission for my use of the above-mentioned material. By signing below, you give ProQuest Information and Learning (UMI) the right to supply copies of this material on demand as part of my master's thesis. Please attach any other terms and conditions for the proposed use of this item below. If you no longer hold the copyright to this work, please indicate to whom I should direct my request.

  
Name  
N. G. Guy

1 Nov 2011  
Date

If you could, please respond to this e-mail or, send a letter as formatted in this e-mail to the address provided below. Thank you for your time and attention to this matter.

Sincerely,

Kyle Myers  
Graduate Research Assistant  
Department of Mechanical Engineering  
Western Michigan University  
4601 Campus Dr.  
Kalamazoo, MI 49008-5343  
(269) 276-3438



## Appendix E

### Impedance Data for Polyester Fiber

The normal specific acoustic impedance ratio of a sample of polyester fiber used in the prototype was experimentally measured and compared to the empirical predictions of Garai [36]. The measurements were conducted using a Bruel & Kjaer Type 4206 impedance tube and follow the method outlined in ASTM E1050-98 [38]. The impedance results are shown below.

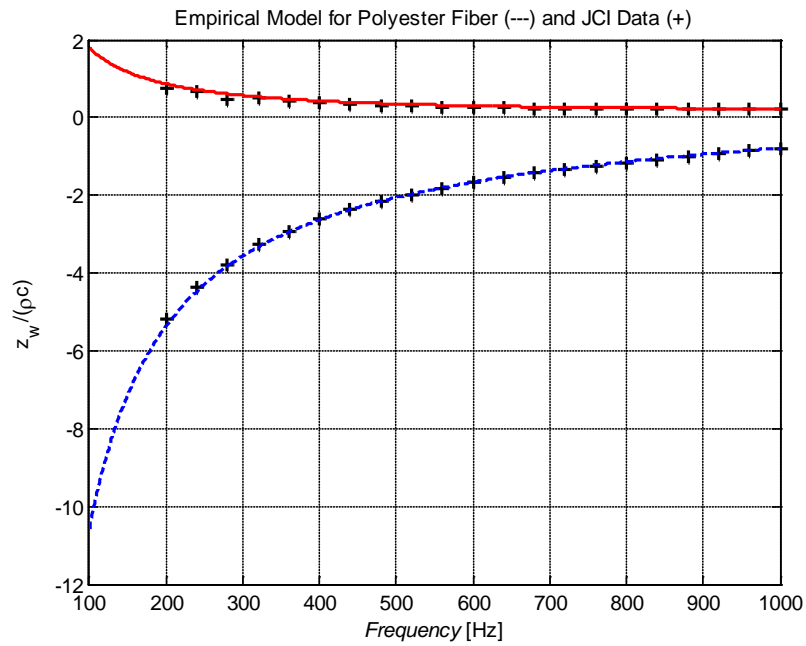


**Figure 58** Normal specific acoustic impedance ratio. Real component (---), imaginary component ( - - - ), and experimental data (+)